



VCU

Virginia Commonwealth University
VCU Scholars Compass

Theses and Dissertations

Graduate School

2023

PMs and Gas Pollutants Removal by Electret Filter Media and Metal-Organic Frameworks (MOFs)

Yu Zhang

Virginia Commonwealth University

Follow this and additional works at: <https://scholarscompass.vcu.edu/etd>



Part of the [Mechanical Engineering Commons](#)

© The Author

Downloaded from

<https://scholarscompass.vcu.edu/etd/7271>

This Dissertation is brought to you for free and open access by the Graduate School at VCU Scholars Compass. It has been accepted for inclusion in Theses and Dissertations by an authorized administrator of VCU Scholars Compass. For more information, please contact libcompass@vcu.edu.

©Yu Zhang _____ 2023

All Rights Reserved

PMs and Gas Pollutants Removal by Electret Filter Media and Metal-Organic Frameworks (MOFs)

A dissertation submitted in partial fulfillment of the requirements for the degree of Doctor of
Philosophy at Virginia Commonwealth University

By

Yu Zhang

M.S., Safety Engineering, Northeastern University, China, 2019

B.S., Safety Engineering, Shenyang University of Chemical Technology, China, 2016

Advisor: Sheng-Chieh Chen

Assistant Professor, Department of Mechanical and Nuclear Engineering

Virginia Commonwealth University

Richmond, Virginia

May 2023

Acknowledgment

First and foremost, I must thank my supervisor, Prof. Shawn Chen, without his assistance and dedicated involvement in every step throughout the process, this dissertation would never have been accomplished. I would like to thank you very much for your support and understanding over these past few years.

I would also like to show my gratitude to my dissertation committee, including Prof. Daren Chen, Prof. Weining Wang, Prof. Dmitry Pestov, and Prof. Xiuli Lin. I'm appreciative of their invaluable and insightful suggestions and comments towards my research work. In addition, I would like to thank Prof. Supathorn Phongikaroon and Prof. Zeyun Wu for their assistance with my academia job search. I would also like to thank Prof. Karla Mossi for her kindness with everything. As the graduate program director of mechanical and nuclear engineering department at VCU, she is an incredible asset to all the graduate students.

Getting through my dissertation required more than academic support, and I have many, many people to thank for listening to and, at times, having to tolerate me over the past several years. I cannot begin to express how grateful I am for their friendship. Dr. Xiang He, Dr. Zan Zhu, Dr. Peng Wang, Hao Tu, Dr. Qijin Huang, Dr. Shihang Li, Dr. Zheng Fan, Dr. Mi Zhou and Fei Liu have been unwavering in their personal and professional support during the time I spent at VCU. I would also like to thank Xiaomei Weng and Lingqiu Jin who welcomed me when I first arrived in Richmond.

Finally, none of this could have happened without my family. I am forever grateful that they offered their endless love, support and encouragement through phone calls and messages every other weeks. Thank you all!

Tables of Contents

Acknowledgment	III
List of Figures	VII
List of Tables	X
Abstract	XI
Chapter 1. Introduction	1
1.1 Indoor air pollution.....	2
1.2 Overview of control strategies	3
1.3 Objectives and arrangement of the dissertation.....	9
Chapter 2. Development of metal-organic framework coated electret filter media for simultaneous removal of VOCs and PM _{2.5}	13
2.1 Introduction	15
2.2 Materials and Methods	17
2.2.1 Electret filter media	17
2.2.2 Synthesis of MOFs particles.....	19
2.2.3 Preparation of E-MOFilters	19
2.2.4 Characterization of MOF particles and E-MOFilters	22
2.2.5 Initial efficiency of E-MOFilters for PMs.....	23
2.2.6 PM aging test.....	24
2.2.7 Removal efficiency and adsorption capacity of toluene by E-MOFilters.....	24
2.3 Results and Discussions	26
2.3.1 Characterization of MOF particles	26
2.3.2 Characterization of different E-MOFilters	28
2.3.3 Initial efficiency of E-MOFilters (MIL-125-NH ₂) for PMs	30
2.3.4 Performance of E-MOFilters on PM loading	32
2.3.5 Performance of E-MOFilters for toluene removal	35
2.4 Conclusions	39
Chapter 3. Mitigating the relative humidity effects on the simultaneous removal of VOCs and PM _{2.5} of a metal–organic framework coated electret filter	41
3.1 Introduction	43

3.2 Materials and Methods	46
3.2.1 Modification of MOF MIL-125-NH ₂ particles.....	46
3.2.2 Electret filter media and modified E-MOFilter	47
3.2.3 Characterization of MOF particles and E-MOFilters	47
3.2.4 Initial efficiency and holding capacity of modified E-MOFilters for PMs	48
3.2.5 RH effects on the initial efficiency and adsorption capacity of the E-MOFilter for toluene	48
3.3. Results and Discussion.....	50
3.3.1 Characterization of MOF particles	50
3.3.2 Characterization of modified E-MOFilters	54
3.3.3 Initial efficiency of modified E-MOFilters for PMs	57
3.3.4 Performance of modified E-MOFilters on PM loading.....	58
3.3.5 RH effects on the initial efficiency and adsorption capacity of the E-MOFilter for toluene	59
3.4 Conclusions	64
Chapter 4. A novel sustainable semiconductor/metal-organic framework coated electret filter for simultaneous removal of PM _{2.5} and VOCs	66
4.1 Introduction	68
4.2 Materials and Methods	71
4.2.1 Synthesis of composite photocatalyst (p-BWO@MIL-125-NH ₂).....	71
4.2.2 PE-MOFilter fabrication.....	73
4.2.3 Characterization of MOF Particles and PE-MOFilters.....	74
4.2.4 PM and toluene removal efficiency by the PE-MOFilter.....	74
4.2.5 Initial PM removal efficiency test	76
4.2.6 Toluene initial efficiency and adsorption capacity test	76
4.2.7 Photodegradation of toluene by the PE-MOFilters	78
4.3 Results and Discussions	80
4.3.1 Characterization of synthesized MIL, p-BWO and p-BWO@MIL-1 Particles	80
4.3.2 Performance of PE-MOFilters.....	83
4.3.3 Initial Efficiency of PE-MOFilters for PMs.....	84
4.3.4 Initial adsorption Efficiency of PE-MOFilters for toluene.....	85
4.3.5 Toluene adsorption capacity and photodegradation of the PE-MOFilters	86
4.4 Conclusions	90
Chapter 5. An empirical equation for quickly qualifying commercial N95 equivalent respirators	92

5.1 Introduction	94
5.2 Materials and Methods	97
5.2.1 Materials	97
5.2.2 Theoretical deposition model	98
5.2.3 Surface potential measurement.....	101
5.2.4 Filtration efficiency testing.....	103
5.3 Results and Discussions	107
5.3.1 Specification of studied masks	107
5.3.2 Comparison of the theoretical and experimental efficiency curve	110
5.3.3 Correlation of Surface potential and charge density	111
5.3.4 Empirical correlation of easily accessible parameters.....	111
5.3.5 Validation and application of the developed empirical equation	114
5.4 Conclusions	116
Chapter 6. Conclusions and Future Directions	117
6.1 Conclusions	118
6.1.1 Development of MOFs-based materials coated electret filter media for indoor air pollution control	118
6.1.2 Development of an empirical equation for quick respirator efficiency evaluation for individual health protection	119
6.2 Future Directions.....	120
Appendix: Vita.....	121
Reference:	123

List of Figures

Figure 1. 1 Schematic illustration of the strategy for addressing the issue of indoor air PM and VOC pollution.	5
Figure 1. 2 Digital images of (a) face masks and filtering facepiece respirators (FFRs) that suggested by CDC for reducing transmission of SARS-CoV-2 and providing self-protection, and (b) Specific respirators: N95s in United States (NIOSH standards) and N95 equivalent respirators--FFP2 from European Union (EN 140:2001 standards), KN95 from China (GB2626-2006/2019) and KF94 from Korean (KMOEL-2017-64).....	6
Figure 2. 1 The experimental setup to coat MOF particles onto charged filter media.	22
Figure 2. 2 Experimental setup for the initial removal efficiency and adsorption capacity of toluene by the E-MOFilters.....	25
Figure 2. 3 SEM image of MIL-125-NH ₂ (a), FT-IR spectrum of the MIL-125-NH ₂ (b), XRD patterns of MIL-125-NH ₂ (c), and BET analysis of pore diameter distribution of MIL-125-NH ₂ (d).	27
Figure 2. 4 BET analysis for the pore size distributions of MIL-125-NH ₂ coated HEPA E-MOFilter (a) and MERV 13 E-MOFilter (b), and SEM images of MIL-125-NH ₂ depositions on two E-MOFilters (c).....	29
Figure 2. 5 Initial size-fractioned efficiency of MERV 13 E-MOFilter coated with different levels of MIL-125-NH ₂ particles.	32
Figure 2. 6 Effects of the MOF loading on the evolution of pressure drop of the MERV 13 E-MOFilters during filtration.....	33
Figure 2. 7 Dynamic size-fractioned efficiency of original (a), low coating (b), medium coating (c), and high coating (d) MERV 13 filters along PM aging process.....	34
Figure 2. 8 Comparison of initial toluene removal efficiency between HEPA and MERV 13 based E-MOFilters coated with different MOF particles (25 wt% high level). (b) Comparison of initial toluene removal efficiency by 1 and 2 layers of MERV 13 filter coated with different levels of MIL-125-NH ₂ particles.....	36
Figure 2. 9 Comparison of breakthrough curve amongst ACFs and MERV 13 based E-MOFilters coated with different levels of MIL-125-NH ₂ particles.	39

Figure 3. 1 Experimental setup for the initial removal efficiency and adsorption capacity of toluene by the E-MOFilters under different RHs.	50
Figure 3. 2 Comparison of SEM images and WCAs (a: MIL-125-NH ₂ , b: MIL-125-R7, c: PDMS@MIL-125-NH ₂ , d: PDMS@MIL-125- R7), XRD patterns (e), FT-IR spectra (f) N ₂ adsorption isotherms (g) between original and modified MIL-125-NH ₂	54
Figure 3. 3 SEM images of the depositions of modified MIL-125-NH ₂ particles on the fibers of MERV13 electret filter (a) and N ₂ adsorption isotherms of original and modified E-MOFilters (b).	56
Figure 3. 4 Initial size-fractioned efficiency of MERV 13 E-MOFilter coated with MIL-125-NH ₂ , PDMS@MIL-125-NH ₂ , MIL-125-R7 and PDMS@MIL-125-R7 MOF particles.	57
Figure 3. 5 Comparison of initial toluene removal efficiency of MERV 13 based E-MOFilters coated with alkylated and PDMS-treated MIL-125-NH ₂ at 5 cm s ⁻¹ (a) and 0.5 cm s ⁻¹ (b).	61
Figure 3. 6 Comparison of breakthrough curves amongst E-MOFilters coated with original and modified MOF particles under 0.5 cm s ⁻¹ face velocity.	63
Figure 4. 1 The schematic diagram and digital images of the newly developed multi-functional filter holder.	75
Figure 4. 2 Experimental setup for initial removal efficiency and adsorption capacity test, and photocatalytic efficiency test for toluene.	78
Figure 4. 3 SEM, XRD patterns and BET analysis of powdered original MIL, p-BWO and p-BWO@MIL (mass ratio: 1:1) (a-f), photoluminescence (PL) analysis of p-BWO (inset image shows the photochromic response of p-BWO under 30s visible light irradiation) (g), UV-vis spectra and Tauc plots of p-BWO and MIL (h and i).	82
Figure 4. 4 SEM image of the deposition of p-BWO@MIL-1 particles on the fibers of MERV 13 electret media (PE-MOFilter).	84
Figure 4. 5 Comparison of initial size-fractioned efficiency of original MERV 13 electret media, PE-MOFilter coated with p-BWO@MIL-1 particles, and discharged MERV 13 electret media.	85
Figure 4. 6 Comparison of initial toluene removal efficiency of original MIL, p-BWO, p-BWO@MIL-0.5 (-1.5) coated MERV 13 electret media.	86
Figure 4. 7 Comparison of toluene conversion rates of p-BWO, MIL and p-BWO@MIL-0.5 (-1.5) coated MERV 13 electret media.	89

Figure 4. 8 Comparison of SEM images (a), XRD patterns (b) of p-BWO@MIL-1 before and after the toluene photocatalytic tests and filtration efficiencies (c) of original, UV treated, and IPA discharged MERV 13 filter media.	90
Figure 5. 1 Schematic of surface potential measurement by the electrostatic voltmeter.....	103
Figure 5. 2 Schematic diagram of experimental setup for measuring filtration efficiency of FFRs.	106
Figure 5. 3 Particle size distribution that was used in the filtration efficiency testing.	107
Figure 5. 4 Comparison of the theoretical and experimental efficiency curve of respirator #16 (N95), (a); respirator #9 (KN95), (b); respirator #21 (KF94), (c); respirator #24 (FFP2), (d) respirators.....	110
Figure 5. 5 Correlation of Surface potential and charge density of tested respirators.....	111

List of Tables

Table 2. 1 Specification of the HEPA and MERV 13 electret media for the MOF coating..... 18

Table 3. 1 BET analysis of original and modified MOF powders and E-MOFilters..... 53

Table 4. 1 Specification of the MERV 13 electret media for the composite photocatalyst coating.
..... 74

Table 4. 2 Experimental conditions for PM and toluene removal tests and photoreaction. 77

Table 4. 3 BET analysis of p-BWO, MIL and p-BWO@MIL particles..... 83

Table 5. 1 Specification of the studied respirators in this work..... 109

Table 5. 2 The comparison of the predicted efficiency by empirical equation model with
experimental efficiency..... 113

Table 5. 3 The new respirator samples that was used to validate the empirical equation. 114

Table 5. 4 Empirical equation application for mechanical filters 115

Abstract

PMS AND GAS POLLUTANTS REMOVAL BY ELECTRET FILTER MEDIA AND METAL-ORGANIC FRAMEWORKS (MOFS)

By Yu Zhang

A dissertation submitted in partial fulfillment of the requirements for the degree of Doctor of
Philosophy at Virginia Commonwealth University

Virginia Commonwealth University, 2023

Advisor: Dr. Sheng-Chieh Chen

Assistant Professor, Department of Mechanical and Nuclear Engineering

Indoor air quality (IAQ) has been becoming a major concern worldwide because statistical data showed that the indoor concentrations of gas pollutants, e.g., volatile organic compounds (VOCs) and particulate matters (PMs) are often 2–5 times higher than that of outdoors. Especially, people spend 87% of their time indoors and increasing to more than 90% during COVID-19 pandemic. The high concentration of these indoor air pollutants is mainly due to the reduced air exchange rate for the design of energy-efficient building construction and the increased usage of furnishings, glues, paints, furnaces, etc., leading to VOC outgassing and particle emission. Evidence has shown that prolonged exposure to these pollutants can cause acute and chronic effects on respiratory and central nervous systems. As typical pollutants of indoor air, PMs and

VOCs pose a significant threat to public health. It is urgent to simultaneously and effectively remove indoor air pollutants to improve the indoor air quality.

To simultaneously mitigate indoor PMs and VOCs, this dissertation investigated the idea of developing metal organic frameworks (MOFs) based materials coated electret filters. The idea is based on the following three facts: (1) Electret filters, with quasi-permanent electrical charges on the fibers, acquiring an additional force of electrostatic attraction, show a high initial filtration efficiency against PMs and a much lower pressure drop (ΔP) compared to mechanical filters. (2) MOFs which are made of metal clusters and organic linkers, have attracted considerable interest owing to their extraordinarily high surface areas, tunable pore size, and adjustable internal surface properties. Because of their controllable pore size and chemical functionality, MOFs outperform traditional porous materials (activated carbon, zeolite, alumina, and silica) in the adsorption of VOCs. (3) MOF-based semiconductor was demonstrated to have large surface area ($> 1000 \text{ m}^2/\text{g}$) and suppressed charge carrier (h^+ and e^-) recombination rate, contributing to high photocatalytic efficiency, which are advantageous for VOC photocatalytic oxidation. The selected MOFs were synthesized via a hydrothermal route and then coated in electret filter media by using a liquid filtration method for fabrication of MOF and semiconductor/MOF coated electret filter, named E-MOFilter and PE-MOFilter, respectively. Various characterizations, such as XRD, SEM, and FT-IR etc., were performed and their results demonstrated that the successful synthesis of samples. The PM filtration tests and VOC absorption and photodegradation tests were further performed. Results demonstrated that the newly developed filters were found to have high PM removal efficiency and decent VOC removal efficiency because of the negligible fiber charge degradation in filters, the highly porous structures of MOFs and the increased charge carrier densities in the photocatalytic systems.

Beyond development of advanced electret HVAC filters for simultaneous PM and VOC control, face masks and filtering facepiece respirators (FFRs), as personal protective equipment (PPE), can be used to provide indoor air pollution control and personal health protection. However, it is reported that approximately 60% of KN95s, the most widely available N95 equivalent respirators on the market that NIOSH evaluated during the COVID-19 pandemic in 2020 and 2021 did not meet the requirements. Besides, the general public has limited access to the standardized testing equipment (required by the National Institute for Occupational Safety and Health (NIOSH)) for evaluating the filtration efficiency of FFRs. Therefore, in this work, an empirical equation by using easily accessible parameters for efficiency prediction of respirator minimum efficiency at most penetrating particle size (MPPS) was provided. In the empirical equation model, the three most easily accessible parameters, pressure drop, mask area and surface potential were utilized. The predicted efficiencies showed less than 4% deviation to the experimental efficiencies, which demonstrated the acceptability of the empirical equation model. This model was further validated by extra new mask samples.

This work from this dissertation sheds light on applying the novel MOF-based materials coated electret filters in the residential and commercial HVAC systems to remove PMs and VOCs simultaneously and effectively. In addition, by providing an empirical equation for predicting filtration efficiency, this work provides an easily accessible screening method for qualifying respirators so that the general public can make informed decisions regarding the use of respirators for individual health protection and indoor air pollution control.

Chapter 1. Introduction

1.1 Indoor air pollution

With the rapid development of society and economy, air pollution has become one of our era's greatest concerns due to its great impact on public health. From the smog hanging over cities to the smoke inside the home, air pollution poses a major threat to public health. The combined effects of indoor and ambient (outdoor) air pollution causes millions of premature deaths every year (Manisalidis et al. 2020; Jiang et al. 2016), largely as a result of increased mortality from stroke, heart disease, chronic obstructive pulmonary disease, lung cancer and acute respiratory infections. Air pollution is contamination of the indoor or outdoor environment by any chemical, physical or biological agent that modifies the natural characteristics of the atmosphere.

Indoor air pollution is a pollution of special concern especially during the COVID 19 pandemic (Du and Wang 2020; Huang et al. 2018; US EPA, 2017). The statistical data has shown that people from all over the world spend more than 87–90% of their time indoors (Klepeis et al. 2001). Exposure to a variety of indoor air pollutants, including particulate matters (PMs), and gaseous pollutants, e.g., volatile organic compounds (VOCs), nitrogen oxides (NO_x), sulfur oxides (SO_x), etc., causes a wide range of adverse health outcomes from respiratory illnesses to cancer problems (Tran et al. 2020; Chen et al. 2019). In developed countries, indoor concentrations of air pollutants, e.g., PM_{2.5} and VOCs etc., are found to be often 2-5 times higher than typical outdoor concentrations (US EPA 2017). It is mainly due to the design of lower air exchange rates for energy-efficient building construction and an increased use of synthetic building materials, furnishings, personal care products, etc. In low- and middle-income countries, exposure to smoke from burning fuels such as dung, wood and coal in inefficient stoves produces a variety of health-damaging pollutants, including PMs, VOCs, methane, carbon monoxide etc., causes 3.8 million premature deaths each year (Huang et al. 2018; Pui et al. 2014; Gustafson et al. 2008). Besides, due to the high

concentration of ambient fine particulate matters, PM_{2.5} (particulate matter with an aerodynamic diameter less than 2.5 μm) can infiltrate into indoor environments (Chang et al., 2019; Tang et al., 2018a). Meanwhile, commercial buildings and apartments are being built and homes are being refurbished due to their improved wealth in developing countries (Jiang et al., 2013). This results in an increase in the use of furniture, glues, and paints etc., leading to an increase in VOC emissions. Therefore, for both developed and developing countries, PM_{2.5} and VOCs are the pollutants of great concern in indoor air environments. Many studies have shown that PM_{2.5} and VOCs can lead to acute and chronic effects on humans' respiratory and central nervous systems and eventually cause hematological problems and cancer (Brasche and Bischof 2005; Chen et al. 2019; Sarigiannis et al. 2011). Therefore, it is essential to effectively remove PM_{2.5} and VOCs in order to enhance indoor air quality.

1.2 Overview of control strategies

Indoor air pollution is a significant environmental health concern that has gained increasing attention in recent years. It is a complex issue that involves various pollutants and sources that can have negative impacts on human health and wellbeing. Indoor air pollutant control strategies are necessary to address the issue and minimize exposure to pollutants.

To mitigate PM_{2.5} which infiltrate into or are originated indoors for healthy indoor environments, air filters are widely utilized in the heating, ventilating, air conditioning (HVAC) system, and indoor air cleaners (IACs) in residential homes, schools, and commercial and hospital buildings. Electret filters, with quasi-permanent electrical charges on the fibers, acquiring an additional force of electrostatic attraction, show a high initial filtration efficiency and a much lower pressure drop (ΔP) compared to mechanical filters. They have been widely used to improve the quality of indoor air in recent years (Chang et al. 2019; Tang et al. 2018a, 2018b). However, to

achieve good indoor air quality (IAQ), not only PM_{2.5} but also VOCs, e.g., formaldehyde, and BTXs (benzene, toluene, xylene), should be mitigated at the same time (Jiang et al. 2013; Zhao et al. 1998). To remove VOCs, traditionally, porous activated carbon air purifiers are utilized to chemically attract organic contaminants to be absorbed (Zhu et al. 2020). Simultaneous removal of PM and VOC pollutions is achieved by combining granular activated carbon (GAC) or other adsorbents, e.g., zeolites, with filter media, either embedded in or separately as an individual filtration module (Rezaei et al. 2016; Zhao et al. 1998). Both assembly strategies make the filtration module bulky and heavy. The activated carbon fiber (ACF) filters were also developed to simultaneously remove PMs and VOCs. However, the ACF is not dielectric and cannot be charged, making them less efficient for PM removal compared with electret media at the same mechanical properties (fiber diameter, porosity, and thickness) (Zhang et al. 2021; Das et al. 2004).

Recently, metal–organic frameworks (MOFs) have gained much attention mainly due to their high surface area, high porosity, and tunable structures (Scott Bobbitt et al. 2017; Zhang et al. 2016; Schneemann et al. 2014; DeCoste and Peterson 2014). MOFs are a major part of nanomaterials science and are composed of metal clusters and organic linkers. MOFs as the inherent porous materials have outperformed the traditional porous materials (activated carbon, zeolite, alumina, and silica) in adsorption of harmful gas/vapor due to their tunable pore size and tunable chemical functionality (Furukawa et al. 2013). Also, MOFs are considered to be a promising photocatalysts to mitigate VOC pollution in indoor air environments, based on the extraordinary variability of their metal nodes and functional linkers and richness of their porous structures (Usman et al. 2017; Li et al. 2014; Alvaro et al. 2007). Motivated by the enormous potential of MOFs to remove harmful gases and the excellent PM_{2.5} filtration performance and low pressure drop of electret filters, it would be a rational strategy to integrate electret filters with MOFs (as shown in Fig. 1.1), where

PM_{2.5} and VOCs can be removed simultaneously via air filtration, gas adsorption and photodegradation, to address the issue of indoor air PM and VOC pollution.

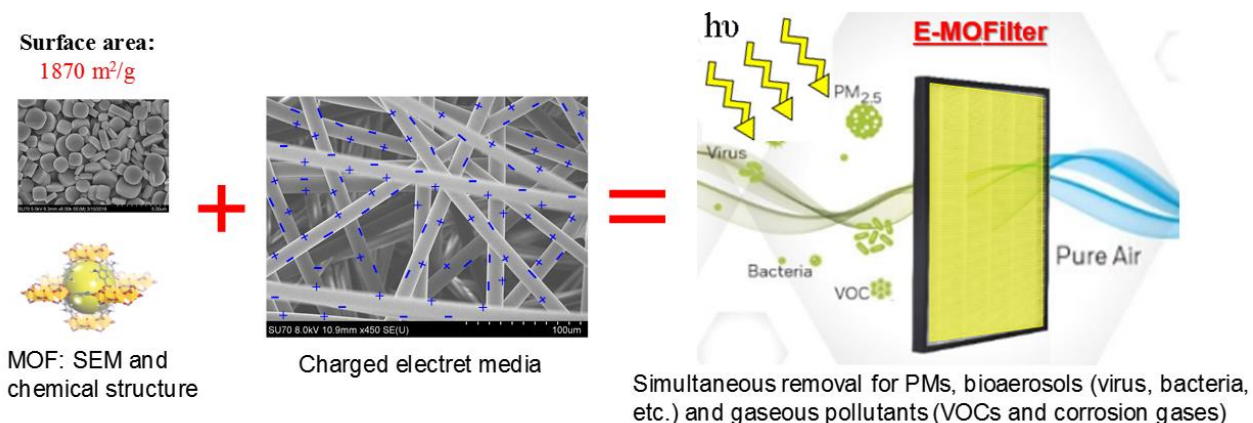


Figure 1. 1 Schematic illustration of the strategy for addressing the issue of indoor air PM and VOC pollution.

In addition to the PM_{2.5} and VOCs pollutants, the bioaerosol pollutants that carry bacteria, fungi and viruses serve as transmission vehicles for diverse infections (Ereth et al. 2021; Kim et al. 2018), are also a great concern. In particular, during COVID 19 pandemic, the novel coronavirus (SARS-CoV-2) causes millions of people infections and death due to its severe fatality rate and high airborne transmission rate (Dhand and Li 2020; Jayaweera et al. 2020; Prather et al. 2020; Yan et al. 2018). It is reported that sneezing, coughing, speaking and breathing release and disperse droplets and aerosols carried with virus and these droplets can travel up to 8 m, and, once desiccated, the residue or droplet nuclei may stay suspended for hours (Dhand and Li 2020; CDC 2020a), which pose a great threat to public health. To provide protection for individuals and prevent the high transmission rate of the coronavirus by droplets and aerosols, face masks and filtering facepiece respirators (FFRs), as shown in Fig. 1.2 (a), are required or highly recommended by Centers for Disease Control and Prevention, CDC, since the outbreak of the COVID 19 pandemic

in March 2020 in the United States (CDC 2022). Face masks are generally looser fitting and made of 2-3 ply with a melt blown layer in-between and designed primarily for one way protection (to capture bodily fluid leaving the wearer in case of cough, sneeze, etc.). Most face masks do not have safety rating and their primary design is not to protect the wearer. Respirators are generally tight fitting with a much better face seal and designed to provide two-way protection (non-valve) by filtering both the outward and inward air. Generally, they have stricter testing and safety ratings depending on how much they protect the wearer.

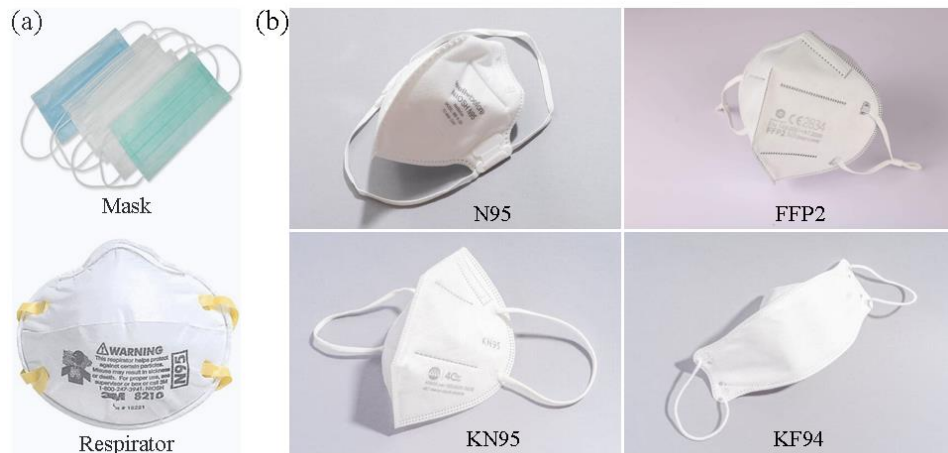


Figure 1. 2 Digital images of (a) face masks and filtering facepiece respirators (FFRs) that suggested by CDC for reducing transmission of SARS-CoV-2 and providing self-protection, and (b) Specific respirators: N95s in United States (NIOSH standards) and N95 equivalent respirators--FFP2 from European Union (EN 140:2001 standards), KN95 from China (GB2626-2006/2019) and KF94 from Korean (KMOEL-2017-64).

It is obvious that the COVID-19 pandemic has highlighted the importance of FFRs as personal protective equipment (PPE) in reducing the risk of infection and disease transmission. It is to be noted that even though the pandemic has almost been over, the research on FFRs filtration

performance is still necessary to prepare for the next possible pandemic. As known, the COVID-19 pandemic severely disrupted the supply chains for many types of Personal Protective Equipment (PPE), particularly surgical N95 respirators earlier during the outbreak in March 2020. As a consequence, on May 27, 2020, an Emergency Use Authorization (EUA) from the United States Food and Drug Administration (FDA) had allowed use of industrial N95 respirators and importation of N95 equivalent respirators (denoted as, N95 equivalent respirators hereafter) manufactured to international standards to be used for health care personnel in health care settings; these include KN95 respirators from China and FFP2 respirators from the European Union (Health 2021). Therefore, many commercial N95 equivalent respirators, e.g., FFP2, KN95, and KF94, as shown in Fig. 1.2, on the market nowadays can be widely accessible and affordable. The N95 equivalent respirators have recently become a common choice for the general public. Though COVID 19 pandemic has almost been over, the viruses have not gone. Hence, it is of great significance that these FFRs have a good quality to protect the general public from getting and spreading viruses. It is worth noting, however, that according to the CDC, approximately 60% of KN95, the most widely available N95 equivalent respirators on the market that NIOSH evaluated during the COVID-19 pandemic in 2020 and 2021 did not meet the requirements i.e., filtration efficiency (FE) > 95% (CDC 2022). In reaction to the unsatisfactory performance of FFRs, several studies have performed evaluation of the filtration performance of commercially available FFRs (Schilling et al. 2021; Plana et al. 2021a; Duncan et al. 2021). As known, the testing protocols standardized by the National Institute for Occupational Safety and Health (NIOSH) require a series of equipment such as airflow regulator, aerosol generator, neutralizer, and particle counters, most of which are expensive devices in certified research lab and usually out of reach to the general public. Therefore, due to the limited access to the facilities that the standardized testing protocols

required for evaluating mask efficiency, many of their filtration tests were not strictly in compliance with N95 testing standards or the equivalent international requirements and thus, their efficiency results are either overestimated or underestimated (Schilling et al. 2021; Patra et al. 2022; Duncan et al. 2021; Stahl et al. 2021; Cai and Floyd 2020). In their tests, the particle size distribution (especially for particle size less than 300 nm), the charge status, and the deliquesce point of the water-soluble contents in the particles were usually not considered when determining the efficiencies. For instance, Plana et al. (2020) simplified filtration testing setup and procedures utilizing non-neutralized particles to challenge the filter, resulting in overestimated filtration efficiencies. Also, in their study, the filtration efficiencies of the filters are only based on the challenging particles larger than 300 nm and did not take the small particle sizes (< 300 nm) into account, which may result in the overestimated filtration efficiencies. Yim et al. (2020) evaluated the filtration efficiency of N95 and KN95 respirators against particles around 20–30 nm with the larger sizes up to about 150 nm, which were generated by a candle, due to their limited access to the collision-type atomizer. The authors did not consider the charges on the aerosols particles when determining the filtration efficiencies of the respirators, which may overestimate the efficiencies. As mentioned above, these simplified testing generated systematic errors when determining the filtration efficiency of a filter media. Therefore, to obtain accurate efficiency results, it is essential that a testing system utilizes the standardized facilities required by NIOSH. Given the limited access to these facilities and the systematic errors that may occur, in addition to experimentally evaluate mask efficiency, theoretical deposition models based on single fiber theory can also be used to evaluate the filtration efficiency of a filter media (Chang et al., 2016). In general, theoretical models can accurately predict the efficiencies. However, the theoretical calculation can be complicated and time-consuming, as it requires knowing many parameters, e.g., fiber size,

thickness, packing density, charge density, and face velocity. Besides, charge density is the most inaccessible parameter due to the complexity of charge figuration in the filters. Also, it is commonly seen that in many studies, only an estimated value of charge density was given to calculate efficiency (Hao et al., 2021). Based on the above mentioned, it is necessary to develop a fast and convenient method to evaluate mask efficiency. As is known, empirical equation models are a useful tool that can quickly provide reliable predictions and insights into complex systems and are often more accessible to non-experts than more theoretical models. Empirical equations are mathematical equations that describe the relationship between variables based on observations, data, or experimental results. These equations are selected because they fit experimental data and are useful for predicting outcomes. For example, a study by You et al. (2012) calculated indoor particle deposition velocity using a modified three-layer model and then generated an empirical equation based on the database. It was worth mentioning that limited work has been reported so far to develop empirical equation models to evaluate mask efficiency.

1.3 Objectives and arrangement of the dissertation

As mentioned above, to simultaneously remove PMs and VOCs in the indoor air, this dissertation aims to develop MOF and MOF-based material coated electret filter media by taking full advantage of the merits of electret filter and MOFs-based materials. Beyond development of advanced electret HVAC filters for simultaneous PM and VOC removal, an empirical equation for quickly qualifying respirators is also of great interest to be developed for general public to make informed decisions regarding the use of respirators for indoor air pollution control and personal health protection.

The objectives of this dissertation are 1) to develop a multifunctional HAVC filter media to simultaneously and efficiently removal PMs and VOCs by integration of electret filter with MOFs;

2) to provide performance evaluation for commercial facepiece filtering respirators (FFRs) and meanwhile, propose an empirical equation to quickly qualifying these commercial FFRs by using easily accessible parameters. Given these two major objectives, this dissertation is divided into two sections. For the first section, it involves the development of a gas-particle removal of filter media capable of simultaneously removal of PMs and VOCs by combing electret filter with MOFs for sustainable design of heating, ventilation, and air conditioning (HAVC) filter (**Chapter 2, 3 and 4**). For the second, it is to provide performance evaluation and an empirical equation for quickly qualifying commercial respirators, thereby enabling the easy access to evaluating mask efficiency (**Chapter 5**).

More specifically, **Chapter 2** developed a novel air filtration media, called E-MOFilter, by combing metal organic frameworks (MOFs) with electret filter media, which can effectively and efficiently simultaneous remove PMs and VOCs. The MOF particles were prepared and successfully deposited onto electret media by utilizing the proposed liquid filtration method. Results showed that the E-MOFilter gained only a few more pascals of air resistance compared with clean electret media. The developed E-MOFilter with MIL-125-NH₂ particle coating not only had a decent toluene removal efficiency (>80%) but also maintained its original PM_{2.5} holding capacity. **Chapter 3** focused on reducing the effects of humidity introduced by MOFs. To lessen the effects of humidity on VOC removal, the performances of five filter modifications to give the MIL-125-NH₂ MOF coating hydrophobic qualities were introduced and investigated. It was revealed that the introduction of an external coating of polydimethylsiloxane (PDMS) produced the best results, with impressive initial VOC removal efficiency and the longest VOC breakthrough time under a relative humidity level of 50%. **Chapter 4** proposed to develop a composite photocatalyst (semiconductor@MOF) coated electret filter, denoted as PE-MOFilter, which not

only captures but effectively photodegrades VOC pollutants via the synergistic action of adsorption and photocatalytic oxidation (PCO). In addition, the proposed photocatalytic PE-MOFilter was demonstrated to maintain its high PM filtration efficiency.

In **Chapter 5**, a filtration testing system was strictly designed according to standards to perform efficiency evaluations of 50 different N95 and N95 equivalent commercial respirators. The respirator samples were measured with their thickness, fiber size, packing density, surface potential, and filtration area. Their efficiencies were evaluated for both mass- and number-based methods. The surface potential was correlated with the charge density derived through the theoretical efficiency model. Findings demonstrated a strong correlation between filter charge density and surface potential. An empirical equation model for predicting the filtration efficiency of minimum mask efficiency at most penetrating particle size (MPPS) has been successfully developed. In this model, the three most readily available parameters were utilized: pressure drop, mask area, and surface potential. The predicted efficiencies obtained by the empirical equation showed less than 4% deviation to the experimental efficiency data. The empirical equation was further validated by experimental efficiency data derived from additional samples. Overall, by providing an empirical equation for predicting the filtration efficiency, this work provides an easily accessible screening method for qualifying respirators so that the general public can make informed decisions about the use of respirators.

This work from this dissertation sheds light on applying the novel E-MOFilter and PE-MOFilter in the residential and commercial HVAC systems to remove PMs and VOCs simultaneously and effectively. Also, by providing an empirical equation for predicting the filtration efficiency of FFRs, the work provides an easily accessible screening approach for qualifying respirators, which should enable organizations that may experience mask/respirator

shortages and uncertain inventories make informed decisions regarding the use and procurement of respirators for personal health protection and indoor air pollution control.

Chapter 2. Development of metal-organic framework coated electret filter media for simultaneous removal of VOCs and PM_{2.5}

Journal of Membrane Science. 618 (2021): 118629

DOI: <https://doi.org/10.1016/j.memsci.2020.118629>

Reproduced by permission of The Elsevier

Abstract

The electret filter media coated with highly porous metal-organic frameworks (MOFs) particles, named E-MOFilter, is newly developed and evaluated for its capacity for simultaneous removal of fine particulate matters ($PM_{2.5}$) and volatile organic compounds (VOCs). Three different MOFs particles, including MIL-125-NH₂, UiO-66-NH₂, and ZIF 67, were synthesized and systematically characterized. The produced MOF particles were suspended in ultrapure water and then a liquid filtration apparatus was used to deposit the MOF particles onto two electret media with different minimum efficiency reporting values (MERV 13 and 17) to form the E-MOFilters. Results showed that the MOF particles deposited in MERV 13 media were more uniform than that of MERV 17. In the PM filtration tests, results showed that the E-MOFilter gained only a few more pascals of air resistance compared with clean electret media. Besides, its PM removal efficiency was found to be close to that of clean electret media. This indicates that a uniform MOF particle deposition and negligible charge degradation from the current coating process were obtained. Further, the E-MOFilter with MIL-125-NH₂ particle coating not only had a decent toluene removal efficiency (> 80%) but also maintained its original $PM_{2.5}$ holding capacity. This work may shed light on applying the novel E-MOFilter in the residential and commercial HVAC systems and indoor air purifiers to simultaneously and effectively remove $PM_{2.5}$ and VOCs.

2.1 Introduction

The statistical data showed that people spend about 87–90% of their time indoors (Brasche and Bischof, 2005; Klepeis et al., 2001; Schweizer et al., 2007). However, indoor air quality (IAQ) has been becoming a major concern not only in developing but also developed countries. In developing countries, commercial buildings and apartments are being built and homes are being refurbished due to improved wealth. That increases the use of a large quantity of furnishings, glues, paints, etc., leading to the increase in the emissions of volatile organic compounds, VOCs (Chen et al., 2019; Huang et al., 2018; C. Jiang et al., 2013). Besides, due to the high concentration of ambient fine particulate matters ($PM_{2.5}$, particulate matter with an aerodynamic diameter less than $2.5\ \mu\text{m}$), $PM_{2.5}$ can infiltrate into indoor environments (Li et al., 2020; Pui et al., 2014). In developed countries, indoor concentrations of some pollutants are found to be often 2-5 times higher than typical outdoor concentrations. It is mainly due to the design of lower air exchange rates for energy-efficient building construction and an increased use of synthetic building materials, furnishings, personal care products, etc. (EPA, 2017). Research has shown that VOCs and $PM_{2.5}$ can lead to acute and chronic effects on humans' respiratory and central nervous systems and eventually cause hematological problems and cancer (Chen et al., 2019; Du and Wang, 2020; Pui et al., 2014; Sarigiannis et al., 2011).

To mitigate $PM_{2.5}$ for healthy indoor environments, air filters are utilized in the heating, ventilating, air conditioning (HVAC) system, and indoor air cleaners (IACs). Electret filters, with quasi-permanent electrical charges on the fibers, acquiring an additional force of electrostatic attraction, show a high initial filtration efficiency and a much lower pressure drop compared to mechanical filters. They have been widely used to improve the quality of indoor air in recent years (Chang et al., 2019; Tang et al., 2018b, 2018a). However, to achieve a good IAQ, not only $PM_{2.5}$

but also VOCs, e.g., formaldehyde, and BTXs (benzene, toluene, xylene), should be mitigated (Du and Wang, 2020; Ohura et al., 2009; Walgraeve et al., 2011; Yu et al., 2009). Traditionally, simultaneous removal of PM and VOC pollutions is achieved by combining granular activated carbon (GAC) or other adsorbents, e.g., zeolites, with filter media, either embedded in or separately as an individual filtration module (Jo and Yang, 2009; Rezaei et al., 2016; Zhao et al., 1998). Both assembly strategies make the filtration module bulky and heavy. There is also an advanced high-end photocatalytic oxidation (PCO) technology applied in IACs. However, the high price and requirement of UV light source cause the inconvenience (Wang et al., 2016; Zhao and Yang, 2003; Zhong and Haghghat, 2015). The activated carbon fiber (ACF) filters were developed to simultaneously remove PMs and VOCs (Das et al., 2004; Yang et al., 2017; Zhu et al., 2020). However, the ACF is not dielectric and cannot be charged, making it less efficient for PM removal compared with electret media at the same mechanical properties (fiber diameter, porosity, and thickness).

Metal-organic frameworks (MOFs), a novel class of porous crystalline polymers, have large surface areas, tailorable pore sizes, tunable functionalities, and relatively high thermal stability and selectivity, which make them promising candidates for gas capture, gas separation and drug delivery, catalysis, sensing, etc. (DeCoste and Peterson, 2014; Furukawa et al., 2013). MOFs are constructed from metal ions and organic ligands. Such materials offer significant chemical and structural diversity and have outperformed the traditional porous materials (activated carbon, zeolite, alumina, and silica) in adsorption of harmful gas/vapor due to their tunable pore size and chemical functionality in a controlled manner (K. Tanabe and M. Cohen, 2011; Lu et al., 2014; Schneemann et al., 2014). Inspired by MOFs having such great potential to remove harmful gases, researchers recently coated MOFs onto mechanical filters, termed MOFilters, to remove PMs and

toxic gas pollutants simultaneously (Chen et al., 2017; Z. Jiang et al., 2013; Ma et al., 2019a). Results demonstrated that certain inorganic toxic gas species, such as SO₂, H₂S, and O₃, can be removed efficiently. However, because of the use of mechanical media, the pressure drop was relatively high and PM efficiency was low (Li et al., 2020).

In this study, for the first time electret filter media is combined with MOF particles, named E-MOFilter, to mitigate PM_{2.5} and VOCs simultaneously. Three MOF particles, including MIL-125-NH₂, UiO-66-NH₂ and ZIF-67, were selected and synthesized for the fabrication of E-MOFilters. These MOFs were chosen due to their small pore sizes, high surface areas, and special functionalities, enabling a promising adsorption of VOCs (Jiang et al., 2013; Katz et al., 2013; Kim et al., 2018). In the aspect of electret filter, two electret filters with different minimum efficiency reporting values (MERVs), i.e., MERV 13 and MERV 17, were used as base substrates for the deposition of MOF particles. The effects of fiber diameter and porosity on the uniformity of MOF particles depositions were studied. The E-MOFilters were tested not only for their initial efficiency but also holding and adsorption capacity for PM_{2.5} and toluene (a common indoor VOC pollutant). The ultimate goal of this study is to demonstrate the E-MOFilter and the developed fabrication method not only maintain the charge of electret media but also keep high removal efficiency and holding capacity for PM_{2.5}. Besides, the E-MOFilter has high efficiency and high adsorption capacity for VOCs.

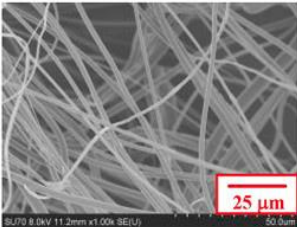
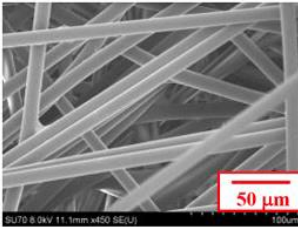
2.2 Materials and Methods

2.2.1 Electret filter media

The flat sheets of the MERV 13 and MERV 17 rated electret filter media were used for the deposition of MOF particles and subsequent PM and toluene removal tests. To be noted that the

MERV 17 rated filter is equivalent to the high efficiency particulate air (HEPA) filter which has a 99.97% efficiency in the removal of 0.3 μm particles. Therefore, the MERV 17 will be labeled as ‘HEPA’ throughout the rest of the article. The filter specifications and scanning electron microscopy (SEM) images of these two media are summarized in Table 2.1. As can be seen, the HEPA media has a much smaller fiber diameter (major layer) than that of MERV 13. It is expected that the HEPA media would be relatively easier for the deposition of MOF particles onto its fibers by sieving mechanism in the liquid filtration (coating) process. Since the MERV 13 has a relatively low pressure drop and its PM removal efficiency may not be high enough, this study intended to use two layers of MERV 13, in addition to 1 layer, to see if the PM and toluene removal efficiency can be further improved. In comparison, due to the existing high pressure and good PM efficiency, the HEPA will be tested with 1 layer only.

Table 2. 1 Specification of the HEPA and MERV 13 electret media for the MOF coating.

Types	HEPA (MERV 17)	MERV 13
SEM images		
Fiber diameter (μm)	2.0 ± 0.5 (fine fibers)	13.1 ± 0.9
Thickness (mm)	0.5 ± 0.03 (0.11 ± 0.01 ,	0.47 ± 0.02
Basic weight (g/m^2)	72 ± 2 (22 ± 1 without	75 ± 2
Solidity (α)	0.102	0.104
Charging density ($\mu\text{C}/\text{m}^2$)	80	50
Initial pressure drop at 5 cm/s (Pa)	46.2 ± 0.7	4.5 ± 0.1
Initial efficiency for 0.3 μm particles	99.97 ± 0.01	91.11 ± 0.23

2.2.2 Synthesis of MOFs particles

Three types of MOFs, including MIL-125-NH₂, UiO-66-NH₂ and ZIF-67, were selected and synthesized to fabricate the E-MOFilters. The three MOFs were synthesized following the procedures reported in the literature with slight modifications (Jiang et al., 2013; Katz et al., 2013; Kim et al., 2018). Briefly, for MIL-125-NH₂, 0.797 mL titanium tetraisopropoxide (TTIP) and 0.651 g 2-aminoterephthalic acid (BDC-NH₂) were dissolved in the mixture of dimethylformamide (DMF)/methanol (15 mL/15 mL). Then, the mixture was transferred to a Teflon-lined steel autoclave reactor and placed in an oven at 150 °C for 15 hours. The obtained yellow products were isolated by centrifugation and washed by 30 mL DMF and 30 mL methanol, respectively, for three times. Finally, the samples were dried under 50 °C overnight in vacuum. For UiO-66-NH₂, 1.875 g ZrCl₄ (pre-dissolved in a mixture of DMF/HCl, 75 mL/15 mL) and 2.011 g BDC-NH₂ (pre-dissolved in DMF 150 mL) were mixed and heated at 80 °C for 3 hours. Then the obtained powders were isolated by centrifugation and washed with 45 mL DMF for three times. Similarly, the product was dried under vacuum at 50 °C overnight. In synthesizing ZIF-67, 0.3577 g cobalt nitrate hexahydrate (pre-dissolved in 25 mL methanol) and 0.4062 g 2-methylimidazolate (pre-dissolved in 25 mL methanol) were mixed and stirred at room temperature for 24 hours. Then the obtained products were isolated by centrifugation and washed with 30 mL methanol for two times. The products were also dried under vacuum at 50 °C overnight.

2.2.3 Preparation of E-MOFilters

In general, there are many ways to incorporate MOF particles with the filter media, including in situ interweaving, electrospinning (physical blending of MOF nanoparticles with polymers, producing MOF-based nanofibers), freeze-drying, hot-pressing, roll-to-roll processing, air

filtration deposition, etc. (Zhang et al., 2016; Chen et al., 2017; Ma et al., 2019). To choose an appropriate method for the current study, the following considerations should be taken into account in the process of combining the MOF particles with the charged fibers. Firstly, the charges of the electret media should not be degraded; secondly, the MOF particles should firmly attach to the electret media with a minimized growth of air resistance; thirdly, the transfer process is simple and cost-efficient. Reviewing the abovementioned methods, none of them is applicable. For example, the interweaving could not tightly hold the MOF particles and particle shedding during filtration may occur; the electrospinning method may not be easily scaled up to the size of real HVAC filters of 12" × 12" or 20" × 20"; both freeze-drying and hot pressing would experience harsh temperature or pressure changes, therefore, the degradation for fiber charges is unavoidable; the roll-to-roll can also cause shedding issue; and the air filtration always leads to a non-uniform deposition of particles in depth of the media.

As none of the existing methods were appropriate, this study proposed a liquid filtration (coating) method to fabricate the E-MOFilters, which was based on the authors' previous research findings (Chen et al., 2016; Lee et al., 2017). The choice of liquid filtration is to utilize the inherent more uniform particle deposition in liquid filtration process especially in the case of pore to particle diameter ratio is not low, e.g., 5-20. Besides, the authors have found that there was a negligible charge degradation in water soaking-drying tests for electret media (Chen et al., 2016; Li et al., 2020). If the MOF particles can be uniformly coated onto the fibers and in depth of the media without the formation of particle cake, the applied quantity of MOF particles and the increase of air resistance can be minimized (lower than dendrite structure in air filtration), therefore, the shielding of charge by the MOF particles should be minimized. Besides, the VOC removal efficiency should be maximized due to the high surface area of MOF particles. Fig. 2.1

shows the experimental setup for the MOF coating. The MOF particles were first suspended in water with a concentration of 0.02 wt%. There were still some minor loading effects causing the upper layers of the media to collect a little more MOF particles than the lower layers. Therefore, the coating flow (or filtration direction) was introduced from the back side of the filter to reduce the deposition quantity of MOF particles on the first few layers of the E-MOFilters. Thus, the attenuation of PM removal efficiency and holding capacity due to charge shielding and reduction in void space by MOF particles can be avoided (Chang et al., 2019). The driving force for the flow circulation in the system was provided by a peristaltic pump under the flow rate of $100 \text{ mL} \cdot \text{min}^{-1}$. In brief, the quantities of the coated MOFs were controlled at 5 (low), 10 (medium) and 25 (high) wt%, of the mass of MERV 13 (1 or 2 layer) and HEPA (1 layer) flat sheet with 47 mm in diameter. For example, the one with 5 wt% low coating uses MOF particles for only 3.75 g per square meter of filter.

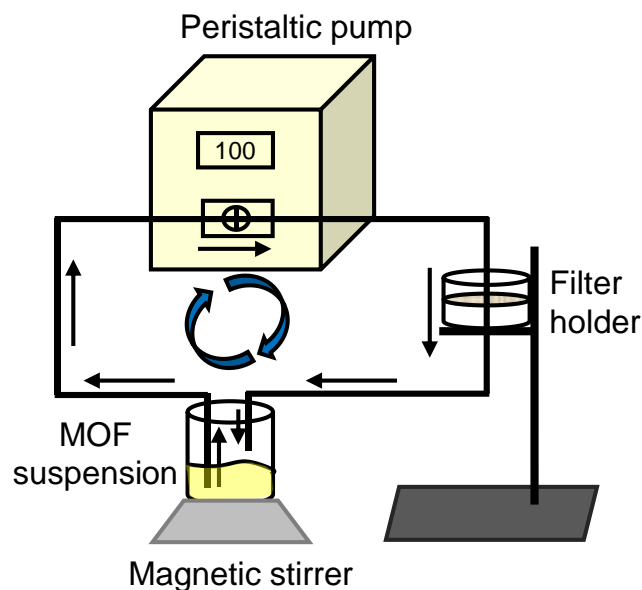


Figure 2. 1 The experimental setup to coat MOF particles onto charged filter media.

2.2.4 Characterization of MOF particles and E-MOFilters

To characterize the MOF particles, the scanning electron microscopy (SEM, HITACHI SU-70, HITACHI Corp., Tokyo, Japan), X-ray diffraction (XRD, PANalytical X'Pert Pro, Malvern PANalytical Ltd., Malvern, UK) and Fourier transform infrared spectroscopy (FT-IR, Nicolet iS50, Thermo Fisher Scientific, Waltham, MA) were utilized to probe the size, morphology, structure, and surface chemistry of the MOF particles, respectively. To measure Brunauer–Emmett–Teller (BET) surface areas of the MOF particles and E-MOFilters, N_2 adsorption/desorption isotherms was measured by a gas sorption analyzer (Autosorb iQ, Quantachrome Instruments Corp., Boynton Beach, FL). In addition to the surface area, the pore diameter distribution was obtained based on the density functional theory (DFT). The SEM analysis was also conducted for E-MOFilter to evaluate the coating uniformity of MOF particles.

2.2.5 Initial efficiency of E-MOFilters for PMs

After the characterization of MOF particles and E-MOFilters, E-MOFilters were evaluated for their PM and VOC removals. This study conducted the PM initial efficiency and PM aging tests first followed by the VOC removal efficiency and adsorption tests of the E-MOFilters. The tests with a reverse order were conducted to confirm the order would not cause many differences. If the two results are close to each other, the experimental data should be applicable to the real operating condition.

The initial PM removal efficiency of E-MOFilter was tested under 5 cm s^{-1} face velocity (commonly used in literature) using the same experimental method of our previous study (Tang et al., 2018a). In brief, atomization (Model 9302, TSI Inc., Shoreview, MN) and classification (Model 3082, TSI Inc., Shoreview, MN) were utilized to produce monodisperse NaCl particles with sizes of 20-700 nm. The classified monodisperse particles were firstly neutralized to reach Boltzmann distribution to minimize and mimic the particles present in the ambient condition before being introduced to challenge the E-MOFilters. The upstream, C_{up} , and downstream, C_{down} , particle concentrations (particle cm^{-3}) were measured by an ultrafine condensation particle counter (UCPC, Model 3776, TSI Inc., Shoreview, MN). Then the initial size-fractioned efficiency, $\eta \%$, can be determined as:

$$\eta \% = \left(1 - \frac{C_{down}}{C_{up}}\right) \times 100\% \quad (2.1)$$

For comparison, the initial efficiency of original and discharged (by IPA vapor) HEPA and MERV 13 electret media without coating MOF particles was also measured (Tang et al., 2018c). Because of the application of classification technique which produced monodisperse particles with low concentration, the loading effect was negligible and would not influence the tests of PM aging (Tien et al., 2020).

2.2.6 PM aging test

The PM aging tests were conducted for the MIL-125-NH₂ coated E-MOFilters only as will be shown later the MIL-125-NH₂ performed the best VOC removal amongst the three MOFs. Similarly, E-MOFilters with three coating levels together with the original electret media will be aged under 5 cm s⁻¹ by PMs with a close size distribution of ambient PM_{2.5} (Tang et al., 2018a, 2018b; Chang et al., 2019). The average number median diameter (NMD) and mass median diameter (MMD) of the NaCl particles used to challenge the E-MOFilter media were ~80 nm and ~500 nm, respectively. The aging tests were conducted under a relative humidity (RH) of ~30%, a relatively dry condition to simulate the worst condition of aging (Tien et al., 2020). The details of the experiments and method to determine the holding capacity, in terms of pressure drop growth versus mass load, can be found elsewhere (Tang et al., 2018a; 2018b).

2.2.7 Removal efficiency and adsorption capacity of toluene by E-MOFilters

The toluene (C₆H₅CH₃) as a common and representative harmful VOC in indoor air, was selected to challenge the E-MOFilters. The experimental setup was shown in Fig. 2.2, in which a gas chromatography (GC, Agilent 7890B, Agilent Technologies Inc., Santa Clara, CA) equipped with a flame ionization detector (FID, Agilent Technologies Inc., Santa Clara, CA) was adopted to measure the toluene concentration. In the GC-FID measurement, three minutes for each run and 30 seconds for each sampling was set. The line of the dummy holder was used to generate the calibration curve, from 0.05 to 50 ppm, for the toluene. Results showed that the relationship between the toluene concentration and peak area had a root square of 0.999.

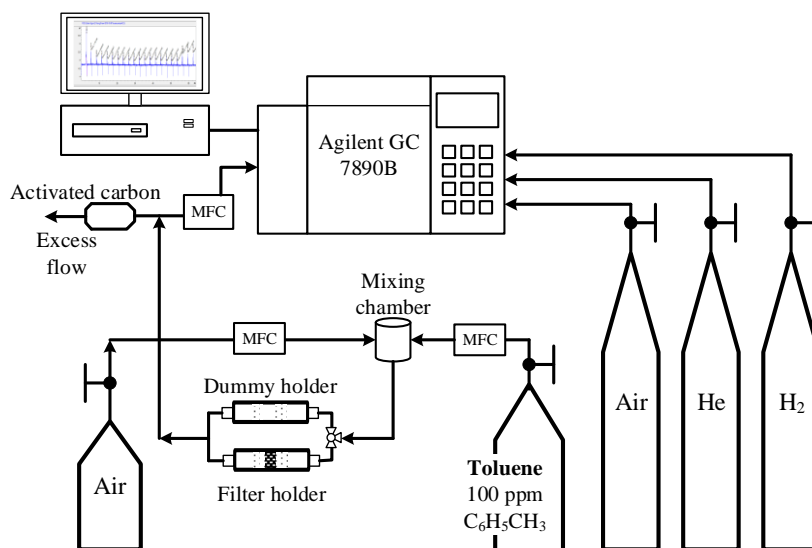


Figure 2. 2 Experimental setup for the initial removal efficiency and adsorption capacity of toluene by the E-MOFilters.

In this study, 5 ppm of toluene with the 5 cm s^{-1} of face velocity were applied for testing. When the measurement started, the toluene flow was introduced to the dummy line first to confirm if a correct toluene concentration was used. Then the flow was switched to the E-MOFilter line by the three-way valve. Usually, the third or fourth peak of the measurement shows the lowest peak area, i.e., the lowest toluene concentration. Thus, using Eq. (2.1), the initial removal efficiency of toluene, $\eta\%$, can be determined from the toluene concentration measured from the dummy line representing the upstream concentration of the E-MOFilter, C_{up} , and the lowest concentration from the E-MOFilter line, representing the downstream concentration, C_{down} . When the toluene flow continued passing the E-MOFilter line, the breakthrough curve, or the adsorption capacity, was determined. To obtain the representative results, measurements for each experimental condition in toluene and PM tests were repeated four times.

2.3 Results and Discussions

2.3.1 Characterization of MOF particles

Fig. 2.3 summarizes the characterization results of MIL-125-NH₂ particles, including SEM image, FT-IR spectrum, XRD patterns, and BET analysis for pore diameter, D_{pore} , distribution. The SEM image shown in Fig. 2.3 (a) reveals that the MIL-125-NH₂ crystals have a morphology of the tetragonal plate, which was in good agreement with that reported by Hu et al. (2014). The average length and thickness were found to be ~900 and ~300 nm, respectively, of the current MIL-125-NH₂ particles. The FT-IR spectrum shown in Fig. 2.3 (b) confirms that the produced MIL-125-NH₂ particles had the typical vibrational bands in the region of 1400–1700 cm⁻¹ representing the carboxylic acid functional group of the Ti-coordinated MOF structure. Besides, the peaks in the region of 400–800 cm⁻¹ indicated the Ti–O–Ti vibrations, and the bands for NH₂ groups were present at 3500 and 3380 cm⁻¹. The band at 1250 cm⁻¹ indicated the symmetric C–H stretching vibrations in the benzene ring. All these stretch vibrations match well with that reported in the literature (Kim et al., 2018). The XRD pattern of the synthesized MOF particles (Fig. 2.3 c) is in an excellent agreement with the simulated pattern, demonstrating the successful formation of the MIL-125-NH₂ structure. Fig. 2.3 (d) shows the N₂ adsorption/desorption isotherms of the synthesized MIL-125-NH₂ particles. As expected, the MOF particles exhibited type I adsorption isotherms at 77 K with no hysteresis, which verifies their microporous nature (Kim et al., 2018). The pore diameter distribution was obtained by the DFT method, and the results show that the dominating pore diameter was about 0.75 nm. This value was in good agreement with that reported by Kim et al. (2018), where two types of cages (octahedral with 12.5 Å and tetrahedral with 6 Å) that are accessible through microporous windows (5–7 Å) were found for the MIL-125-NH₂. The surface area of MIL-125-NH₂ was calculated to be 1871 m² g⁻¹ using the multiple layer BET

method which confirms the highly porous structure of the MIL-125-NH₂. The kinetic diameter of the toluene molecule is 5.85 Å (or 0.585 nm) (Jahandar Lashaki et al., 2012; Webster et al., 1998), which is expected to be easily captured by the MIL-125-NH₂ particles due to their high surface area and suitable pore diameter.

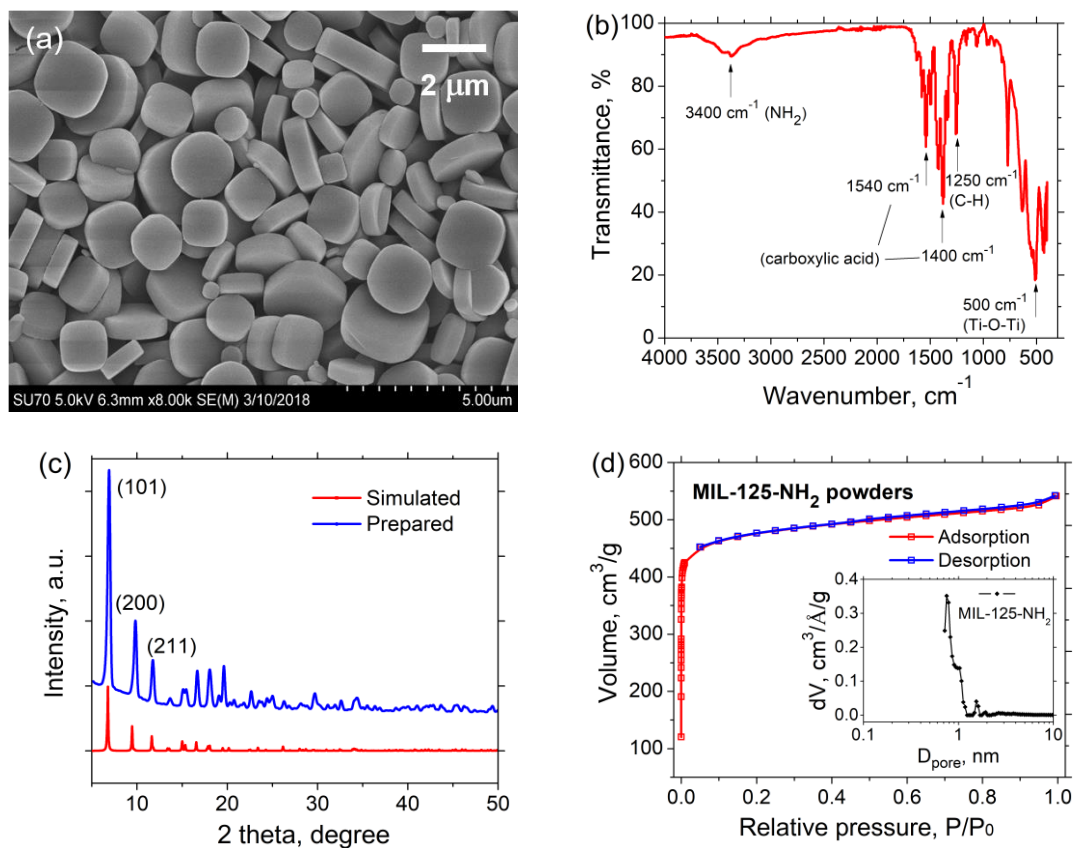


Figure 2. 3 SEM image of MIL-125-NH₂ (a), FT-IR spectrum of the MIL-125-NH₂ (b), XRD patterns of MIL-125-NH₂ (c), and BET analysis of pore diameter distribution of MIL-125-NH₂ (d).

Theoretically, there are two main mechanisms for the adsorption of toluene molecules by the MIL-125-NH₂ particles. Firstly, it is the pore filling mechanism due to diffusion and the forces between the adsorbents and adsorbates are Van de Waal force as a result of dipole interactions (Zhang et al., 2016; Vellingiri et al., 2017; Kim et al., 2018), which can be assigned to

physisorption process. The second one is due to the hydrogen bonding between the adsorbate (toluene) and adsorbent (MIL-125-NH₂), which can be assigned to the chemisorption process (Kim et al., 2018). According to the plausible pore filling adsorption mechanism, it is expected that the toluene molecules were easy to be trapped in the pore holes of MIL-125-NH₂ particles due to the matching sizes between the toluene and MIL-125-NH₂ particle cages. In the aspect of chemisorption, the hydrogen bonding between adsorbents and adsorbates that have ample H-donor moieties and H-acceptor moieties enhanced the capture of toluene (Seo et al., 2016; Wen et al., 2019). To be mentioned, to include ZIF-67 and UiO-66-NH₂ particles allows us to understand the effects of different pore diameters and ligands of different MOFs on toluene adsorption. The characterization results of ZIF-67 and UiO-66-NH₂ particles for SEM, FT-IR and XRD analysis (ZIF-67 only) were analyzed. The results confirm that the ZIF-67 and UiO-66-NH₂ particles were also successfully synthesized.

2.3.2 Characterization of different E-MOFilters

Figs. 2.4 (a) and (b) show the pore size distribution for the HEPA and MERV 13 based E-MOFilters coated with MIL-125-NH₂ particles (25 wt%). It was found the peak pore sizes of all E-MOFilters were smaller than that of ACFs and the total surface areas of E-MOFilters were close to that of ACFs. It is expected the toluene removal efficiency between E-MOFilters and ACFs are comparable. The detailed discussion will be presented in the following. Compared with the MIL-125-NH₂ particles (Fig. 2.3 d), the MIL-125-NH₂ coated E-MOFilters remained a similar peak pore diameter of ~0.8 nm. That is, the coated MIL-125-NH₂ particles contributed most of the microporous structures of the E-MOFilter, and a certain level of removal efficiency for toluene is expected. However, the pore volume for the pure MIL-125-NH₂ particles is much higher than that

of E-MOFilters.

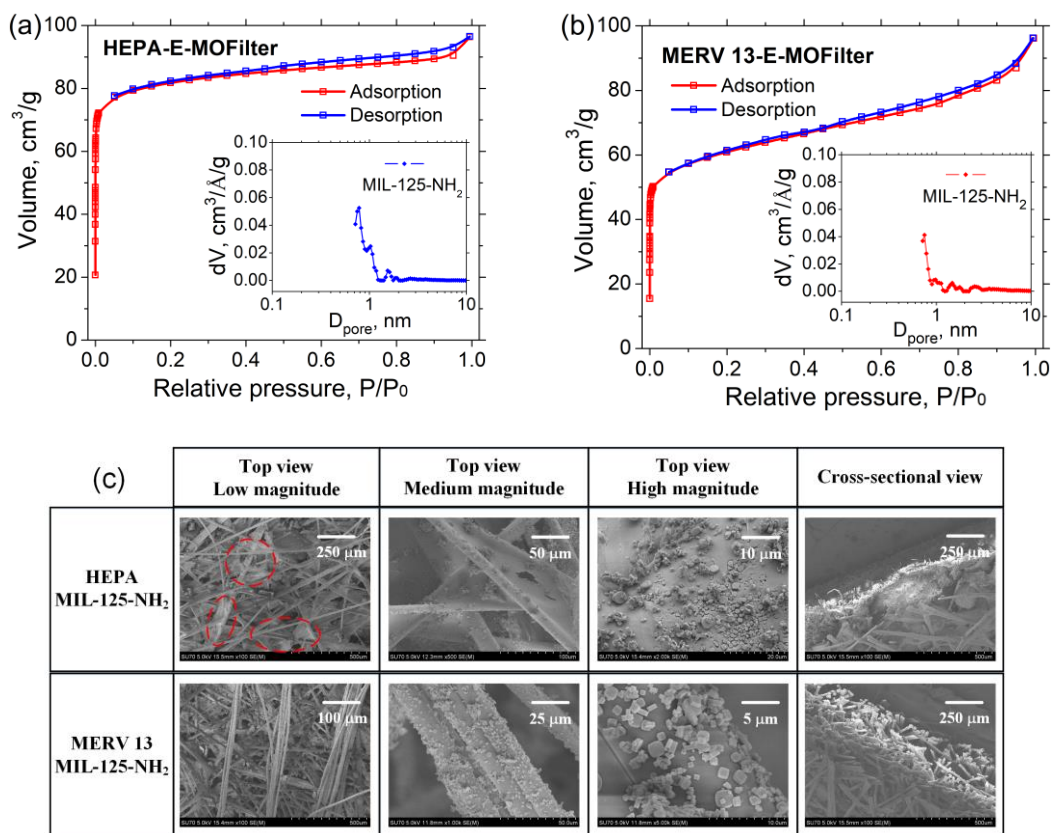


Figure 2. 4 BET analysis for the pore size distributions of MIL-125-NH₂ coated HEPA E-MOFilter (a) and MERV 13 E-MOFilter (b), and SEM images of MIL-125-NH₂ depositions on two E-MOFilters (c).

Under the high coating level of 25 wt%, Fig. 2.4 (c) shows the SEM images of the depositions for MIL-125-NH₂ particles in HEPA (first row) and MERV 13 (second row) based E-MOFilters. The cross-sectional views of the two E-MOFilters are shown in the last column of Fig. 2.4 (c). It is seen that the MOF particles were more uniformly deposited in MERV 13 based E-MOFilter, not only on individual fibers but also in depth (the cross-sectional view), than that of HEPA filter. In different magnitudes, from an overall view to the view with zoomed in of the filter media, it

was found the smaller pore sizes and higher packing density (fine fiber part) of HEPA filters caused the occurrence of bridging and clogging in many portions of the filter, highlighted with circles, especially at interstitial spaces between fibers. Similar results were found for the low- and medium-level coated HEPA based E-MOFilter as the media pore to MOF particle size ratio dominated the coating uniformity. In the coating of ZIF-67 particles, as its average size is close to that of MIL-125-NH₂ particles, a non-uniformity of coating is expected. However, the effects were minor when coating UiO-66-NH₂ particles to the HEPA media, which was due to their small sizes (~250 nm). Because of the small size of UiO-66-NH₂, this study found that they were not easy to be coated onto MERV 13 and a longer coating time is needed.

As will be shown later, the E-MOFilter coated with MIL-125-NH₂ particles had a better toluene removal efficiency than that of UiO-66-NH₂ and ZIF-67 particles, therefore, the results of MIL-125-NH₂ E-MOFilters will be focused and discussed in the following. To be concluded that from the coating experiments, without considering the adsorption ability amongst different MOFs, the ratio of the media pore size to MOF particle diameter is a crucial parameter determining if a uniform deposition can be achieved.

2.3.3 Initial efficiency of E-MOFilters (MIL-125-NH₂) for PMs

In order to investigate the effects of MOF coating on the performance of E-MOFilter against PMs, the size-fractioned efficiency of E-MOFilters was measured. Fig. 2.5 shows the results for the MIL-125-NH₂ coated MERV 13 (2 layers) E-MOFilters with different coating levels measured at 5 cm s⁻¹ face velocity. The original MERV 13 without MIL-125-NH₂ particles and the discharged MERV 13 by isopropyl alcohol (IPA) vapor were also tested to determine the efficiency decline due to charge degradation and remainder from the coating. The decline of PM

removal efficiency gets severer with increasing loading level due to charge shielding, nevertheless, the declines in all particle sizes were less than 10% for all three levels of coating. The E-MOF filter with a high-level MOF coating had a higher efficiency in the removal of larger particles than that with medium-level MOF coating, which should be attributed to loading effects. There were substantial efficiency differences between the E-MOF filters with that of discharged one, indicating a negligible efficiency degradation due to the coating. Although more MIL-125-NH₂ coating should enhance the capture of toluene, to compromise the decay of PM efficiency and the increase of pressure drop, and the decline of PM holding capacity (shown later), low or medium level of coating might be more desirable. A similar result with only minor efficiency decline was obtained for the HEPA E-MOF filters coated with high level of MIL-125-NH₂.

One question may be asked is that if the shedding of MOF particles can occur during the filtration of E-MOF filters. To address this issue, the MERV 13 E-MOF filters coated with all three levels of MIL-125-NH₂ were tested. In the experiments, E-MOF filters were blown with clean air at face velocities of 5 and 10 cm s⁻¹, the common filtration velocities, and a raised velocity of 30 cm s⁻¹ for challenging the stability of the current coating method. The air downstream of the filter was introduced to the UCPC which was operated with the accumulation counting mode. Ten times with one minute for each was run. Results of the particle shedding, in which the average values and standard deviations were rounded to the nearest integer. It is seen the shedding of particles does increase with increasing velocity and coating level. However, a quick calculation shows that there will be only ~0.001-0.01% of MOF particles released for the high coating E-MOF filter being operated at 30 cm s⁻¹ for 7/24 for a year. Therefore, the coating method presented here maintains the merits of electret media, including high efficiency and low pressure drop, and has a negligible shedding effect.

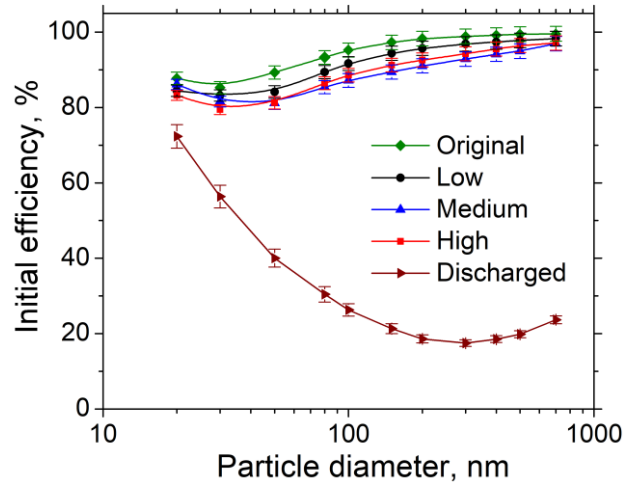


Figure 2. 5 Initial size-fractioned efficiency of MERV 13 E-MOFilter coated with different levels of MIL-125-NH₂ particles.

2.3.4 Performance of E-MOFilters on PM loading

For an IAC or HVAC filter, in addition to the initial efficiency, its performance over a period of operation, e.g., a few months, is of great concern. A commonly applied criterion is the PM holding capacity, i.e., the loaded PM mass versus the pressure drop growth which relates to the energy consumption in operating the filtration. Besides, as an electret media, its efficiency usually declines from the beginning of the operation, due to charge shielding, until loading effects occur and beat the decline. Therefore, this time-dependent and dynamic filter efficiency should also be considered as the second criterion. Since the focus of this study was to examine if the coating of MOF particles could deteriorate the performance of the electret media, only the two criteria about PM loading will be compared, as follows. The insights into PM loading characteristics for electret media, i.e., mechanisms of charge decay, transitions in the pressure drop growth curve, loading effects on efficiency enhancement, etc., can be found elsewhere (Tien et al., 2020), thus, will not be discussed here.

Fig. 2.6 compares the PM_{2.5} holding capacities of the clean MERV 13 and MERV 13 E-

MOFilters coated with different levels of MIL-125-NH₂ particles. The initial pressure drop of these filters are also shown in the figure and it was found the increase of initial pressure drops were very minor with only 1.5 and 3.7 Pa for the low and medium coated E-MOFilters, respectively. In comparison, the highly coated E-MOFilter gained a significant pressure drop (12.5 Pa). In the PM_{2.5} aging tests, the endpoint was set at 1.0 in-H₂O (249 Pa) and the more mass of PMs can be collected the better the filter is. As expected, the clean MERV 13 had the highest holding capacity (19.1 g m⁻²) and it was about 10, 25, and 50% higher than that of the low, medium, and high coating, respectively. It becomes clear that, in terms of deterioration of PM holding capacity, the E-MOFilters with low and medium coating should be acceptable, whereas, not for the high coating.

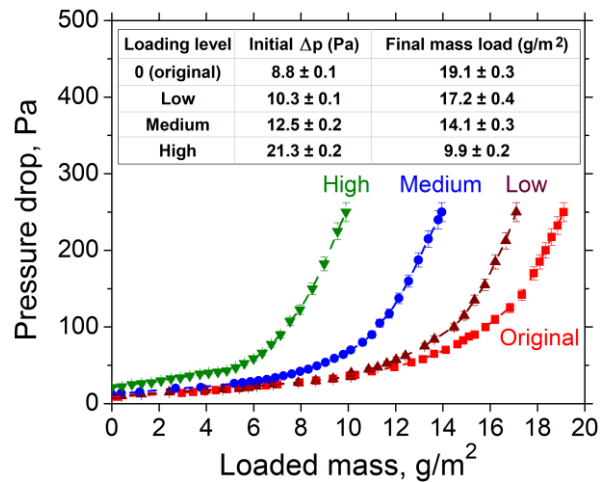


Figure 2. 6 Effects of the MOF loading on the evolution of pressure drop of the MERV 13 E-MOFilters during filtration.

Fig. 2.7 compares dynamic size-fractionated efficiency at different mass loads amongst original MERV 13 and E-MOFilters with the three coating levels (MIL-125-NH₂). The curves in each figure correspond to the efficiencies at initial (0 loading), minimum values (onset of efficiency increase for most particle sizes), pressure drop at 0.5 in-H₂O, and 1.0 in-H₂O (endpoint of aging),

respectively. The minimum efficiency is important as it represents the worst filtration condition in the use of electret-based filters (Tien et al., 2020). When the loading started, due to charge degradation the size-fractionated efficiency of these electret filters began declining (except for small particles in original and low coating level media) from their initial efficiency to the minimum efficiency, after which filter efficiency kept increasing because of loading effects (Li et al., 2020; Tien et al., 2020).

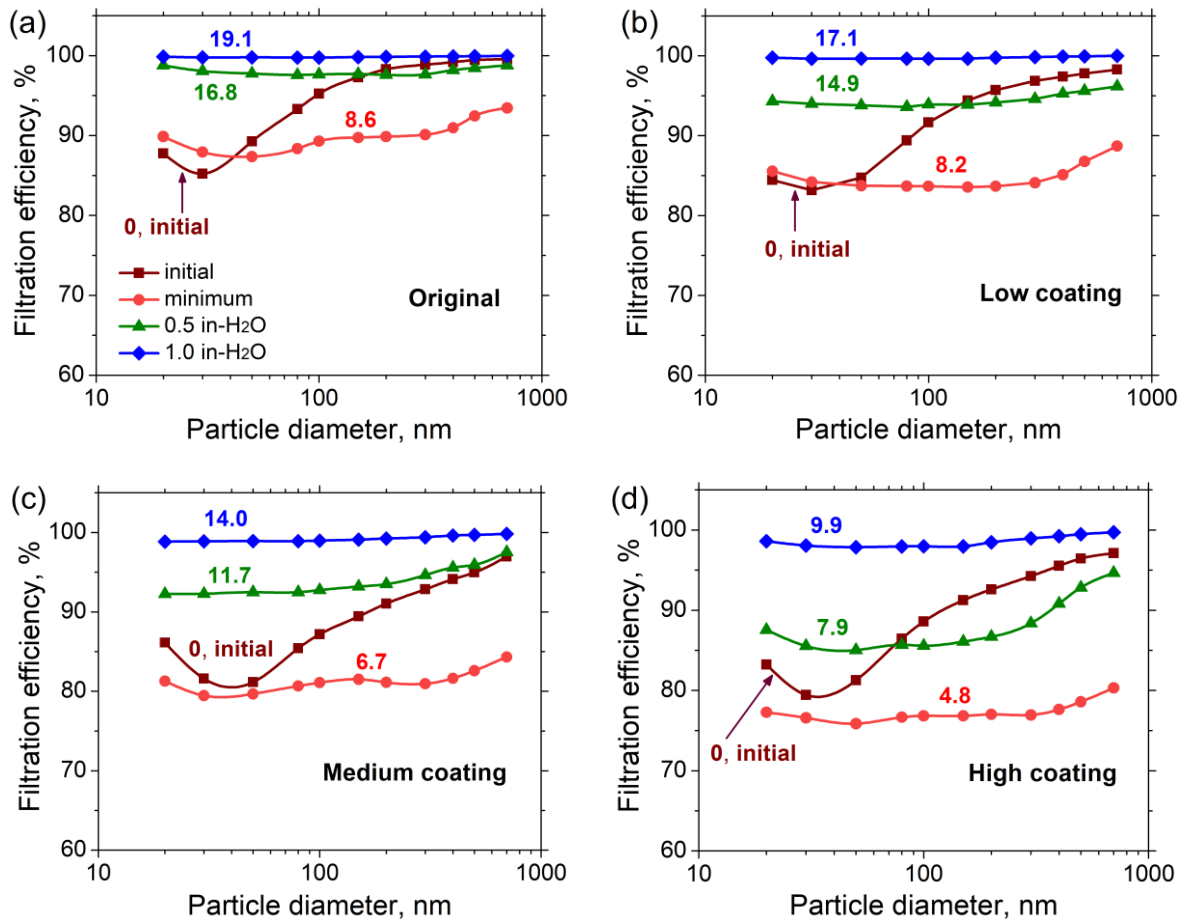


Figure 2. 7 Dynamic size-fractionated efficiency of original (a), low coating (b), medium coating (c), and high coating (d) MERV 13 filters along PM aging process.

The minimum efficiencies of low and medium coated E-MOFilters remain to be greater than 80%, whereas the minimum efficiency for the one with high MOF coating was found to be less

than 80%. To be highlighted, the small particles (< 50 nm) did not or almost had no efficiency reduction during the PM loading. This was because their deposition mechanism inherently relied mainly on diffusion rather than electrostatic force. From Fig. 2.7, it is seen the dynamic efficiency curves of E-MOFilters did differ quite much from the original MERV 13, nevertheless, the trend remained a very close characteristic as the original MERV 13. In summary, the test results for PM loading for E-MOFilters confirmed the current coating method, liquid filtration and from back to front, did not degrade the fiber charge too much or alter the fiber structure of electret media.

2.3.5 Performance of E-MOFilters for toluene removal

2.3.5.1 Initial removal efficiency

In the previous section, the performances of E-MOFilters for PM removal have been demonstrated to be comparable to that of the original electret filters, especially for the E-MOFilters with low and medium level coating. In this section, the removal of toluene by the E-MOFilters will be quantitatively compared amongst different base substrates, MERV 13 (1 or 2 layers) and HEPA, and different MOF particles and different levels of coating.

Fig. 2.8 (a) compares the initial toluene removal efficiency under 5 cm s^{-1} face velocity between the MERV 13 (1 layer) and HEPA (1 layer) E-MOFilters coated with high levels (25 wt%) of the three MOF particles. An order of $\text{MIL-125-NH}_2 > \text{UiO-66-NH}_2 > \text{ZIF-67}$ for the toluene removal efficiency was found for both MERV 13 and HEPA E-MOFilters. In comparison, the MERV 13 exhibited better performance than HEPA towards the toluene removal when coated with MOF particles. This was attributed to the uniformity of coating influenced by the ratio of media pore to MOF particle diameter as discussed in section 2.3.2. The ZIF-67 (29% with MERV 13) and UiO-66-NH₂ (44% with MERV 13) may not be qualified to be applied in the E-MOFilter

as their efficiencies were too low. While for MIL-125-NH₂, the efficiency was as good as 72%. This promising result should be highlighted because the method proposed within this study does prove not only the coating method retains the charge of electret media but also the coated MOF particles can remove toluene efficiently. From the above discussion, the HEPA, ZIF-67, and UiO-66-NH₂ could be excluded from the further tests in examining the effects of the coating level and using two layers of MERV 13 on toluene removal efficiency and adsorption capacity.

Fig. 2.8 (b) compares the toluene removal efficiency amongst 1 and 2 layers of MERV 13 E-MOFilters coated with three levels of MIL-125-NH₂ under 5 cm s⁻¹ face velocity. Reasonably, the efficiency increases with one additional layer of MERV 13 and coating level of MOF particles, however, not as large as expected. An average improvement of ~20% from 1 layer to 2 layers and ~8% from increasing coating level was obtained. To be mentioned, the 2-layer low coated E-MOFilter already had a decent efficiency of 74%. Besides, 2 layers of MERV 13 are required as it would enhance the PM removal efficiency and toluene adsorption capacity which will be shown later.

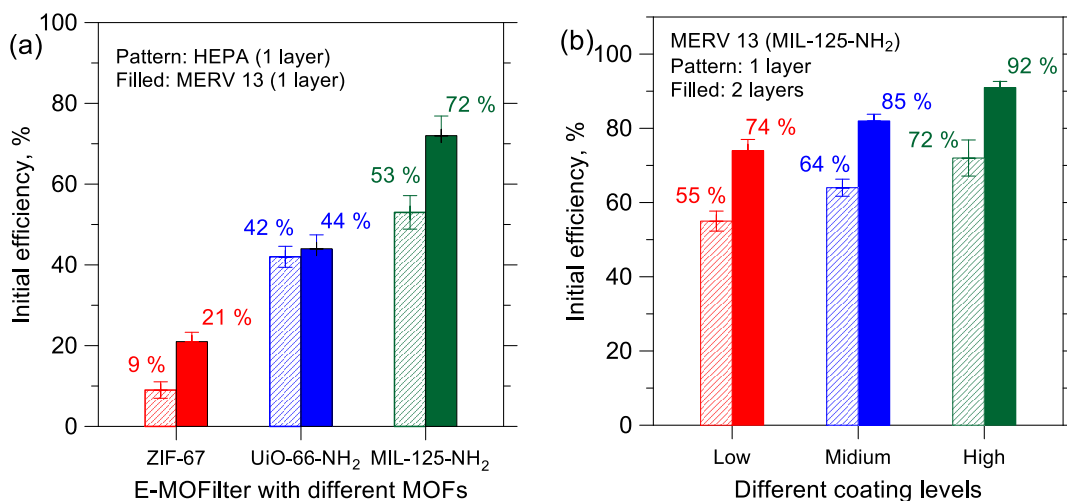


Figure 2. 8 Comparison of initial toluene removal efficiency between HEPA and MERV 13 based E-MOFilters coated with different MOF particles (25 wt% high level). (b) Comparison of initial

toluene removal efficiency by 1 and 2 layers of MERV 13 filter coated with different levels of MIL-125-NH₂ particles.

From the results of the initial toluene removal efficiency shown in Fig. 2.8, it becomes clear that the ratio of the filter pore size to MOF particle size is a crucial parameter for achieving a good coating and thus a good toluene removal. Besides, the amino functional group in ligand should also contribute to the toluene removal via chemisorption. Although HEPA filter has high initial efficiency, however, as has been reported in literature (Li et al., 2020; Tien et al., 2020), electret HEPA filter has a much lower holding capacity for PM, therefore, applying MERV 13 (two layers here) as the coating substrate is more desirable. Its larger pore size increases the flexibility to be the base substrate for coating many other MOF particles with different sizes, which may extend the applications for removing other gaseous pollutants.

2.3.5.2 Toluene adsorption capacity

Fig. 2.9 shows the toluene adsorption capacity, or breakthrough curve, of the 2-layer MERV 13 E-MOFilter coated with different levels of MIL-125-NH₂. The breakthrough curve for 2 ACF filters used in respirators for welding workers and the 1-layer E-MOFilter with high coating are also shown for comparison. It can be seen that the adsorption capacity increases substantially with increasing coating quantity. The two ACFs do have higher initial efficiency, ~90-95%, however, their adsorption capacity is only comparable with the low coating E-MOFilter, and worse than the medium and high coating E-MOFilters. The capacity of the 1-layer highly coated E-MOFileter is close to that of medium coated 2-layer E-MOFilter but lower than the 2-layer highly coated one, indicating the doubling of MOF particles does increase the toluene adsorption capacity. A rough calculation considering the area of the right triangle upper the breakthrough curve shows the

captured quantity of toluene is about double by the 2-layer E-MOFilter.

Fig. 2.9 also compares the adsorption capacity between the E-MOFilters evaluated for PM loading first (particle first) and toluene adsorption first (toluene first) to understand whether the treatment order would lead to different results. Results showed that the adsorption capacity for treating toluene first was only a little better than that of particle first, indicating loading of PM did not decay the toluene adsorption, thus, the current results are applicable for the real operation when particle and toluene filtrations are taking place simultaneously. Based on the decent results obtained, the newly developed method for the fabrication of E-MOFilter should be extended to the applications in making filter media for IAC, HVAC, and respirator filters. Although the 2-layer highly coated E-MOFilter had an outstanding performance towards the removal of toluene, an overall evaluation on the trade-off of gained pressure drop and charge degradation causing the decline of PM initial efficiency and PM holding capacity is needed. Both low and medium coated 2-layer MOFilter would be good choices for now before an optimized coating condition and better MOF particles are found.

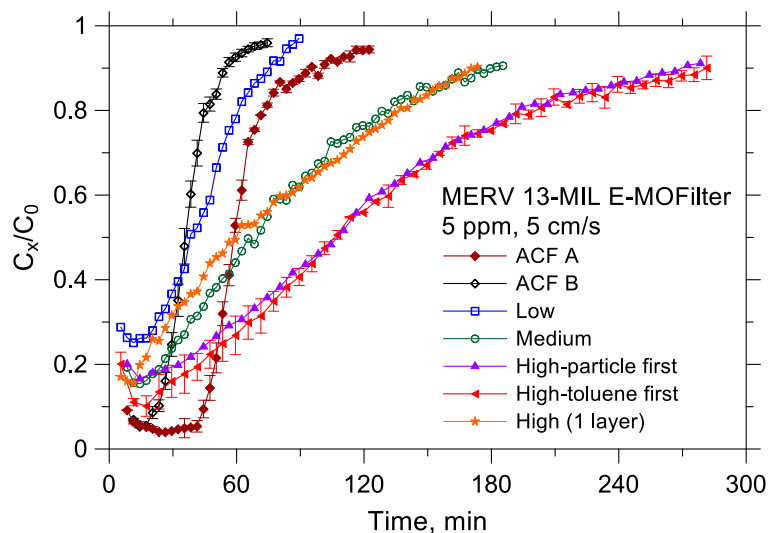


Figure 2. 9 Comparison of breakthrough curve amongst ACFs and MERV 13 based E-MOFilters coated with different levels of MIL-125-NH₂ particles.

2.4 Conclusions

Three MOF particles, including MIL-125-NH₂, UiO-66-NH₂ and ZIF 67, were synthesized, characterized, and coated to a MERV 13 and a HEPA grade electret filter media to form E-MOFilters for the simultaneous removal of fine particulate matters (PM_{2.5}) and volatile organic compounds (VOCs). As for the MOF coating, 5, 10 and 25 wt% were applied to figure out which level is the most appropriate, in terms of low increase of air resistance, low charge degradation, and sufficient VOC removal efficiency and adsorption capacity. A series of measurements were conducted to test the initial efficiency and holding/adsorption capacity of PM and toluene by the E-MOFilters.

The characterization results show that the MOF particles were successfully synthesized with similar morphology, size, surface area, pore diameter, FT-IR spectrum, and XRD patterns to those reported in the literature. The PM removal performances, in terms of initial efficiency, holding capacity, and dynamic efficiency, of the low and medium coated E-MOFilter were found to be

comparable to the original MERV 13. However, the highly coated one gained an essential air resistance and had a much lower PM holding capacity. The comparison of the time-dependent size-fractionated efficiency along the aging between E-MOFilter and original electret media shows that they have a similar trend of efficiency decline due to charge shielding and efficiency enhancement caused by loading effects. This indicates the coating method presented here does not significantly deteriorate the charge density and change the fibrous structure to a considerable extent.

The initial toluene removal efficiency of the MERV 13 E-MOFilters coated with MIL-125-NH₂ reaches 74% and 85% for the low and medium coating levels, respectively. It was found that the pore of filter media to MOF particle size is a crucial parameter for achieving a good coating and good toluene removal. Although HEPA filter had high initial efficiency, its lower holding capacity for PM and small pore size result in clogging during the MOF coating. Therefore, using MERV 13 as the coating substrate is more desirable. From the toluene adsorption capacity results, it is seen the newly developed MERV 13 E-MOFilter had a comparable capacity to that of two ACF media used in the respirators for welding workers. The low medium and high coating MOFilter predominated the ACFs. However, to consider the deterioration of the PM removal for the highly coated E-MOFilter, the parameters of the low and medium coated E-MOFilter may be more desirable to be applied in the designs of IAC, HVAC, and respirator filters.

Chapter 3. Mitigating the relative humidity effects on the simultaneous removal of VOCs and PM_{2.5} of a metal–organic framework coated electret filter

Separation and Purification Technology. 285 (2022): 120309.

<https://doi.org/10.1016/j.seppur.2021.120309>

Reproduced by permission of The Elsevier

Abstract:

An electret filter media coated with highly porous metal-organic framework (MOF, i.e., MIL-125-NH₂ in this work) particles, called E-MOFilter, has been developed to remove fine particulate matters (PM_{2.5}, particulate matter less than 2.5 micrometers in diameter) and volatile organic compounds (VOCs, e.g., toluene) simultaneously. However, its adsorption efficiency and capacity of toluene deteriorated at an elevated relative humidity (RH). This was due to the hydrophilic nature of MIL-125-NH₂ leading to competitive adsorption between toluene and water molecules. To address this issue, five modification methods were conducted to alter MIL-125-NH₂ from inherent hydrophilic into hydrophobic, which included the internal (alkylation method), external (coating with polydimethylsiloxane, PDMS), combined (alkylation plus PDMS coating), polyvinylpyrrolidone (PVP) surfactant, and N-coordination modifications. The new E-MOFilters were fabricated based on these modified MIL-125-NH₂ and then systematically compared for their toluene adsorption efficiency and capacity under various RH levels (from 10, 30, 40, 50 to 60%). In addition to toluene, the PM removal efficiency and PM_{2.5} holding capacity by the modified E-MOFilters were also evaluated. The toluene adsorption results revealed the PDMS-coated E-MOFilter outperformed all other modifications. The PM removal ability were retained for all modified E-MOFilters indicating the charge and structure of the electret media were not altered. This study is the first to combine the MOFs with electret filter media for a low pressure drop and simultaneous removal of PM and toluene under different RHs. The effectiveness and performance towards toluene adsorption under elevated RH conditions for E-MOFilters with various modifications were comprehensively evaluated and discussed.

3.1 Introduction

Indoor air quality (IAQ) has been becoming a major concern worldwide because statistical data showed that the indoor concentrations of gas pollutants, e.g., volatile organic compounds (VOCs) and particulate matters (PMs) are often 2-5 times higher than that of outdoors (Gustafson et al., 2008). Especially, people spend 87% of their time indoors and increasing to more than 90% during COVID-19 pandemic (Brasche and Bischof, 2005; Klepeis et al., 2001). The high concentration of these indoor air pollutants is mainly due to the reduced air change rate for the design of energy-efficient building construction and the increased usage of furnishings, glues, paints, furnaces, etc., leading to outgassing and particle emission. Prolonged exposure to these pollutants can cause acute and chronic effects on respiratory and central nervous system (Chen et al., 2019; Du and Wang, 2020; Pui et al., 2014; Sarigiannis et al., 2011). Therefore, it is urgent to effectively remove PMs and VOCs to increase the indoor air quality.

To mitigate indoor PMs, electret filters, with quasi-permanent electrical charges on the fibers have been widely used in the heating, ventilation, and air conditioning (HVAC) systems and indoor air purifiers, which show a high initial PMs filtration efficiency and a much lower pressure drop (ΔP) compared to the mechanical filters (Tang et al., 2018b). To remove VOCs, gas adsorbents, e.g., activated carbon (AC) and zeolites, are usually used because of their high efficiency and relatively low price. However, low selectivity and weak affinity to polar pollutants of these adsorbents are of a great concern (DeCoste and Peterson, 2014; Zheng et al., 2020). In addition to these common adsorbents, the metal-organic frameworks (MOFs), a type of novel porous materials, have been receiving increased attention due to their large surface area, tailorable particle size and tunable functionality, making them promising candidates for capturing gaseous pollutants (Furukawa et al., 2013; Scott Bobbitt et al., 2017). To simultaneously remove PMs and VOCs, the

MIL-125-NH₂ MOF was synthesized and successfully integrated into a commercially available electret filter with a minimum efficiency reporting value of 13 (MERV 13), named E-MOFilter (Zhang et al., 2021). This E-MOFilter demonstrated a low pressure drop (< 15 Pa at 5 cm s⁻¹ face velocity) and a high removal efficiency (~90%) for both PMs and toluene (C₆H₅CH₃) under a relative humidity (RH) less than 30%. However, the adsorption efficiency of toluene reduces with increasing RH levels (Zhang et al., 2012; Zhang et al., 2019; Li et al., 2020; Zheng et al., 2020). This RH effect on VOC adsorption degradation is commonly seen in many traditional adsorbents, including AC and zeolites (Zhu et al., 2020). Because under high RH conditions the adsorption sites of the adsorbents are competitively occupied by the water molecules. This adverse RH effect is more significant for hydrophilic adsorbents, such as MIL-125-NH₂ where the adsorption sites have stronger affinity to water molecules than the less polar VOC molecules (Zhu et al., 2017). To address this issue, researchers often modified the adsorbents to increase their hydrophobicity to repel water molecules (Isaka et al., 2019; Kawase et al., 2019; Kim et al., 2012; Liu et al., 2016; Nguyen and Cohen, 2010; Sun et al., 2017; W. Zhang et al., 2014; Zheng et al., 2020). The water contact angle (WCA) tests are usually conducted to evaluate the hydrophobicity of the adsorbents. Typically, a WCA less than 90°, within 90°-150° and larger than 150° is considered to be hydrophilic, hydrophobic, and superhydrophobic, respectively (Nguyen and Cohen, 2010)

The modifications can be categorized into three major methods, including internal, external and others. Internal modifications usually involve the reactions of ligand or metal cluster functionalization at the molecular level (Kawase et al., 2019). External modification is completely different, where a layer of hydrophobic materials is coated on the surface of adsorbents (Kim et al., 2012). Other modifications mainly involve adding surfactants or nitrogenous compounds into the solution during MOFs synthesis (Hu et al., 2018; Zhang et al., 2019). Basically, there exists an

inherent tradeoff between the increase of hydrophobicity of MOFs for the water resistance and a reduction of surface area of MOFs due to the modification. Thus, it is important to conduct these modifications systematically to find the optimal condition and to compare their effectiveness on minimizing the RH effects.

In this study, the MIL-125-NH₂ MOF was synthesized and modified to increase its hydrophobicity in order to mitigate the adverse effects of RH on the removal efficiency towards toluene, a representative indoor VOC. Several modification methods, i.e., internal (alkylation method), external (PDMS-coating method), combined (alkylation plus PDMS-coating method), and other modifications (PVP and N-coordination methods) were conducted. The modified MIL-125-NH₂ MOFs were then transported to MERV13 electret filter media to form modified E-MOFilters. Systematic evaluations on the toluene removal efficiency by the original and modified E-MOFilters under different RHs (10-60%) were conducted. This study aims to compare and report the effectiveness of different modifications on mitigating the RH effects for both initial removal efficiency and adsorption capacity of toluene. As a simultaneous gas-particle removal filter, the modified E-MOFilters were also examined for their PM removal efficiency and PM_{2.5} (particulate matter less than 2.5 micrometers in diameter) holding capacity to confirm the modifications would not cause any degradation for PM removal performances. The ultimate goal of this study is to demonstrate the modified E-MOFilters not only have a high PMs filtration performance, but also an enhanced efficiency and adsorption capacity for toluene under elevated RH conditions.

3.2 Materials and Methods

3.2.1 Modification of MOF MIL-125-NH₂ particles

MIL-125-NH₂ was synthesized according to our previous report (Zhang et al., 2021). Then, the original MOFs MIL-125-NH₂ were undertaken alkylation, PDMS, surfactant and N-coordination modifications to obtain the modified MOFs.

For the alkylation modification, the MIL-125-NH₂ was grafted with long alkyl chains to yield MIL-125-R7 by following the procedures published elsewhere (Isaka et al., 2019). Briefly, the prepared MIL-125-NH₂ (49 mg) was activated at 200 °C for 2 h in air before further modification. Then the MOF was dispersed in 5.0 mL of acetonitrile, to which 40 equivalent of n-octanoic anhydride was then added. The suspension was stirred for 24 h at 80 °C. The final product was washed by CH₂Cl₂ three times.

In the PDMS coating method, a fresh PDMS stamp was placed inside a 100 mm glass petri dish on the top with MIL-125-NH₂ particles uniformly spread on the bottom. The above glass petri dish containing both PDMS and MIL-125-NH₂ was sealed and kept in the oven at 235 °C for 6 hours and then cooled down to room temperature (Yuan et al., 2008). The obtained products are named PDMS@MIL-125-NH₂ and PDMS@MIL-125-R7 (combination of internal and external modification). It should be noted that the mass ratios of PDMS stamps to MOF particles were set from 3:1 to 400:1, for different coating amounts of PDMS on MOFs. The Energy Dispersive X-Ray (EDX, HITACHI SU-70, HITACHI Corp., Tokyo, Japan) analysis was conducted to determine the atomic ratio of Si and Ti and quantify the PDMS coated on the MOFs.

The PVP surfactant modification (MIL-125-NH₂/PVP) and N-coordination method (MIL-125-NH₂/N_x) were conducted according to Zhang et al. (2020) and Hu et al. (2018), respectively.

Noteworthy, in addition to MIL-125-NH₂, the inherent hydrophobic MOF ZIF-8 was also synthesized for comparison (Jafari et al., 2018).

3.2.2 Electret filter media and modified E-MOFilter

The 50 mm diameter flat sheets of the MERV 13 electret filter media were used for the deposition of modified (hydrophobicity) MOF particles to form modified E-MOFilter for the PM_{2.5} and toluene removal tests. The experimental setup and parameters for the MOF coating onto electret filter media can be found in our previous work (Zhang et al., 2021). The coating level of differently modified MOFs was controlled at 10 wt% (MOFs/media). Two layers of MERV 13 flat sheet were used to enhance the removal efficiency of both PM_{2.5} and toluene. In total, there were seven kinds of E-MOFilters fabricated and tested, which were coated with MIL-125-NH₂, MIL-125-R7, PDMS@MIL-125-NH₂, PDMS@MIL-125-R7, MIL-125-NH₂/PVP, MIL-125-NH₂/N_x and ZIF-8 MOFs.

3.2.3 Characterization of MOF particles and E-MOFilters

The scanning electron microscopy (SEM, HITACHI SU-70, HITACHI Corp., Tokyo, Japan), x-ray diffraction (XRD, PANalytical X'Pert Pro, Malvern PANalytical Ltd., Malvern, UK) and fourier transform infrared spectroscopy (FT-IR, Nicolet iS50, Thermo Fisher Scientific, Waltham, MA), optical contact angle goniometer (OCA 15 goniometer, DataPhysics Instruments Corp., Charlotte, NC) were utilized to characterize the size and morphology, crystal structure, surface chemistry and WCA, respectively, of the modified MOF particles. The energy dispersive x-ray (EDX, HITACHI SU-70, HITACHI Corp., Tokyo, Japan) analysis were conducted to determine the atomic ratio of Si and Ti to confirm the quantity of PDMS coated on the MOFs. Besides,

nitrogen adsorption-desorption isotherms were collected using a gas sorption analyzer (Autosorb iQ, Quantachrome Instruments Corp., Boynton Beach, FL) at 77 K to characterize the pore size distribution and Brunauer-Emmett-Teller (BET) surface area. The SEM analysis was also conducted for the modified E-MOFilters to evaluate if the MOF particles were coated uniformly on the filters.

3.2.4 Initial efficiency and holding capacity of modified E-MOFilters for PMs

After the characterization of the modified MOFs and E-MOFilters, the E-MOFilters were evaluated for their performance of PM and VOC removal under different test conditions. Table S3 of SI C. (Test conditions for the modified E-MOFilters against PM and VOC) summarizes the test conditions for the E-MOFilters against PM and VOC. Basically, the filtration face velocity for the PM tests was 5 cm s^{-1} . As demonstrated in our previous work (Zhang et al., 2021), the order of the PM filtration and VOCs removal tests would not cause different results. Therefore, this study conducted the PM initial efficiency and PM aging (size distribution close to ambient $\text{PM}_{2.5}$) tests first followed by the VOC removal and adsorption tests. The details of experiments for conducting PM removal performance tests and methods to determine the PM initial removal efficiency and holding capacity of E-MOFilters can be found elsewhere (Tang et al., 2018a; 2018b).

3.2.5 RH effects on the initial efficiency and adsorption capacity of the E-MOFilter for toluene

Toluene, a common and representative harmful indoor VOC, was selected to challenge the E-MOFilters. Fig. 3.1 shows the experimental setup for investigating the RH effects on the toluene adsorption of the E-MOFilter. Different RHs were controlled by adjusting the flow rates of the

compressed air (~5% RH) and the water mists generated by the single jet atomizer (Model 9302, TSI Inc., Shoreview, MN). The toluene removal efficiency at 10% RH was first measured and the results were treated as dry condition and the baseline for examining the efficiency degradation at elevated RH values. The RH was raised to 30, 40, 50 and 60% and then followed by the efficiency measurement. Two face velocities, 0.5 and 5 cm s⁻¹, were applied to investigate their toluene removal efficiency. 5 cm s⁻¹ is commonly used in an HVAC application (velocity in pleated media) and 0.5 cm s⁻¹, a fairly low face velocity, is to simulate the relatively static flow condition that was often seen in the literature (Zheng et al., 2021). The toluene with 5 ppm concentration was prepared by adjusting the air and toluene flow rates via the mass flow controller (MFC, MKS Instruments Inc., Andover, MA) and confirmed by a gas chromatography (GC, Agilent 7890B, Agilent Technologies Inc., Santa Clara, CA) equipped with a flame ionization detector (FID, Agilent Technologies Inc., Santa Clara, CA) to challenge the E-MOFilters. The toluene removal efficiency, $\eta\%$, was calculated from the measured upstream (C_{up} , through the dummy holder) and downstream (C_{down} , through the filter holder) toluene concentration of the E-MOFilter as:

$$\eta \% = \left(1 - \frac{C_{down}}{C_{up}}\right) \times 100\% \quad (3.1)$$

When the toluene flow continued passing the E-MOFilter, the breakthrough curve, or the adsorption capacity, was determined. To obtain the representative results, measurements for both toluene and PM removal efficiency were repeated at least four times.

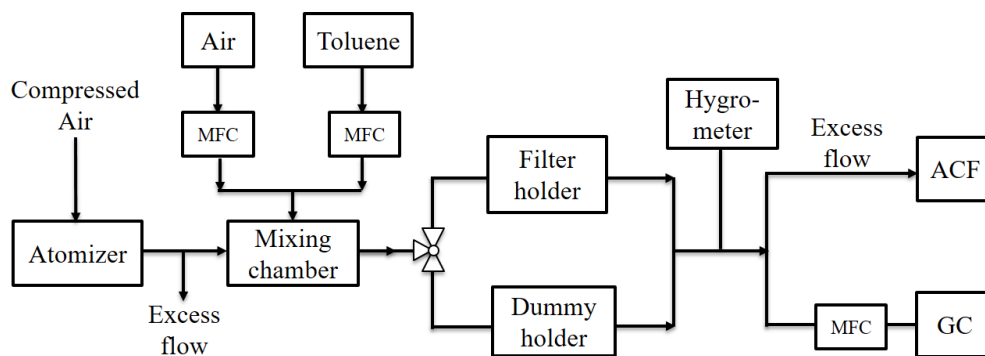


Figure 3. 1 Experimental setup for the initial removal efficiency and adsorption capacity of toluene by the E-MOFilters under different RHs.

3.3. Results and Discussion

3.3.1 Characterization of MOF particles

Fig. 3.2 summarizes the SEM images, XRD patterns, N₂ adsorption isotherms and FT-IR spectra for both original and modified MIL-125-NH₂ MOF particles. Fig. 3.2 (a)-(d) show the SEM images and WCAs of original MIL-125-NH₂, MIL-125-R7 (alkylated MIL-125-NH₂), PDMS@MIL-125-NH₂ (PDMS-coated MIL-125-NH₂), and PDMS@MIL-125-R7 (alkylated and PDMS-coated MIL-125-NH₂) MOFs, respectively. The modified MIL-125-NH₂ particles have an almost identical tetragonal plate morphology as the original MOFs (Kim et al., 2018a; Kim et al., 2013). Besides, the WCAs were found to be 0°, 131.5°, 155.5° and 151.5° for the four MOFs, respectively. According to the WCA results, the original MIL-125-NH₂ MOF was hydrophilic, and the PDMS-coated samples showed the best hydrophobicity amongst all modified MOFs, which should be a desired modification method for the current MIL-125-NH₂ as it was relatively simple and straightforward.

The mass ratio of PDMS to MIL-125-NH₂ was evaluated by determining the atomic ratios of Si/Ti using EDX, where Si and Ti were from PDMS and MIL-125-NH₂, respectively. The atomic ratios of Si/Ti were from 0.1 to 1.23, corresponding to the counterpart mass ratio of PDMS to MOF particles as desired. With various amounts of PDMS coating, the PDMS@MIL-125-NH₂ with a Si/Ti ratio of 0.43 and PDMS@MIL-125-R7 with a Si/Ti ratio of 0.22 showed the best toluene removal efficiency as compared to other ratios.

The XRD patterns of original MIL-125-NH₂, MIL-125-R7, PDMS@MIL-125-NH₂ and PDMS@MIL-125-R7 are shown in Fig. 3.2 (e). In Fig. 3.2 (e), it is seen the alkylated and PDMS-treated MOFs maintained their original crystal structures of MIL-125-NH₂. Similar results were also seen in the analysis of other modified MOFs. It is concluded here that the crystal structure remained unchanged after the modification.

The FT-IR spectra shown in Fig. 3.2 (f) confirms that the major functional groups of modified MIL-125-NH₂ remained unchanged from the original MIL-125-NH₂ but some new peaks appeared. For MIL-125-R7, a new small peak at 3400-3500 cm⁻¹ ascribed to the symmetric stretching vibration of the amino group disappeared after MIL-125-NH₂ was post-treated with n-octanoic anhydrides, indicating that the N-H band was replaced by other functional groups. A new small peak appeared at 1690 cm⁻¹ due to the C=O stretching vibrations of the amide group (Zheng et al., 2020), confirming the reaction between the amino group and anhydrides. For PDMS@MIL-125-NH₂, the appearing of peak at 1020–1074 cm⁻¹ was assigned to the stretching mode of Si-O-Si bond (Bodas et al., 2006), which can be a confirmation of a PDMS film coated on the external surface MOFs. To be noted, the Si/Ti here is 0.43, which is a relatively high ratio and thus the vibrations of Si-O-Si can be observed clearly. In comparison, there was a lower Si/Ti (0.22) for PDMS@MIL-125-R7, thus the absence of a peak appearing at 1690 cm⁻¹ should be attributed to

the low Si/Ti. This result was in agreement with that found by Zheng et al. (2020), where no peak was seen at Si/Al=0.2.

Fig. 3.2 (g) shows the N₂ adsorption/desorption isotherms of MIL-125-NH₂ and modified MIL-125-NH₂ MOFs. As expected, both original MIL-125-NH₂ and the modified MOFs exhibited type I adsorption isotherms at 77 K with no obvious hysteresis, which verified their microporous structure (Kim et al., 2013). The BET specific surface area (SSA) and micropore volume of all modified MIL-125-NH₂ MOFs are summarized in Table 3.1. The SSA had an order of MIL-125-NH₂ > PDMS@MIL-125-NH₂ > MIL-125-R7 > PDMS@MIL-125-R7, which illustrated that PDMS@MIL-125-NH₂ has the largest SSA and micropore volume amongst the modified MOF. In addition, the results also indicated that both internal and external surface modification reduced the SSA and pore volume of MIL-125-NH₂ to some extent. That was because the pores were partially occupied by the long alkyl chains for the MIL-125-R7 (Isaka et al., 2019) and PDMS would cover some of pores of MOFs, and the more PDMS coating there were lower SSA. For PDMS@MIL-125-R7, two factors as aforementioned, i.e., alkyl groups blockage and PDMS-coating, synergistically led to a significant decrease of its SSA and micropore volume. Therefore, based on the analysis above, it is of great importance to find out an optimal Si/Ti to not only enhance the hydrophobicity of PDMS-coated MOFs but also retain the toluene adsorption performance under humid conditions. In addition to SSA and micropore volume, the peak pore size of the PDMS@-MIL-125-NH₂ were found to be 0.75 nm independent on Ti/Si. This value was in good agreement with that reported by Kim et al. (2018). The kinetic diameter of the toluene molecule is 5.85 Å (or 0.585 nm) (Jahandar Lashaki et al., 2012; Webster et al., 1998; Y. Zhang et al., 2014), which is expected to be easily captured by the PDMS@-MIL-125-NH₂ particles due to their suitable pore to molecule diameter ratio.

Table 3. 1 BET analysis of original and modified MOF powders and E-MOFilters.

	Adsorbents	BET surface area (m ² /g)	Total /Micro pore volume (cm ³ /g)	Pore diameter (nm)
Original and modified MOF powder	MIL-125-NH ₂	1871	0.837/0.667	0.78
	MIL-125-R7	771	0.379/0.223	0.72
	PDMS@MIL-125-NH ₂	1417	0.726/0.463	0.78
	PDMS@MIL-125-R7	561	0.263/0.155	0.72
	MIL-125-NH ₂ /PVP	1580	0.744/0.544	0.75
	MIL-125- NH ₂ /N _x	1388	0.673/0.468	0.75
	ZIF-8	1357	0.735/0.627	1.08
Original and modified E-MOFilter	MIL-125-NH ₂	320	0.149/0.114	0.78
	MIL-125-R7	206	0.089/0.073	0.72
	PDMS@MIL-125-NH ₂	301	0.135/0.105	0.78
	PDMS@MIL-125-R7	181	0.071/0.063	0.72

According to the results of WCA and BET analysis, the WCAs of PDMS coated MOFs remained ~ 150° without strong correlation of PDMS coating amount in the ranges of 0.1-1.23 of Si/Ti. However, SSA and micropore volume of PDMS coated MOFs exhibited a significant reduction with increasing PDMS coating. In this study, it is found that both PDMS@MIL-125-NH₂ (Si/Ti=0.43) and PDMS@MIL-125-R7 (Si/Ti=0.22) had better humidity resistance and remained acceptable SSA area and micropore volume. The lower PDMS coating for the latter was to compensate for its already reduced SSA due to alkylation.

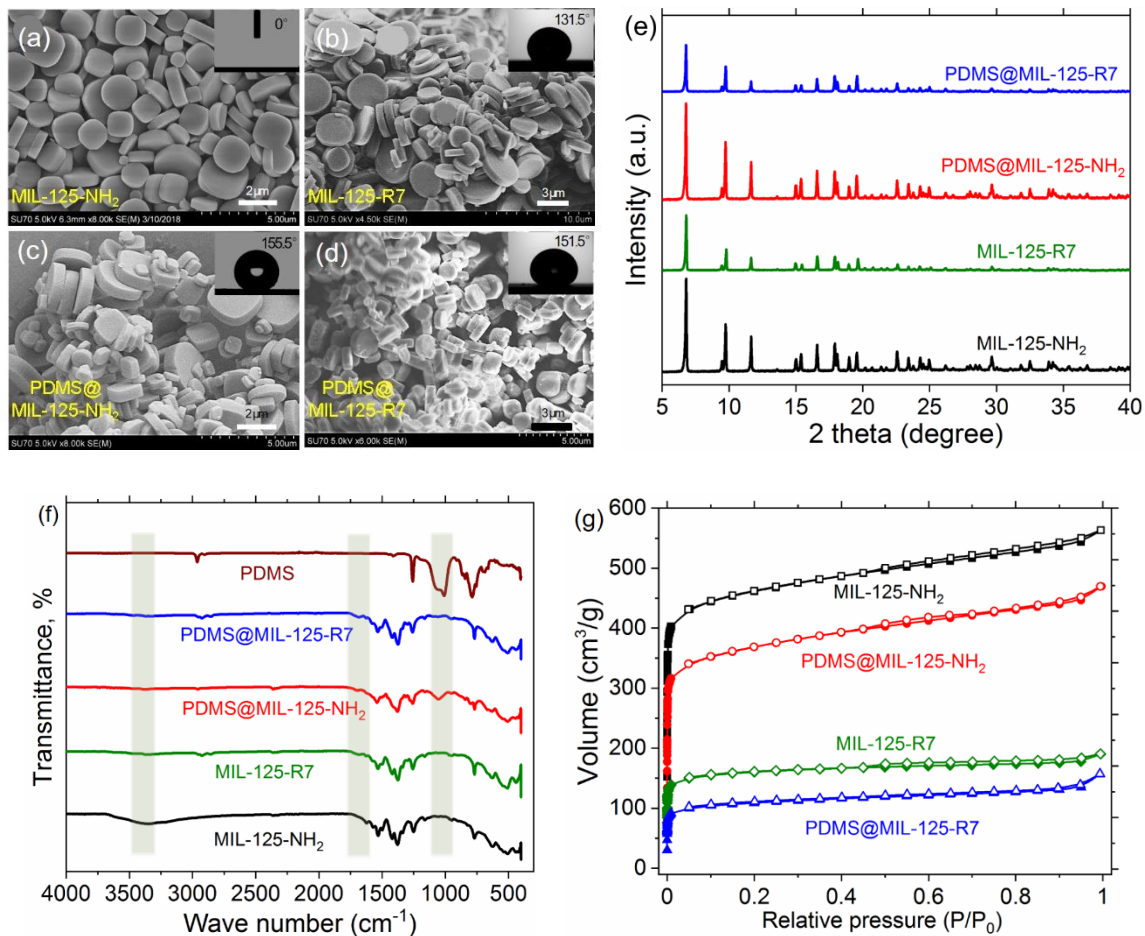


Figure 3. 2 Comparison of SEM images and WCAs (a: MIL-125-NH₂, b: MIL-125-R7, c: PDMS@MIL-125-NH₂, d: PDMS@MIL-125-R7), XRD patterns (e), FT-IR spectra (f) N₂ adsorption isotherms (g) between original and modified MIL-125-NH₂.

3.3.2 Characterization of modified E-MOFilters

The modified MIL-125-NH₂ MOFs were transported to MERV13 electret filter media to fabricate modified E-MOFilters. Fig. 3.3 (a) shows the SEM images of the depositions of modified MIL-125-NH₂ particles on the fibers of MERV13 electret filter. It is seen that the modified MOF particles were uniformly deposited on individual fibers and in-depth of the E-MOFilter, which

again illustrated that the liquid filtration coating method was feasible and effective in practice (Zhang et al., 2021).

Fig. 3.3 (b) shows N_2 adsorption/desorption isotherms for the original and modified E-MOFilter. Table 1 summarizes the results of BET analysis, including SSA, pore volume, and peak pore diameter for the original and modified E-MOFilters. Compared with the MIL-125-NH₂ particles (1871 m² g⁻¹), the original E-MOFilter already had a significant SSA reduction to 320 m² g⁻¹. Nevertheless, this SSA is still higher than activated carbon fiber respirators used to protect welding workers. The PDMS@MIL-125-NH₂ coated E-MOFilters have a similar SSA value compared to the original E-MOFilter. However, MIL-125-R7 and PDMS@MIL-125-R7 E-MOFilters had a SSA of only 206 and 181 m² g⁻¹, respectively. Nevertheless, they all maintain a peak pore diameter of ~0.75 nm. This is because the MIL-125-NH₂ particles rather than the coated polymers contributed most of the microporous structures of the E-MOFilters. From above BET and SEMs results, it is expected that the modified E-MOFilters would be capable of capturing toluene under different humidity due to their remained microporous structures, successful in-depth hydrophobic MOF particles coating and acceptable SSA.

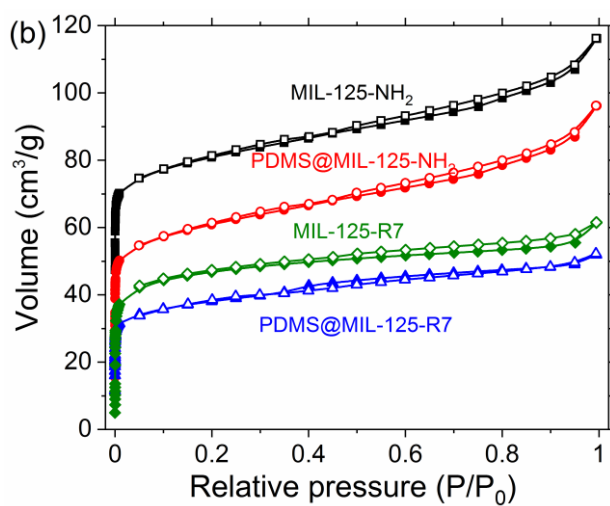
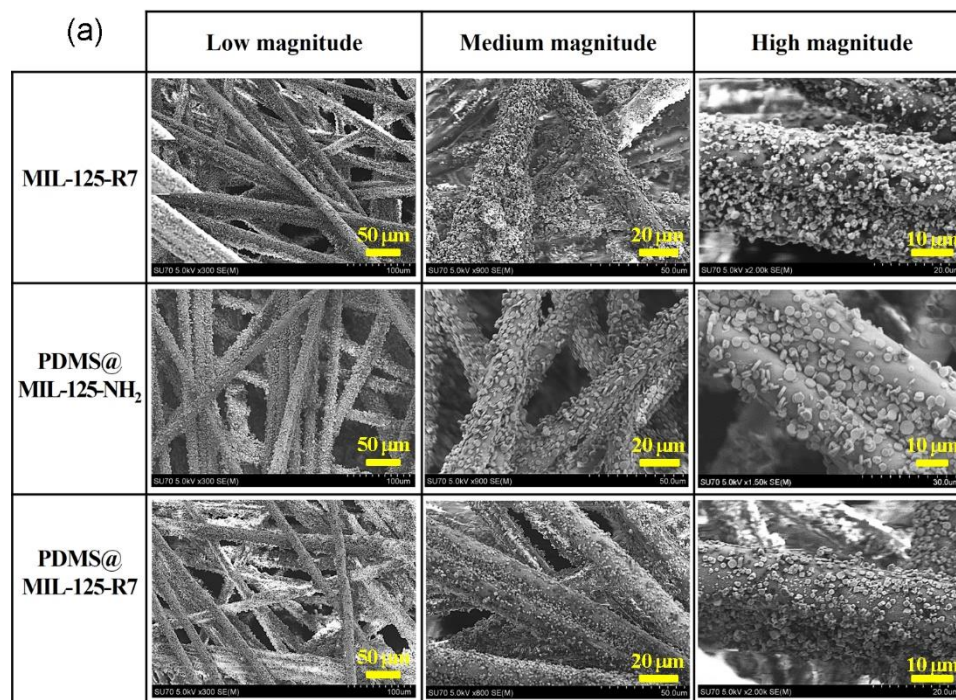


Figure 3. 3 SEM images of the depositions of modified MIL-125-NH₂ particles on the fibers of MERV13 electret filter (a) and N₂ adsorption isotherms of original and modified E-MOFilters (b).

3.3.3 Initial efficiency of modified E-MOFilters for PMs

To investigate the effects of MOF coating (10 wt%) on the PM removal of fabricated E-MOFilters, the size-fractionated efficiencies of the MERV13 and original and modified E-MOFilters were measured (5 cm s^{-1} face velocity) and compared. The efficiency of discharged MERV 13 (by isopropyl alcohol, IPA, vapor) was also compared to evaluate the efficiency decline due to charge degradation by the coated MOFs. As shown in Fig. 3.4, a decline of less than 10% of PM removal efficiency in all particle sizes was observed for the alkylated and PDMS modified E-MOFilters as compared to the original MERV 13. The substantially higher efficiency of all modified E-MOFilters than the discharged MERV 13 indicates a significant retention of fiber charges after the coating of MOFs. It is noted that the PM removal performance was not evaluated for other modified E-MOFilters due to their relatively poor VOCs removal performance compared to those shown in Fig. 3.4.

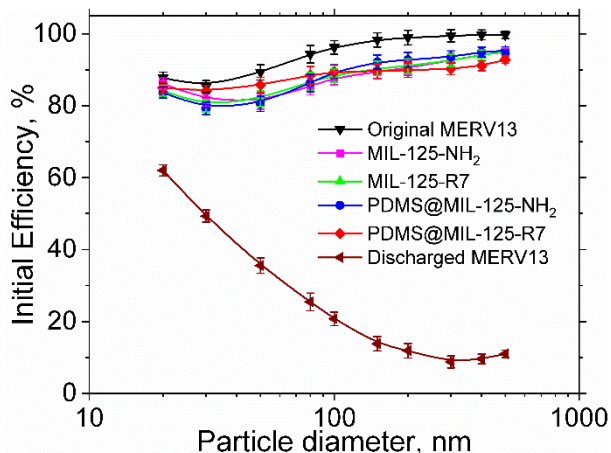


Figure 3. 4 Initial size-fractionated efficiency of MERV 13 E-MOFiler coated with MIL-125-NH₂, PDMS@MIL-125-NH₂, MIL-125-R7 and PDMS@MIL-125-R7 MOF particles.

3.3.4 Performance of modified E-MOFilters on PM loading

In addition to the initial efficiency, the filtration performance of the filters over a period of operation, e.g., a few months, is of great concern. A common criterion is the PM holding capacity, i.e., the loaded PM mass versus the pressure drop growth which relates to the energy consumption in operating the filtration.

Table 3.2 summarizes the initial pressure drop and holding capacity of fabricated E-MOFilters. To be noted again that there were two layers of MERV 13 flat media used in each fabricated E-MOFilters. It was found that the increase of initial pressure drops was very minor with around 4 Pa for all the E-MOFilters. In the PM_{2.5} aging tests, the endpoint was set at 1.0 in-H₂O (250 Pa) and the more mass of PM_{2.5} can be collected the better the filter is. As shown in Table 3.2, the clean MERV 13 had the highest holding capacity (19.1 g m⁻²) and all fabricated E-MOFilters remained a decent holding capacity of ~14.2 g m⁻². Therefore, it can be concluded that, in terms of degradation of PM holding capacity, the alkylated and PDMS E-MOFilters should be acceptable. To be noted, the PM_{2.5} holding capacity tests were conducted at 30±5% in this study and the RH effects on PM loading were discussed in our previous study (Tang et al., 2018c).

Table 3.2 Initial pressure drops and holding capacities of fabricated E-MOFilters (2 layers of MERV13 as the substrate)

Type	Initial ΔP (Pa)	Holding capacity (g m ⁻²)
MERV 13	8.8	19.1
MIL-125-NH ₂	12.5	14.3
MIL-125-R7	12.6	14.1
PDMS@ MIL-125-NH ₂	12.7	14.0
PDMS@ MIL-125-R7	12.4	14.5

3.3.5 RH effects on the initial efficiency and adsorption capacity of the E-MOFilter for toluene

3.3.5.1 Initial removal efficiency

In the previous section, the PM filtration performances of the modified E-MOFilters have been demonstrated to be comparable to that of the clean electret filters. In this section, the toluene removal performance will be quantitatively compared amongst different modified E-MOFilters under different RHs. Figs. 3.5 (a) and (b) compare the initial toluene (5 ppm) removal efficiency of original, alkylated and PDMS coated E-MOFilters under different RH conditions (10-60%) at 5 cm s⁻¹ and 0.5 cm s⁻¹ face velocity, respectively. It is seen the initial removal efficiency was decreased with increasing RH and it was higher at reduced filtration face velocity. Under extremely dry condition of 10% RH, the efficiency of the four modified E-MOFilters was very close with an efficiency of about 80-85%. However, it is clearly seen the efficiency of original E-MOFilter (MIL-125-NH₂) decreases dramatically with increasing RH, especially when RH is higher than 30%, indicating the MIL-125-NH₂ does need a hydrophobic modification. At elevated RHs, the toluene removal efficiency had an order of PDMS@MIL-125-NH₂ > PDMS@MIL-125-R7 > MIL-125-R7 > MIL-125-NH₂. This is consistent with the order of the measured WCAs. However, from the results tested at 50 and 60% RH, only the PDMS@MIL-125-NH₂ could remain a fairly good initial toluene removal efficiency (56% and 41%, respectively). Its better toluene removal was attributed to its superhydrophobicity and larger surface area compared with the PDMS@MIL-125-R7 and MIL-125-R7.

In Fig. 3.5 (b), it is seen the initial toluene removal efficiency under 0.5 cm s⁻¹ face velocity amongst fabricated E-MOFilters remained higher at elevated RHs than that under 5 cm s⁻¹. The

higher toluene removal efficiency at dry conditions ($RH \leq 30\%$) was due to the longer residence time in the filtration. Again, a significant efficiency degradation is seen at elevated RH for the original MIL-125-NH₂ E-MOFilter, which was due to its inherent hydrophilicity. The higher efficiency for modified E-MOFilters at elevated RHs was due to the lower amount of water molecules at reduced flow velocity, which reduced their occupancy at the adsorption sites facilitating the adsorption of toluene. Similar to the results under 5 cm s^{-1} , the toluene removal efficiency had an order of PDMS@MIL-125-NH₂ > PDMS@MIL-125-R7 > MIL-125-R7 > MIL-125-NH₂ at elevated RHs. It is worth mentioning that PDMS@MIL-125-NH₂ E-MOFilter exhibited a decent toluene initial removal efficiency of 83% and 71%, respectively, at 50 and 60% RH. Besides, the toluene initial removal efficiencies by PDMS@MIL-125-R7 were 63 and 45%, respectively, and that of MIL-125-R7 were 45 and 31%, respectively.

The toluene removal efficiencies of other modified E-MOFilters, i.e., PVP surfactant modified (MIL-125-NH₂/PVP) and N-coordination modified (MIL-125-NH₂/N_x), and hydrophobic ZIF-8 E-MOFilter were also investigated under different RHs at both 5 and 0.5 cm s^{-1} face velocity. As expected, the efficiencies of these three filters were also decreased with increasing RH under both face velocities. The MIL-125-NH₂/N_x and MIL-125-NH₂/PVP E-MOFilters had a close performance for toluene removal and much better than the ZIF-8. The low efficiency of ZIF-8 E-MOFilter under any RH conditions was due to its smaller pore diameter (0.34 nm) than the size of toluene molecules (dynamic molecules length, 0.58 nm) causing obstacles for toluene molecules to diffuse into its pores (Lashaki et al., 2012; Webster et al., 1998). Although MIL-125-NH₂/PVP and MIL-125-NH₂/N_x performed closely, a trend with the former performing better at low RH and the latter better at raised RH can be seen. This was because the MIL-125-NH₂/PVP had a higher surface area than that of MIL-125-NH₂/N_x (Table 3.1). In comparison, at raised RHs 30-60%, N

groups in MIL-125-NH₂/N_x replaced part of oxygen in the metal clusters (Ti-O-Ti) to coordinate with Ti⁴⁺, which will weaken the interaction between hydrophilic metal sites and water molecules and promote the toluene adsorption (Hu et al., 2018). Comparing the results shown in Fig. 3.5, it is concluded that the PDMS-coating E-MOF filter exhibited the best toluene removal efficiency amongst all the methods.

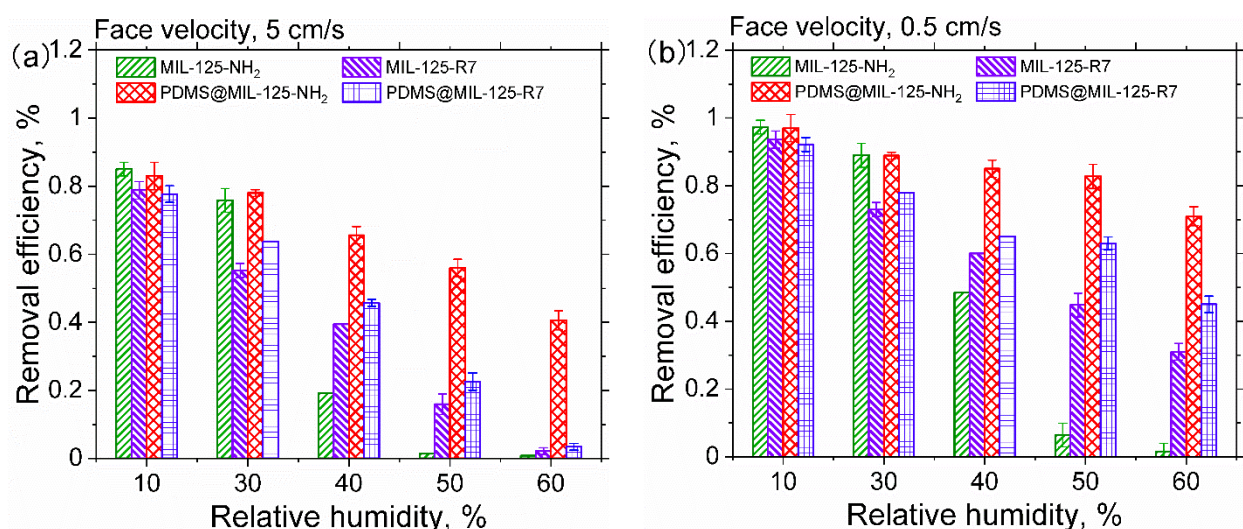


Figure 3. 5 Comparison of initial toluene removal efficiency of MERV 13 based E-MOFilters coated with alkylated and PDMS-treated MIL-125-NH₂ at 5 cm s⁻¹ (a) and 0.5 cm s⁻¹ (b).

3.3.5.2 Toluene adsorption capacity

In the previous section, the toluene initial removal efficiency of E-MOFilters under different RHs (10-60% RH) were systematically tested. In this section, toluene adsorption capacity of alkylated and PDMS modified E-MOFilters under 50% RH at 0.5 cm s⁻¹ face velocity was specially shown to illustrate the breakthrough curves of the fabricated E-MOFilters. The adsorption capacities for other E-MOFilters were not tested as their efficiency for toluene were not as good as the alkylated and PDMS modified E-MOFilters. In addition, the 50% RH is not only a typical

indoor air RH, but also a recommended value for assessing the performance of air cleaning systems by ASHRAE 145.2.

Fig. 3.6 compares the toluene adsorption capacity, or breakthrough curves, between alkylated and PDMS modified E-MOFilters under 50% RH. As seen, the original MIL-125-NH₂ E-MOFilter did not show an obvious toluene adsorption capacity (shortest breakthrough time), due to water vapor competitive adsorption caused by its abundant metal sites and hydrophilic amine groups. In comparison, the PDMS@MIL-125-NH₂ showed the highest toluene adsorption capacity (longest breakthrough time) due to its superhydrophobic surface property demonstrated by the WCA results and its relatively high SSA, then followed by PDMS@MIL-125-R7 and MIL-125-R7. It is worth mentioning that the PDMS coated MIL-125-R7 showed a slightly higher toluene adsorption capacity than the MIL-125-R7. This could be again due to the higher hydrophobicity induced by PDMS coating, as evidenced by its higher WCA.

It was calculated that the adsorption capacity of PDMS@MIL-125-NH₂ E-MOFilter was 8 times of the original MIL-125-NH₂ E-MOFilter. Furthermore, it is also worth mentioning that the breakthrough time for PDMS@MIL-125-NH₂ E-MOFilter only lasted for ~1.5 hours under current experiment conditions even if it showed the highest hydrophobicity and surface area among all the modified E-MOFilters. This breakthrough time is fairly shorter than that reported by Zheng et al. (2020). This was because the current E-MOFilter coated relatively low quantity of MOFs (only ~30%) compared with that of Zheng et al (2020), besides, the toluene concentration in the challenge was five times higher in this study (5 vs. 1 ppm). We also compares the challenging toluene concentration, filtration flow rate, removal efficiency, breakthrough time and adsorption capacity at RH=50% amongst the current E-MOFilters with different modifications and the MOFs CAU-1 ([Al₄(OH)₂(OCH₃)₄(H₂N-BDC)₃]·xH₂O) tested by Zheng et al. (2020). It is observed that

the performance of the PDMS modified E-MOFilter is comparable with the MOF CAU-1 in terms of adsorption capacity. To be concluded, PDMS@MIL-125-NH₂ E-MOFiter was demonstrated to have the best toluene adsorption performance under 50% RH amongst all modified E-MOFilters. Besides, since this method is relatively facile and cost effective, it could be used in practical application to decrease the RH effects on the gas removal filter media.

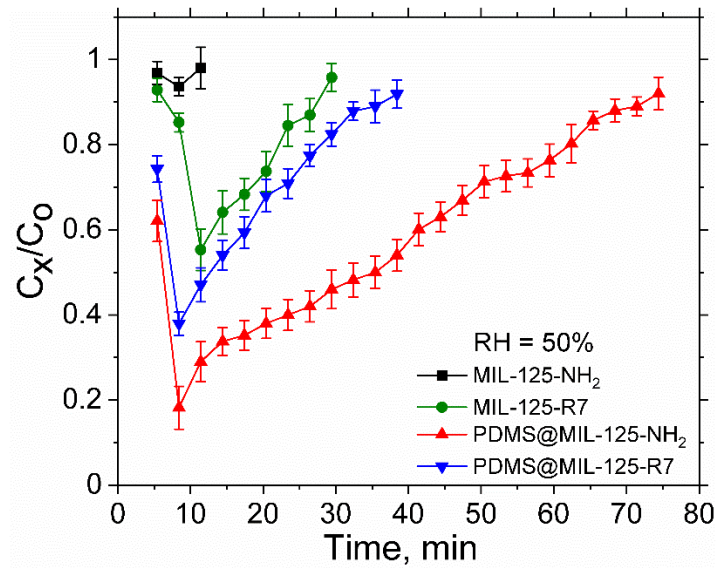


Figure 3. 6 Comparison of breakthrough curves amongst E-MOFilters coated with original and modified MOF particles under 0.5 cm s⁻¹ face velocity.

To evaluate the mechanical stability of the modified E-MOFilter, we conducted the MOF shedding test using an ultrafine condensation particle counter according to Zhang et al. (2021) to realize whether MOFs would detect from the MERV13 fibers. Besides, morphologies and crystalline structures of PDMS modified E-MOFilter after toluene adsorption were compared with the untreated one using the SEM and XRD, respectively. A negligible MOF shedding under the filtration velocity of 5-30 cm s⁻¹ was obtained which concluded a good physical stability of the E-

MOFilter. Our SEM and XRD analysis results indicated the morphology and crystal structure of the modified E-MOFilter remained unchanged after adsorption tests.

3.4 Conclusions

In this study, a representative MOF (MIL-125-NH₂) was successfully synthesized and modified via internal, external and combined modifications, i.e., alkylation, PDMS and both. Then these modified MOFs were coated to a MERV 13 grade electret filter media to develop a water/moisture resistant E-MOFilter for a simultaneous removal of PM_{2.5} and volatile organic compounds (VOCs) under different humid conditions (10-60% RH). The modified MOFs were characterized by SEM, EDX, XRD, FTIR and WCA and BET analysis and demonstrated to be hydrophobic. A series of systematic experiments for the toluene removal by the original and modified E-MOFilter under different RHs were conducted. Results showed the toluene initial removal efficiency of the original E-MOFilter was decreased to almost below 10% when RH was increased to 60%. However, the hydrophobically modified E-MOFilters performed much better than the original filter. Amongst the modified filters, the PDMS modified MIL-125-NH₂ E-MOFilter outperformed all filters having a decent initial removal efficiency (~80% at 0.5 cm s⁻¹ face velocity and ~60% at 5 cm s⁻¹ face velocity) and the longest breakthrough time for toluene under 50% RH. This was because of the high hydrophobicity and retaining high surface area and pore volume of the PDMS modified MIL-125-NH₂. Meanwhile, a series of measurements were conducted to test the PM removal performances, in terms of initial efficiency and holding capacity by the modified E-MOFilters. Results showed that the PM removal performance by the modified E-MOFilters were found to be comparable to the original MERV 13 filter. This indicates the modifications did not deteriorate the fiber charges and structures.

Comparing all the modifications in this work, it becomes clear that SSA, micropore volume and hydrophobicity are of great significance for achieving a good toluene removal efficiency under elevated humid conditions. Besides, regardless of the hydrophobicity of the adsorbents, there is a prerequisite that the relative pore size of the MOFs and three-dimensional size of VOC molecules are crucial for achieving good toluene adsorption performance of the filters. It is not easy to fundamentally tackle the water competitive adsorption issue and much more efforts should be made to extend the E-MOFilter applications in high humid conditions. Nevertheless, the systematic tests and the results from this study provided some new insights into the application of E-MOFilter under elevated RHs.

In conclusion, the significance and distinction of this study include: 1. The first to combine the MOF (MIL-125-NH₂) particles on electret filter media (as the E-MOFilter) for a low pressure drop and simultaneous removal of PM and VOC; 2. The E-MOFilter readily for both gas and particle purification towards a good indoor air quality. 3. Providing a series of modifications and optimization for the MIL-125-NH₂ MOFs and a systematic evaluation of the modified E-MOFilter against toluene under different RH levels. 4. Showing and ranking the effectiveness of the modifications on the mitigation of RH effects for the reference of future study.

Chapter 4. A novel sustainable semiconductor/metal-organic framework coated electret filter for simultaneous removal of PM_{2.5} and VOCs

Aerosol and Air Quality Research 23: 220445.

<https://doi.org/10.4209/aaqr.220445>

Reproduced by permission of Taiwan Association for Aerosol Research

Abstract

A MIL-125-NH₂ metal-organic framework (MOF) coated electret filter, named E-MOFilter, was previously developed to simultaneously remove PM_{2.5} (particulate matter less than 2.5 μm in aerodynamic diameter) and volatile organic compounds (VOCs, e.g., toluene). This E-MOFilter captures toluene primarily through physical adsorption, however, degradation of the adsorbed VOCs is desirable to increase the service life of the filter. In this study, photocatalytic nanosheets Bi₂WO₆/BiOCl (p-BWO) were synthesized, grafted on the MIL to be p-BWO@MIL, and then coated to the electret filter to form a new filter termed PE-MOFilter. The physical characterizations, including size, morphology, crystal structure, optical properties, and surface area for the semiconductor p-BWO nanosheets, p-BWO@MIL and PE-MOFilter were first examined to find out the optimal p-BWO to MIL ratio and coating wt% of p-BWO@MIL particles on the electret filter. Results demonstrated that the p-BWO nanosheets were successfully coated on the surface of MIL and the p-BWO@MIL retained the surface area and micropore volume of the MIL. The capability of the PE-MOFilter on adsorption and degradation of VOCs and the removal efficiency of PM_{2.5} was examined. The results showed that this PE-MOFilter not only captured but also effectively photodegraded VOC pollutants via the synergistic action of adsorption and photocatalytic oxidation (PCO). The photodegradation efficiency was found to be as high as 68.7% and it depended on the ratio of p-BWO to MIL. The results of PM_{2.5} removal efficiency also demonstrated that the coating of p-BWO@MIL particles had a negligible influence on the degradation of fiber charge. This research sheds light on the development of semiconductor@MOF coated electret media to simultaneously remove particulate and gaseous pollutants to improve indoor air quality with low energy consumption.

4.1 Introduction

The statistical data have shown that people spend 87–90% of their time indoors (Klepeis et al., 2001). However, the concentrations of indoor air pollutants, e.g., fine particulate matter, PM_{2.5} (particulate matter with an aerodynamic diameter less than 2.5 μm), and volatile organic compounds (VOCs), are often 2-5 times higher than the outdoor concentrations (Huang et al., 2018; US EPA, 2017). Besides, due to the high concentration of ambient PM_{2.5}, particles can infiltrate into indoor environments to pose threat to people's health (Chang et al., 2019; Tang et al., 2018b). Many researches have shown that PM_{2.5} and VOCs can lead to acute and chronic effects on humans' respiratory and central nervous systems and eventually cause hematological problems and cancer (Brasche and Bischof, 2005; Chen et al., 2019; Sarigiannis et al., 2011; Zhu et al., 2021). Therefore, it is urgent to simultaneously remove PM_{2.5} and VOCs to enhance indoor air quality.

Recently, metal organic frameworks (MOFs) coated electret filter, named E-MOFfilter, has been developed to simultaneously and effectively remove PM and VOC. It had a PM filtration efficiency of 85% and toluene adsorption efficiency of 90% (Zhang et al., 2021). However, the E-MOFfilter reduces VOCs primarily through adsorption, which only captures VOC pollutants. This non-destructive adsorption process is simple but reduction of adsorption due to saturation and desorption by concentration gradient are of great concerns (Schreck et al., 2019). Therefore, to also destroy the VOCs, it is rational to utilize the photocatalytic oxidation (PCO) technology which was discovered by Fujishima and Honda in 1972 (Fujishima A. and Honda K., 1972). The photocatalysts adopt solar energy (or visible lights) and operate at room temperature to degrade VOCs to harmless final products (mostly H₂O and CO₂) (Mamaghani et al., 2017). Inspired by the merits of PCO technology, extensive efforts have been made to expand the application of PCO in the mitigation of indoor air pollutants (Mo et al., 2009). In PCO technology, TiO₂, is the most

widely used catalyst because of its stability, corrosion resistance, and non-toxicity (Augugliaro et al. 1999; Li et al. 2011; Maira et al. 2001; Sun et al. 2012; Xie et al. 2020). However, its high excitation energy, low electron transfer rate to oxygen, and high recombination rate of electron/hole pair limit its photocatalytic performance (Dong et al., 2015). Recently, MOF/semiconductor composites, such as ZIF-8/TiO₂, ZIF-8/ZnO, MIL-100(Fe)/TiO₂, UiO-66-NH₂/TiO₂, UiO-66-NH₂/g-C₃N₄, MIL-125(Ti)-NH₂/TiO₂, MIL-125(Ti)/GO, MIL-125-NH₂/g-C₃N₄, MIL-125-NH₂/BiOCl, MIL-125-NH₂/Bi₂WO₆ etc., exhibit significantly improved catalytic performance as compared with the individual components, and have drawn an increasing attention (He et al., 2019; Hu et al., 2019; Huang et al., 2019; Li et al., 2018; Wang et al., 2016, 2019; Xu et al., 2020; Zeng et al., 2016; Zhang et al., 2018, 2020; Zhu et al., 2023). In these new composites, MOFs provide abundant adsorption sites to pre-concentrate and store a large amount of VOCs, meanwhile, the semiconductor particles serve as photocatalysts to photodegrade the VOC molecules that diffuse from the internal pores of MOF to the surfaces of semiconductors (Qian et al., 2021). For instance, Li et al. (2018) combined NH₂-MIL-125 (Ti) and graphene oxide (GO) to form a heterojunction photocatalyst via a microwave heating technique. The prepared 10-GO/NH₂-MIL-125(Ti) sample exhibited much enhanced photocatalytic efficiency of gaseous acetaldehyde under visible-light compared to its two pure components. It was concluded that the enhanced photocatalytic performance of the composite was a comprehensive result of the increased visible-light absorbance, more electron carrier density, more efficient charge transfer and less electron-hole recombination rate. Huang et al. (2019) developed a composite photocatalyst TiO₂@NH₂-MIL-125 via an in-situ solvothermal method for formaldehyde (HCHO) removal under UV irradiation. Their results showed that the synthesized TiO₂@NH₂-MIL-125 exhibited significantly enhanced photocatalytic performance for HCHO removal (HCHO removal rate of 90%) in

comparison with pure TiO₂ and NH₂-MIL-125, which was owing to the synergistic combination of high adsorption capacity of NH₂-MIL-125, high dispersion of TiO₂ and efficient interfacial charge transfer between TiO₂ and NH₂-MIL-125. Zhang et al. (2020) developed a TiO₂-UiO-66-NH₂ nanocomposites through a simple solvent evaporation method. This nanocomposite photocatalyst demonstrates 72.7% and 70.74% conversion efficiency for toluene and acetaldehyde, respectively, which was about 9.7 and 10.5 times higher than that of UiO-66-NH₂, due to the enhanced surface area of the photocatalyst and the suppressed recombination rates of the charge carriers. As demonstrated by these studies, it is obvious that the formation of heterojunction can considerably improve the performance of MOF/semiconductor photocatalyst in VOCs remediation.

In this study, to improve the E-MOFilter towards VOC degradation, Bi₂WO₆/BiOCl was selected as the semiconductor photocatalyst, termed p-BWO, as it showed the photocatalytic oxidation of toluene with a conversion rate 166-fold higher than that of pristine Bi₂WO₆ and BiOCl, because the layered and amorphous structures of the nanosheets effectively facilitate the separation of electron-hole pairs (Cao et al., 2018). The p-BWO nanosheets were grafted on the surface of MOF MIL-125-NH₂, a representative porous MOF, by using a cationic metal-ion adhesive, poly(ethylenimine) (PEI, 50 wt%). This integration technique differs from the common hydrothermal method (an in situ self-assembly method). The specific details were shown in the later Section 4.2.1.3. The composite photocatalyst (p-BWO@ MIL-125(Ti)-NH₂) was then transported to MERV 13 electret filter media to fabricate the photocatalytic filter, named PE-MOFilter. The MERV 13 electret filter here acted as the substrate for deposition of the composite photocatalyst, which would promise this photocatalytic filter remains charged and has a high PM filtration efficiency based on prior research (Chang et al., 2019; Li et al., 2020; Tang et al., 2018a,b; Tien et al., 2020). Various characterizations, such as XRD, SEM and UV-vis, were performed to

demonstrate the effective synthesis of the composite photocatalyst. The photocatalytic efficiency of toluene, a representative indoor VOC, by the PE-MOFilter was examined. As a simultaneous gas-particle removal filter, the PE-MOFilter was also examined for their PM removal efficiency to confirm the coating of the composite photocatalyst would not cause any degradation for PM removal performances. The ultimate goal of this study is to demonstrate the PE-MOFilter not only captures but effectively photodegrades VOC pollutants via the synergistic action of adsorption and photocatalytic oxidation (PCO).

4.2 Materials and Methods

4.2.1 Synthesis of composite photocatalyst (p-BWO@MIL-125-NH₂)

4.2.1.1 p-BWO synthesis

The p-BWO nanosheets were synthesized via a hydrothermal method according to Cao et al. (2018). In brief, 165 mg Na₂WO₄·2H₂O and 80 mg octadecyltrimethylammonium chloride (OTAC) as the surfactant were dissolved in 40 mL deionized water (DI water). 486 mg Bi(NO₃)₃·5H₂O (1 mmol) milled powders were added to this solution under stirring. After 60 min of stirring, the mixture was moved into a 100 mL Teflon-lined autoclave and then heated at 140°C for 24h. Finally, the product was collected by centrifuge and then dried in vacuum oven for 10 hrs. The OTAC used in this study not only aided in reducing the thickness of the nanosheets, but also played a crucial role in imparting photochromic properties by providing a source of chlorine that facilitated the rich crystalline-amorphous boundaries in the crystal structure, thereby boosting the photoactivity of the semiconductor photocatalyst p-BWO nanosheets.

4.2.1.2 MIL-125(Ti)-NH₂ synthesis

The MIL-125(Ti)-NH₂ was prepared according to Zhang et al. (2021) as follows: 0.797 mL titanium tetraisopropoxide (TTIP) and 0.651 g 2-aminoterephthalic acid (BDC- NH₂) were

dissolved in the mixture of dimethylformamide (DMF)/methanol (15 mL/15 mL). Then, the mixture was transferred to a Teflon-lined steel autoclave reactor and placed in an oven at 150 °C for 15 h. The obtained yellow products were separated by centrifugation and washed by 30 mL DMF and 30 mL methanol, respectively, for three times. Finally, the samples were dried under 50 °C for 12 hr in vacuum. To be brief, MIL-125(Ti)-NH₂ was abbreviated as MIL hereafter.

4.2.1.3 p-BWO@MIL composite photocatalyst preparation

The composite photocatalyst p-BWO@MIL was prepared via a metal-ion adhesive. This synthesis method differs from the common hydrothermal method, in which a simple in situ self-assembly method was used but the stabilization of semiconductors on MOFs was still a challenge because the interfacial contact between MOF and semiconductor was not yet sufficiently strong. The synthesis process of the composite photocatalyst in our method was based on the electrostatic attraction occurred on the interface of MOF and semiconductor, because two components and the adhesive had the opposite surface charges as demonstrated from their zeta potential values, (Barick et al., 2015; Lv et al., 2016; Zhu et al., 2023). 0.25 g poly(ethylenimine) (PEI, 50 wt%) as a metal-ion adhesive was dissolved in 10mL DI water to form PEI/DI water solution (solution I) and then a certain amount of p-BWO nanosheets were dispersed in the solution I and then were stirred for 12 hours to form p-BWO/PEI water solution (solution II). After that, the solution II was centrifuged to obtain p-BWO/PEI solid. The solid was washed with DI water for two times to remove PEI residues and then dispersed in 15mL DI water again to form p-BWO/PEI water solution (solution III). Subsequently, a certain amount of MIL was added and dispersed in the solution III and stirred for 4 hrs. The final yellow product p-BWO@MIL was collected by centrifuge and then dried in vacuum oven for 10 hrs. The composite photocatalysts are, hereafter,

termed p-BWO@MIL-ratio (0.5 to 1.5 of p-BWO/MIL mass ratio), where the mass of MIL was kept at 0.1 g.

4.2.2 PE-MOFilter fabrication

To fabricate the p-BWO@MIL coated electret filter media, PE-MOFilter, the following properties should be considered in the process. Firstly, the charges of the electret media should not be degraded; secondly, the MOF particles should firmly attach to the electret media with a minimized growth of air resistance; thirdly, the transfer process is simple and cost-efficient. Here, we chose the liquid filtration coating method. The experimental setup and parameters for the composite photocatalyst coating onto electret filter media can be found elsewhere (Zhang et al., 2021).

The PE-MOFilter was fabricated by using the 50 mm diameter flat sheets of a MERV 13 electret filter media for the deposition of the p-BWO@MIL particles for the PM_{2.5} and toluene removal tests. Table 4.1 summarizes the specifications of the MERV 13. The coating amount of the composite photocatalyst was controlled at 10 wt% (photocatalyst/media) based on Zhang et al. (2021). Two layers of MERV 13 flat sheets were used to enhance the removal efficiency of both PM_{2.5} and toluene. In total, three kinds of PE-MOFilters were fabricated and tested, which were MERV 13 electret filter media coated with p-BWO@MIL-0.5, p-BWO@MIL-1, and p-BWO@MIL-1.5 particles.

Table 4. 1 Specification of the MERV 13 electret media for the composite photocatalyst coating.

Grade	Fiber diameter (μm)	Thickness (mm)	Basic weight (g m^{-2})	Solidity (α)	Charge density ($\mu\text{C m}^{-2}$)	Pressure drop at 5 cm s^{-1} (Pa)	Initial efficiency for $0.3 \mu\text{m}$ particles at 5 cm s^{-1} (%)
MERV13	13.1 ± 0.9	0.47 ± 0.02	75 ± 2	0.1 ± 0.03	~ 50	4.5 ± 0.1	91.1 ± 0.2

4.2.3 Characterization of MOF Particles and PE-MOFilters

The scanning electron microscopy (SEM, Hitachi SU-70, Hitachi Corp., Tokyo, Japan), X-ray diffraction (XRD, PANalytical X'Pert Pro, Malvern PANalytical Ltd., Malvern, UK), UV-Visible spectrophotometer (Evolution 220, ThermoFisher) and photoluminescence (PL) spectroscopy (QuantaMaster 400, Photon Technology International) were utilized to characterize the size and morphology, crystal structure, and optical properties, respectively, of the synthesized samples. Besides, nitrogen adsorption–desorption isotherms were collected using a gas sorption analyzer (Autosorb iQ, Quantachrome Instruments Corp., Boynton Beach, FL) at 77 K to characterize the pore size distribution and Brunauer-Emmett-Teller (BET) surface area. The SEM analysis was also conducted for the composite PE-MOFilters to evaluate if the p-BWO@MIL particles were coated uniformly in the filters.

4.2.4 PM and toluene removal efficiency by the PE-MOFilter

After the chemical and physical characterizations of the p-BWO@MIL and its corresponding PE-MOFilter, the filters were evaluated for their PM and VOC removal efficiencies. By comparing the PM and toluene removal results of the PE-MOFilter with that of pristine MERV 13 and MIL, the effects of p-BWO@MIL coating on charge degradation and p-BWO coating on the reduction of toluene adsorption were determined.

The filter holder applied to conduct the experiments was a newly fabricated multi-functional holder, as shown in Fig. 4.1. It can be used not only in the PM filtration, but also VOC adsorption and VOC photoreaction tests. This holder had an inner diameter of 4 cm, length of 6 cm and volume of 75 cm³. It clamps and seals the filter media in the middle and has two quartz windows on both sides. In the PM filtration tests, 1 and 2 taps were used to measure the upstream and downstream particle concentration to determine efficiency. The taps 3 and 4 were for the pressure drop measurement. For adsorption tests, all the taps were closed and then filter was challenged by toluene. For photoreaction, all the taps were also closed and the wide opened quartz windows on both sides allowed the majority of p-BWO@MIL being exposed to the light source. This new filter holder significantly made it convenient for performing all the tests in this study. The test methods for the PE-MOFilter against PM_{2.5} and toluene are discussed in the flowing and the test conditions are summarized in Table 4.2.

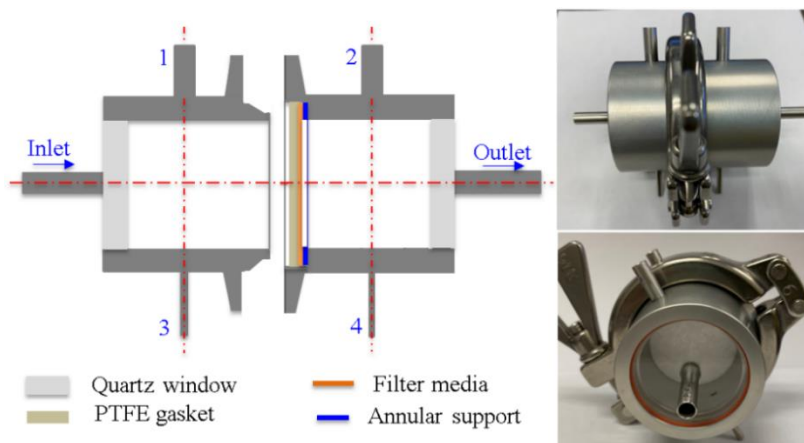


Figure 4. 1 The schematic diagram and digital images of the newly developed multi-functional filter holder.

4.2.5 Initial PM removal efficiency test

The initial PM removal efficiency of PE-MOFilter was tested under 5 cm s^{-1} face velocity by using the same experimental setup as shown in Tang et al. (2018a). In brief, atomization (Model 9302, TSI Inc., Shoreview, MN) and classification (Model 3082, TSI Inc., Shoreview, MN) were utilized to produce monodisperse NaCl particles with sizes between 20–500 nm. The classified monodisperse particles were firstly neutralized to reach Boltzmann distribution to mimic the particles present in the ambient condition before challenging the PE-MOFilters. The upstream, $C(d_x)_{up}$, and downstream, $C(d_x)_{down}$, concentrations (particle cm^{-3}) of particles with diameter of d_x were measured by an ultrafine condensation particle counter (UCPC, Model 3776, TSI Inc. Shoreview, MN). Then the initial size-fractioned efficiency, η_{PM} , can be determined as:

$$\eta_{PM}, \% = \left(1 - \frac{C(d_x)_{down}}{C(d_x)_{up}} \right) \times 100\% \quad (4.1)$$

For comparison, the initial efficiency of the original and discharged (by IPA vapor) MERV 13 electret media without coating p-BWO@MIL particles was also measured.

4.2.6 Toluene initial efficiency and adsorption capacity test

Toluene ($\text{C}_6\text{H}_5\text{CH}_3$) as a common and representative harmful indoor VOC (Chen et al., 2019; Jafari et al., 2018; Kim et al., 2018a; Rezaei et al., 2016) was selected to challenge the PE-MOFilters. The experimental system shown in Fig. 4.2 was used to find the toluene initial adsorption efficiency and adsorption capacity and photoreaction. The light source was not used in the adsorption process. The line of the dummy holder was used to generate the calibration curve between the toluene concentration, i.e., 0.05 to 50 ppm, and peak area, determined by a gas chromatography (GC, Agilent 7890B, Agilent Technologies Inc., Santa Clara, CA) equipped with

a flame ionization detector (FID, Agilent Technologies Inc., Santa Clara, CA). 5 ppm of toluene with the 5 cm s^{-1} of face velocity was applied in the testing. When the adsorption started, the 3-way valve was switched to dummy line first to confirm if a correct toluene concentration was produced from the dilution of a 100 ppm toluene cylinder. When it was correct, the 5 ppm toluene flow was switched to the filter line and continued challenging the filter until breakthrough (90% of 5 ppm in this study). The relative humidity (RH) was controlled to be 10% in the adsorption tests by adjusting the flow rates of the compressed air ($\sim 5\%$ RH) and the water mists generated by the single jet atomizer (Model 9302, TSI Inc., Shoreview, MN). The equations to determine the toluene initial efficiency and adsorption capacity can be found elsewhere (Zhang et al., 2021).

Table 4. 2 Experimental conditions for PM and toluene removal tests and photoreaction.

PE-MOFilter	PM tests (5 cm s^{-1}) Initial efficiency	5 ppm toluene Adsorption tests (5 cm s^{-1} , RH = 10%)	PCO test UV light illumination (RH = 50%)
MIL	√	√	√
p-BWO	√	√	√
p-BWO@MIL-0.5	√	√	√
p-BWO@MIL-1	√	√	√
p-BWO@MIL-1.5	√	√	√

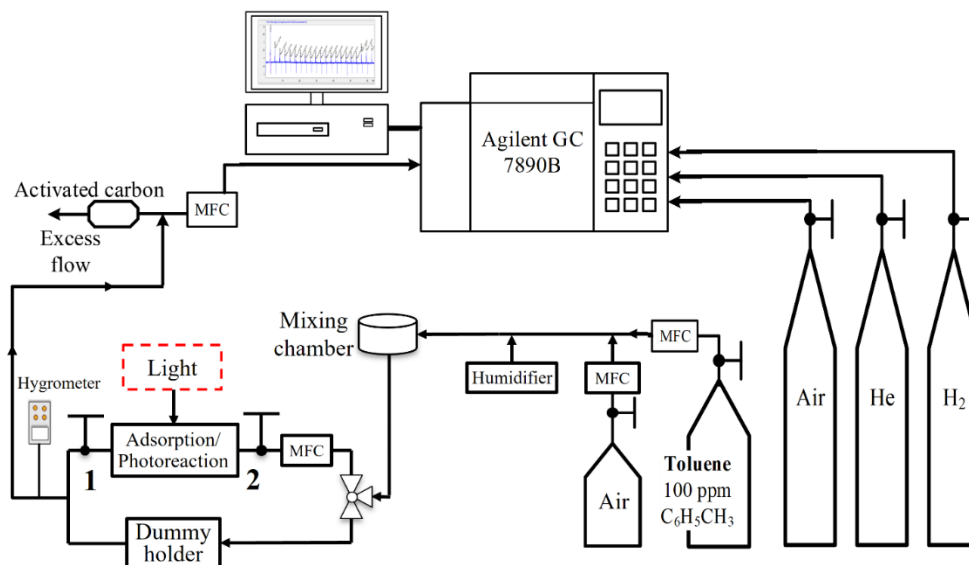


Figure 4. 2 Experimental setup for initial removal efficiency and adsorption capacity test, and photocatalytic efficiency test for toluene.

4.2.7 Photodegradation of toluene by the PE-MOFilters

The photocatalytic degradation of gaseous toluene was performed under static flow condition at ambient temperature of 20 °C, atmospheric pressure of 1 bar, and room RH (~50%). The static means both valves 1 and 2 were closed after the PE-MOFilter was saturated with the toluene in the breakthrough test. Meanwhile, the UV lights irradiated the PE-MOFilter on both sides for a certain time for photoreaction. The light sources were two 25W UV bulbs with a wavelength of 254 nm. They were placed against the two quartz windows to initiate the photocatalytic processes. The power density of the UV light in the reaction chamber was calculated to be 9.5 mW cm⁻². Be noted, the static test conducted here is very relevant to the realistic operation of filter in an air purifier. For example, a residential purifier is normally turned on in the evening and overnight when people are home. During the day, people are out for school and work so the blower of purifier

can be off, and UV can be on to conduct photoadaptation for the adsorbed VOCs. Similarly, for the purifiers used in offices or schools, the photodegradation can be launched during the night.

To determine the efficiency of photodegradation for the PE-MOFilter under UV irradiation, this study developed a simple procedure. That was, we compared the toluene mass from the desorption with a 5 cm s^{-1} air flow blowing under three different conditions. The first condition, called “Blank”, was to initiate the toluene desorption right after the breakthrough (saturated with toluene). The second condition, called “Dark”, was to switch off the room light to keep the holder in dark after saturation and then to initiate the toluene desorption after the sample stayed in dark for 16 hours. The third condition, called “Photoreaction”, was similar to the “Dark” condition except the holder was continued to be irradiated with UV lights for 16 hours.

Ideally, the results between Blank and Dark might be very close if there was no leakage. The efficiency of the photodegradation, η_{Photo} , was calculated as:

$$\eta_{Photo} \% = \left(1 - \frac{\int_0^t C_{t,Photo} \times Q dt}{\int_0^t C_{t,Blank} \times Q dt} \right) \times 100\% = \left(1 - \frac{m_{Photo}}{m_{Blank}} \right) \times 100\% \quad (4.2)$$

where $C_{t,Photo}$ (mg m^{-3}) is the concentration of toluene at the time t (min) in the desorption process of Photoreaction condition, $C_{t,Blank}$ (mg m^{-3}) is the concentration of toluene at the time t in the adsorption process for the Blank condition, Q is the total flowrate (mL min^{-1}), m_{Photo} and m_{Blank} are the toluene desorption mass under Photoreaction and Blank condition, respectively.

4.3 Results and Discussions

4.3.1 Characterization of synthesized MIL, p-BWO and p-BWO@MIL-1 Particles

Fig. 4.3 summarizes the characterization results of original MIL, p-BWO and p-BWO@MIL-1 particles. Their SEM images shown in Figs. 4.3(a-c) reveal the morphologies of the synthesized particles. Fig. 4.3(a) demonstrates that MOF MIL-125-NH₂ has a morphology of tetragonal plate, having an average length and thickness of ~900 and ~300 nm, respectively, which were in good agreement with literature (Kim et al., 2018a). The p-BWO nanosheets shown in Fig. 4.3(b) are hundreds of nanometers long and comprised of multiple units of tiny nanoplates with a thickness of ~10 nm. The image of the photocatalyst p-BWO@MIL in Fig. 4.3(c) shows that the p-BWO nanoplates are well distributed on the surfaces of MOF MIL, which is not only beneficial to the diffusion of toluene from the internal pores of MOF to the surface of p-BWO, but also favorable of the interface charge transfer in the PCO process (He et al., 2019; He and Wang, 2018).

The XRD patterns were measured to investigate the crystallinity of the synthesized p-BWO, MIL and p-BWO@MIL particles. As shown in Fig. 4.3(d), the XRD characteristic peaks of p-BWO and MIL are clearly displayed in the composite p-BWO@MIL particles, indicating a two-phase composition of MIL and p-BWO (Zhang et al., 2020). The specific surface area and porosity of the synthesized samples were determined by BET analysis using N₂ adsorption-desorption tests at 77 K. As shown in Fig. 4.3(e), the isotherm of MIL-125-NH₂ exhibits a typical Type I curve with a sharp increase at low pressure regions, indicating its microporous structures and the corresponding high surface area. The isotherm of p-BWO shows a Type IV curve with a typical hysteresis loop due to the aggregations of p-BWO nanosheets (Zhang et al., 2020), which indicates the non-porous characteristics of p-BWO. This is consistent with its low pore volume and small surface area shown in Table 3. The isotherm of p-BWO@MIL exhibits hybrid Type I/IV, and the

hysteresis loops occur at high-pressure zone ($P/P_0 > 0.85$), suggesting the presence of coexistence of micropore and mesopores. Table 4.3 shows the composite photocatalyst p-BWO@MIL shows high pore volume and surface area. As aforementioned, the high surface area of the composite photocatalyst is beneficial to pre-concentrate a large amount of toluene molecules, and in turn, is facilitated to the photodegradation process. Meanwhile, it is well acknowledged that gas-solid photocatalytic reactions usually occur on the surfaces of catalysts, thus, it is expected that the photocatalytic efficiency would be greatly enhanced because of the increased photoreaction sites when compared to pure MOFs and pure semiconductor materials (He et al., 2019). Fig. 4.3(f) shows the pore size distribution of the prepared samples. It is seen that the original MIL and p-BWO@MIL had the same peak pore size of 0.78 nm, a pore size which is beneficial for toluene adsorption (kinetic diameter, 0.58 nm) (Webster et al., 1998). However, pure p-BWO had the peak pore size of 3.16 nm, which is significantly larger than the toluene molecular size, and unfavorable for toluene capture. In Fig. 4.3(i), the drastically lowered photoluminescence intensity demonstrated the suppressed recombination of photogenerated carriers in p-BWO. It could be predicted that the synthesized p-BWO nanosheets have excellent photocatalytic activity because of the significantly enhanced charge carrier (h^+ , e^-) separation in PCO process (Cao et al., 2018).

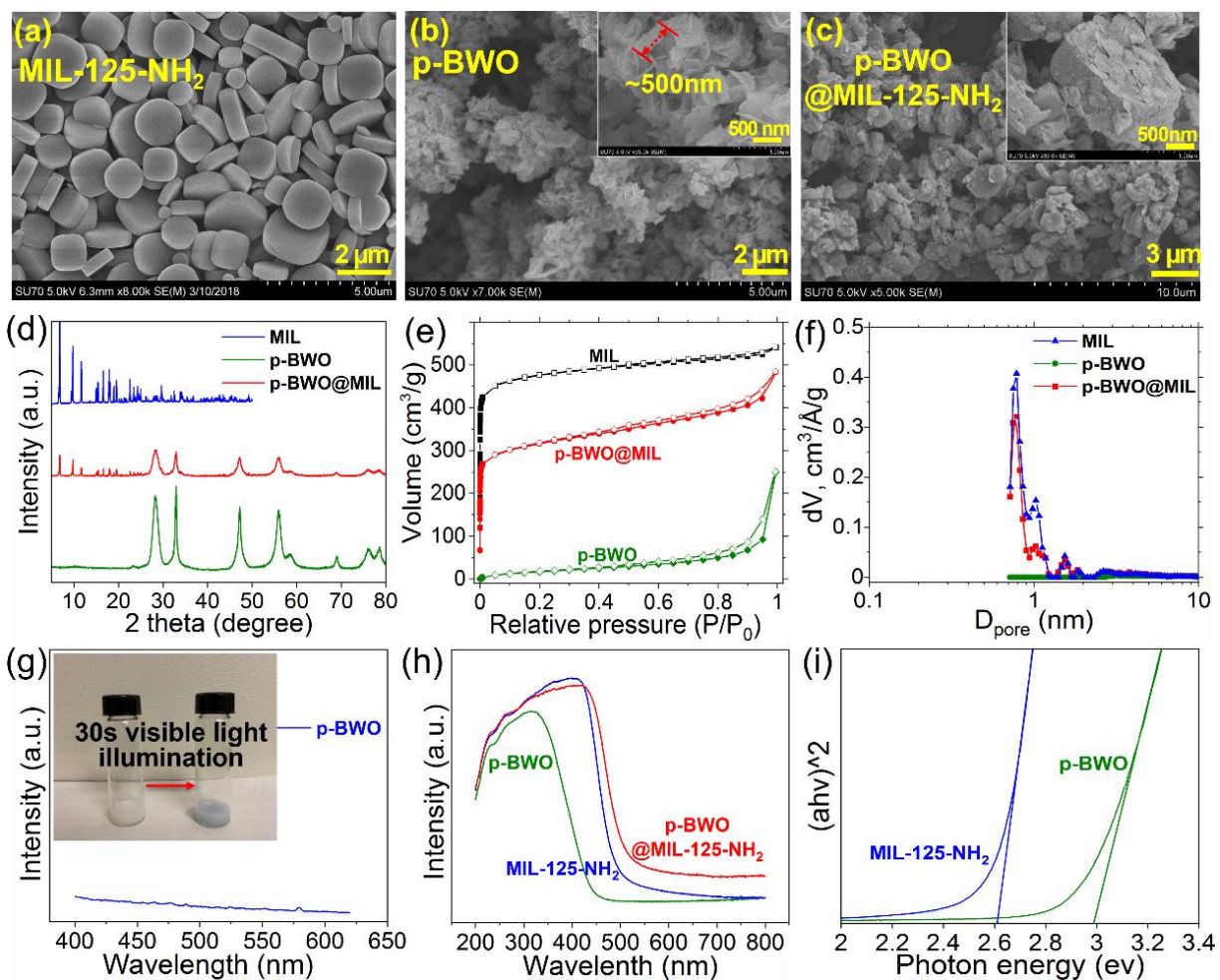


Figure 4. 3 SEM, XRD patterns and BET analysis of powdered original MIL, p-BWO and p-BWO@MIL (mass ratio: 1:1) (a-f), photoluminescence (PL) analysis of p-BWO (inset image shows the photochromic response of p-BWO under 30s visible light irradiation) (g), UV-vis spectra and Tauc plots of p-BWO and MIL (h and i).

The photocoloration response shown in the inset of Fig. 4.3(i) is a macroscopic manifestation of prompt charge carrier separation. The UV-vis spectra were evaluated to explore the optical properties of the samples. As shown in Fig. 4.3(g), the pure p-BWO exhibits light absorption (< 450 nm). After the incorporation of MOF MIL, the light absorption extends to the visible light range (< 600 nm), indicating the enhanced light absorption of the composite

photocatalyst p-BWO@MIL. Tauc plots in Fig. 4.3(h) were derived from the UV-vis spectra to calculate the band gaps. As displayed in Fig. 4.3(h), the band gaps of p-BWO and MIL were determined to be 2.96 eV and 2.62 eV, respectively. It is expected that the incorporation of MIL would narrow down the band gap, which would boost the light utilization during the photocatalytic processes (He et al., 2019).

Table 4. 3 BET analysis of p-BWO, MIL and p-BWO@MIL particles.

Adsorbents	BET surface area ($\text{m}^2 \text{g}^{-1}$)	Total pore volume ($\text{cm}^3 \text{g}^{-1}$)	Micro pore volume ($\text{cm}^3 \text{g}^{-1}$)	Pore diameter (nm)
p-BWO	47	0.387	0	3.16
MIL	1871	0.911	0.667	0.78
p-BWO@MIL-0.5	1439	0.837	0.519	0.78
p-BWO@MIL-1	1213	0.811	0.459	0.78
p-BWO@MIL-1.5	983	0.623	0.289	0.75

4.3.2 Performance of PE-MOFilters

The p-BWO@MIL were transported to MERV 13 electret filter media (~10 wt%) to form PE-MOFilters. Fig. 4.4 shows the SEM images of the depositions of p-BWO@MIL particles on the fibers of MERV 13 media. It is seen the p-BWO@MIL particles were uniformly deposited on individual fibers and in-depth of the PE-MOFilter (Zhang et al., 2021; 2022; 2023).



Figure 4. 4 SEM image of the deposition of p-BWO@MIL-1 particles on the fibers of MERV 13 electret media (PE-MOFilter).

4.3.3 Initial Efficiency of PE-MOFilters for PMs

To investigate the effects of p-BWO@MIL coating (10 wt%) on the PM removal of fabricated PE-MOFilters, the size-fractionated efficiencies of the original MERV 13 and p-BWO@MIL coated PE-MOFilters were compared in Fig. 4.5. The efficiency of discharged MERV 13 was also shown to evaluate the efficiency decline due to charge degradation of PE-MOFilters. As seen in Fig. 4.5, the decline of PM removal efficiency in all particle sizes was less than 10% compared to the original MERV 13. The substantial higher efficiency of the PE-MOFilters than the discharged MERV 13 indicates a significant retention of fiber charges after the coating of the p-BWO@MIL. It is noted that the PM removal efficiencies for MERV 13 electret media coated with p-BWO@MIL-0.5 and p-BWO@MIL-1.5 have the similar trend as p-BWO@MIL-1. Thus, they are not shown here. In addition, the results also showed that the coating of p-BWO@MIL caused a negligible increase of pressure drop. Therefore, the proposed PE-MOFilter here remains the merits of electret media, including high PM removal efficiency and low pressure drop.

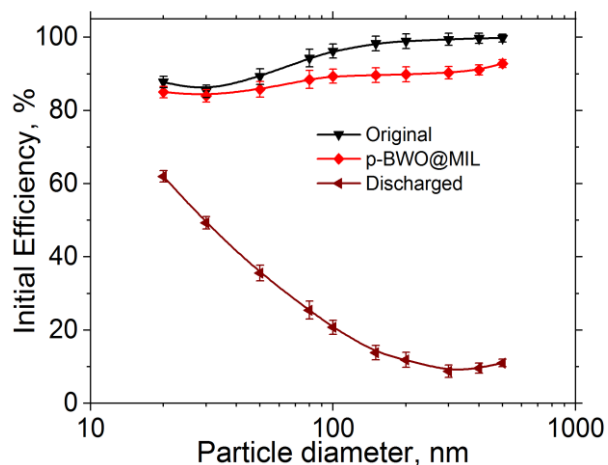


Figure 4. 5 Comparison of initial size-fractionated efficiency of original MERV 13 electret media, PE-MOFilter coated with p-BWO@MIL-1 particles, and discharged MERV 13 electret media.

4.3.4 Initial adsorption Efficiency of PE-MOFilters for toluene

In this section, the toluene removal performance was quantitatively compared amongst PE-MOFilters with different p-BWO to MIL ratios. Fig. 4.6 compares the initial toluene (5 ppm) removal efficiency of the original MIL, pure p-BWO and p-BWO@MIL-0.5 (-1.5) coated on MERV 13 under 5 cm s^{-1} face velocity. It is seen that the initial removal efficiencies of the PE-MOFilters, 80-88%, had a comparable toluene removal performance with the original E-MOFilter of 92%. The efficiency slightly reduced with increasing ratio of p-BWO to MIL, which was in agreement with the BET surface area shown in Table 4.3. It is noted that the pure p-BWO nanosheets coated MERV 13 had a low toluene initial removal efficiency due to the extremely low surface area and large pore size as shown in Table 3 and Fig. 4.3(f). It is concluded that with the appropriate amount of p-BWO@MIL coating, there were negligible adverse effects of coating on the surface area and porous structure of MOF and toluene adsorption.

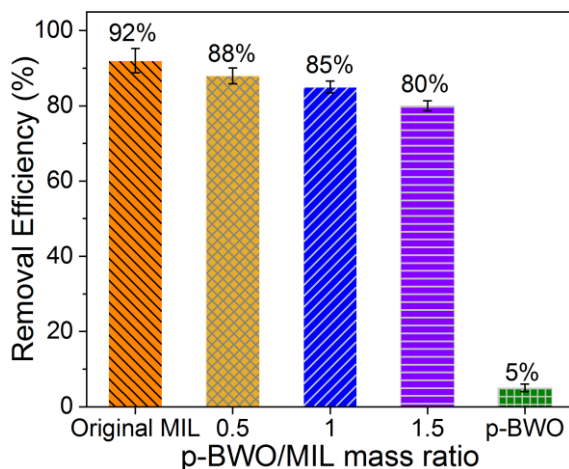


Figure 4. 6 Comparison of initial toluene removal efficiency of original MIL, p-BWO, p-BWO@MIL-0.5 (-1.5) coated MERV 13 electret media.

4.3.5 Toluene adsorption capacity and photodegradation of the PE-MOFilters

Fig. 4.7(a) compares the adsorption capacity (breakthrough) of original MIL, p-BWO and p-BWO@MIL coated electret media. The C_0 and C_x in Fig. 4.7(a) refer to the feeding 5 ppm toluene and monitored downstream toluene concentration of the PE-MOFilter, respectively. The adsorption capacity from greatest to least was original MIL > p-BWO@MIL-0.5 > p-BWO@MIL-1 > p-BWO@MIL-1.5 > p-BWO. Notably, the PE-MOFilters exhibited only slight reduction of adsorption capacity compared to the original E-MOFilter, which was due to their retention of highly porous structure, while p-BWO coated media showed a very low adsorption capacity due to its low surface area. These results are consistent with the order of their corresponding surface area shown in Table 4.3.

Figs. 4.7(b–f) compared the toluene desorption curves amongst Blank, Dark and Photoreaction conditions. The C_0 in these figures was the first detected toluene desorption concentration from the conditions of Blank and C_x is the desorption concentration under Dark or

Photoreaction conditions. As expected, the results between the Blank and Dark were very close indicating a good leakage free of the photoreactor chamber. It can be seen the order of toluene conversion rate is p-BWO@MIL-1 > p-BWO@MIL-1.5 > p-BWO@MIL-0.5 > p-BWO > MIL. The results indicate that all the composite photocatalysts exhibit higher efficiencies of photodegradation for toluene than the original MIL and p-BWO coated electret media, which can be attributed to the rapid charge transfer at the interface of p-BWO and MIL, as verified by the photoluminescence in previous studies (Xu et al., 2020; Yin et al., 2020a, 2020b). In Fig. 4.7(b), the original E-MOFilter was demonstrated to have the lowest photocatalytic efficiency (3.5%), indicating the poor photocatalytic performance of the pure MIL. Meanwhile, the pure p-BWO coated electret media shows a toluene conversion rate of 25.3% (Fig. 7(c)), suggesting pure semiconductor p-BWO could not serve as an effective photocatalyst towards photodegradation of VOCs. This can be explained by its extremely small surface area and the consequently small number of photoreaction sites. In the contrary, p-BWO@MIL coated PE-MOFilters (shown in Figs. 7(d–f)) exhibited good photocatalytic performances, and the conversion of toluene increased from 45.0% to 68.7% and then reduced to 52.5% for p-BWO to MIL ratio from 0.5 to 1.0 and 1.5, respectively. Based on the results, it is concluded that the ratio of p-BWO to MOF plays a significant role in enhancing the photocatalytic efficiency of the composite photocatalyst. This is because the appropriate amount of MOF facilitates the interfacial charge transfer and suppresses the charge carrier recombination. However, if the amount of MOF exceeds the optimal value, the extra MOF would lower light absorption, diminish the density of excited charge carriers, and impair interfacial charge transfer in the PCO process, which would result in a reduction in the photodegradation efficiency (He et al., 2019). In contrast, semiconductors serve as a photoactive center to photodegrade toluene. If it is higher than ideal value, the micropore of MOFs would be

partially blocked and thus the surface area would be reduced (Molavi et al., 2018), meanwhile, the interface charge transfer would also be restricted, causing a reduced photocatalytic efficiency.

To evaluate the structural stability of the prepared samples, SEM and XRD analysis of p-BWO@MIL-1 before and after photocatalytic tests were conducted. As shown in Fig. 8, the morphology and crystal structure remained unchanged after photoreaction process, demonstrating that the UV light will not cause damage to the MOF structure. Additionally, to demonstrate that the UV light will not degrade the charge of the electret filter, the filtration efficiencies of the original and UV light treated MERV 13 electret filter media were examined and compared. Results shown in Fig. 8 indicated that UV light treated MERV 13 electret media has a negligible filtration efficiency change compared with the original one.

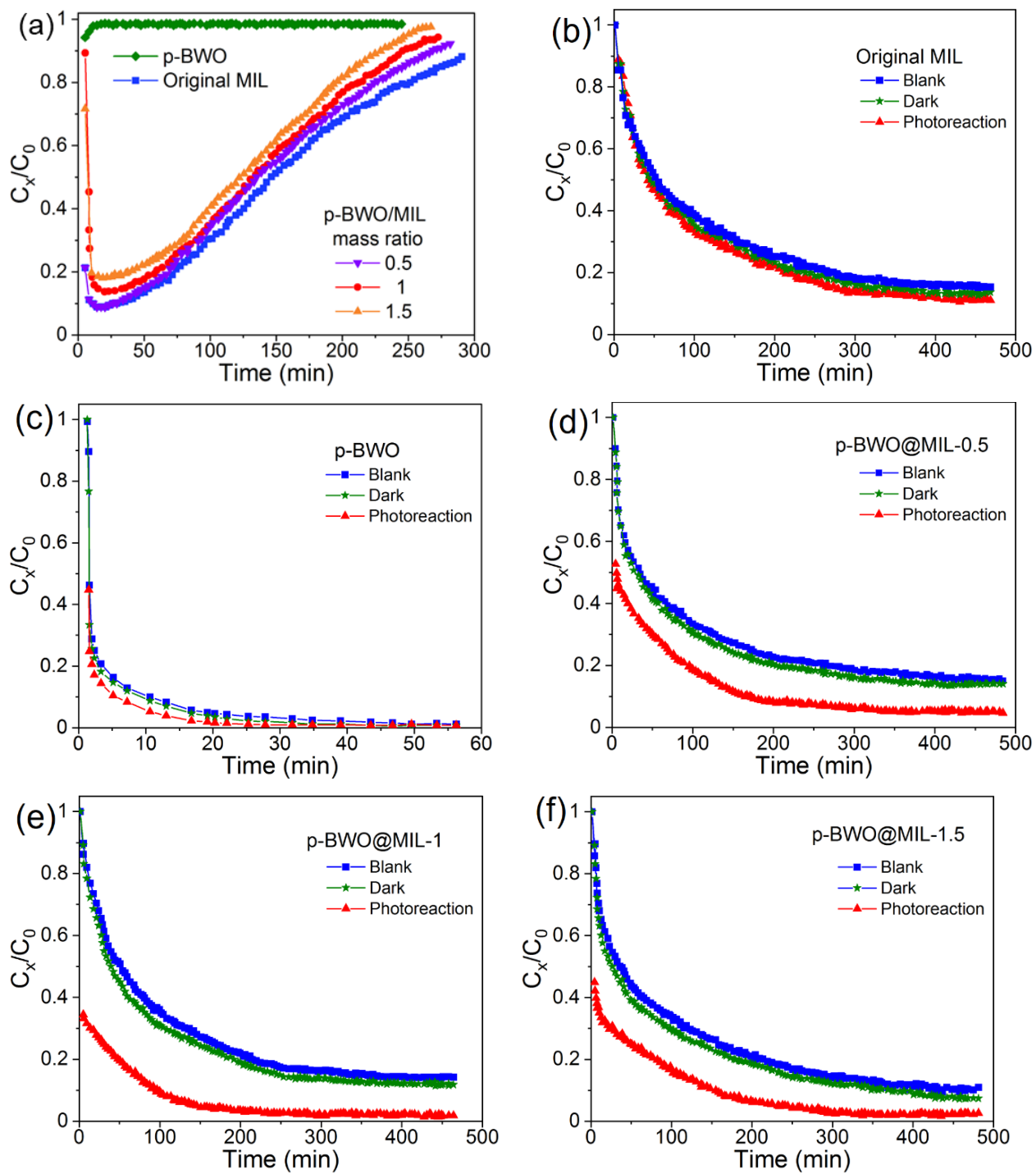


Figure 4. 7 Comparison of toluene conversion rates of p-BWO, MIL and p-BWO@MIL-0.5 (-1.5) coated MERV 13 electret media.

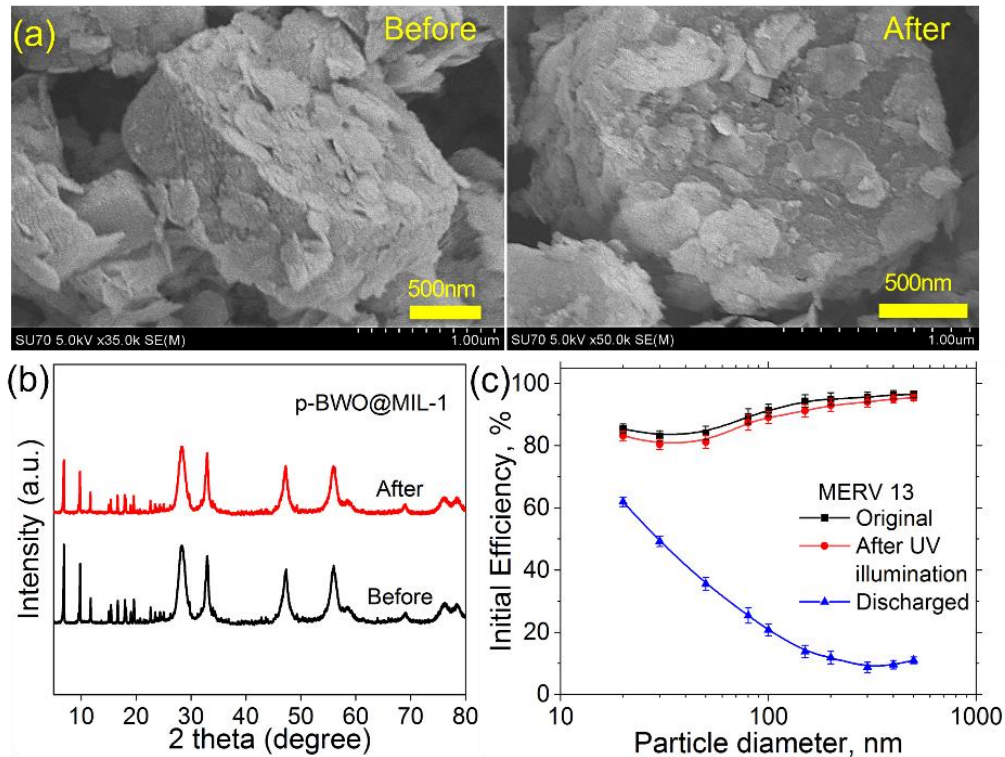


Figure 4. 8 Comparison of SEM images (a), XRD patterns (b) of p-BWO@MIL-1 before and after the toluene photocatalytic tests and filtration efficiencies (c) of original, UV treated, and IPA discharged MERV 13 filter media.

4.4 Conclusions

In this study, a representative MOF (MIL-125-NH₂) was successfully synthesized and coated with amorphous semiconductor p-BWO nanosheets to form a composite photocatalyst p-BWO@MIL-125-NH₂ (p-BWO@MIL). Then the composite photocatalyst was coated to a MERV 13 grade electret filter media to develop a photocatalytic PE-MOFilter for a simultaneous removal of PM_{2.5} and VOCs. The composite photocatalysts were characterized by SEM, XRD, UV-vis, photoluminescence and BET analysis. The characterization results demonstrated the successful synthesis of the composite photocatalyst p-BWO@MIL, as the p-BWO nanosheets formed an intimate contact on the surface of MOF MIL-125-NH₂. The PL spectrum of p-BWO demonstrated

this composite photocatalyst a promising photocatalytic activity. The XRD analysis for the crystallinity of p-BWO@MIL indicated a two-phase composition of MIL and p-BWO. The BET surface area of the PE-MOFilter also remained high ($1213 \text{ cm}^2 \text{ g}^{-1}$).

The newly fabricated PE-MOFilter was found to have an initial toluene adsorption efficiency of more than 80% and a comparable adsorption capacity to that of the MIL-125-NH₂ based E-MOFilter. The PM removal efficiency was found to remain higher than 85% indicating the coating of p-BWO@MIL on the MERV 13 electret media had a negligible degradation of fiber charge based on 10 wt% of coating.

A simple method was developed to evaluate the photocatalytic performance of the PE-MOFilter. The method compares the toluene desorption mass of PE-MOFilter right after saturation to that of PE-MOFilter after 16 hours of UV illumination. It was found the p-BWO@MIL-1 based PE-MOFilter displayed the best photodegradation rate of about 70%.

To conclude, this study is the first to combine the semiconductor/MOF particles and coat them to electret filter media (denoted as PE-MOFilter) for the simultaneous removal of PM and VOC with low pressure drop. We found out the promising photocatalytic performance of the p-BWO@MIL towards toluene removal. The semiconductor/MOF particles could be regenerated by UV illumination enabling sustainable gas purification and elongated life span of the PE-MOFilter. The physical and chemical characteristics of the semiconductor/MOF are analyzed and discussed for the reference of future development. However, more in-depth explorations are needed to unravel the PCO mechanisms of toluene degradation by the p-BWO@MIL coated electret filter, PE-MOFilter.

**Chapter 5. An empirical equation for quickly qualifying commercial N95
equivalent respirators**

Abstract

The COVID-19 pandemic has highlighted the significance of facepiece filtering respirators (FFRs), especially N95 and N95 equivalent respirators, as personal protective equipment (PPE) for reducing the risk of infection and disease transmission. However, the extensive prevalence of poor-performing N95 equivalent respirators has presented substantial obstacles to achieving this goal. It is essential that respirators have their advertised high filtration efficiencies (FEs) (i.e., FEs > 95%) in order to prevent individuals from getting and spreading the virus. Therefore, it is of great significance to measure/screen the efficiencies of these commercial respirators before distributing them to the end users. Although there have been studies evaluating mask efficiency, limited access to standardized facilities required by the National Institute for Occupational Safety & Health (NIOSH) testing protocol may lead to inaccuracies in efficiency measurements. Theoretical efficiency models can accurately predict FEs, but they require knowledge of various parameters, such as fiber diameter, thickness, packing density, charge density, and face velocity. The objective of this study is to develop an empirical equation to predict the FEs of commercial N95 equivalent respirators by using easily accessible and the most influential parameters. Hence, in this work, a standardized testing system was first developed in accordance with a NIOSH equivalent testing standard (i.e., GB2626-2006) to obtain the accurate efficiencies of 30 different commercial respirators. An empirical equation model was then developed to predict the filtration efficiency of minimum mask efficiency at the most penetrating particle size (MPPS) by using three easily accessible parameters: pressure drop, mask area, and surface potential. Results showed that the predicted efficiencies had less than 5% deviation from the experimental efficiencies, indicating the acceptability of the empirical equation model. This model was further validated using additional new mask samples. The ultimate goal of this study is to develop a simple, accessible, and fast

method for the evaluation of mask efficiency, which should enable widely available access to quantitatively benchmark respirator efficiency, thereby providing guidance for the general public in mask selection and practical use.

5.1 Introduction

Since the outbreak of COVID 19 pandemic, the novel coronavirus (SARS-CoV-2) causes millions of people infections and death due to its severe fatality rate and high airborne transmission rate (Dhand and Li 2020; Jayaweera et al. 2020; Prather et al. 2020). It is reported that the coronavirus is transmitted through the coronavirus-laden droplets and aerosols, which are released by sneezing, coughing, speaking, and breathing. These droplets and aerosols can travel up to 8 m, and, once desiccated, the residue or droplet nuclei may stay suspended for hours (CDC 2020a; Dhand and Li 2020), which extremely enhanced the transmission rate. To provide protection for individuals and prevent the high transmission rate of the coronavirus by droplets and aerosols, face masks and filtering facepiece respirators (FFRs) are required or highly recommended by Centers for Disease Control and Prevention, CDC, since the outbreak of the COVID 19 pandemic in March 2020 in the United States (CDC 2022). N95, KN95, FFP2, and KN94 respirators etc., whose filtration efficiencies are designed to be larger than 95%, are widely commercially available and affordable for the general public use.

It is of great significance that these FFRs have a good quality to protect the general public from getting and spreading viruses. It is worth noting, however, that according to the CDC, approximately 60% of KN95, the most widely available N95 equivalent respirators on the market that NIOSH evaluated during the COVID-19 pandemic in 2020 and 2021 did not meet the requirements i.e., filtration efficiency (FE) > 95% (CDC 2022; Brochot et al., 2020). In reaction to the unsatisfactory performance of FFRs, several studies have performed evaluation of the

filtration performance of commercially available FFRs (Schilling et al. 2021; Plana et al. 2021a; Duncan et al. 2021). As known, the testing protocols standardized by the National Institute for Occupational Safety and Health (NIOSH) require a series of equipment such as airflow regulator, aerosol generator, neutralizer, and particle counters, most of which are expensive devices in certified research lab and usually out of reach to the general public. Due to limited access to the facilities that the standardized testing protocols required for evaluating mask efficiency, many of their filtration tests were not strictly in compliance with N95 testing standards or the equivalent international requirements and thus, their efficiency results are either overestimated or underestimated (Schilling et al. 2021; Patra et al. 2022; Duncan et al. 2021; Stahl et al. 2021; Cai and Floyd 2020). In their tests, the particle size distribution (especially for particle size less than 300 nm), the charge status, and the deliquesce point of the water-soluble contents in the particles were usually not considered when determining the efficiencies. For instance, Plana et al. (2020) simplified filtration testing setup and procedures utilizing non-neutralized particles to challenge the filter, resulting in overestimated filtration efficiencies. Also, in their study, the filtration efficiencies of the filters are only based on the challenging particles larger than 300 nm and did not take the small particle sizes (< 300 nm) into account, which may result in the overestimated filtration efficiencies. Yim et al. (2020) evaluated the filtration efficiency of N95 and KN95 respirators against particles around 20–30 nm with the larger sizes up to about 150 nm, which were generated by a candle, due to their limited access to the collision-type atomizer. The authors did not consider the charges on the aerosols particles when determining the filtration efficiencies of the respirators, which may overestimate the efficiencies. As mentioned above, these simplified testing generated systematic errors when determining filtration efficiency. Therefore, to obtain accurate efficiency results, it is essential that the testing systems utilize the standardized facilities

required by NIOSH. On the other hand, given the limited access to these facilities, it is worth mentioning that in addition to experimentally evaluating mask efficiency, theoretical deposition models based on the single fiber theory can also be used to evaluate filtration efficiency (Chang et al., 2016). In general, theoretical models can accurately predict mask efficiency. However, the theoretical calculation can be complicated and time-consuming, as it requires knowing many parameters, e.g., fiber size, thickness, packing density, charge density, and face velocity. Besides, charge density is the most inaccessible parameter due to the complexity of charge figuration in the filters. Also, it is commonly seen that in many studies, only an estimated value of charge density was given to calculate efficiency (Hao et al., 2021). Based on the above mentioned, it is necessary to develop a fast and convenient method to evaluate mask efficiency. As is known, empirical equation models are a useful tool that can quickly provide reliable predictions and insights into complex systems and are often more accessible to non-experts than more theoretical models. Empirical equations are mathematical equations that describe the relationship between variables based on observations, data, or experimental results. These equations are selected because they fit experimental data and are useful for predicting outcomes. For example, a study by You et al. (2012) calculated indoor particle deposition velocity using a modified three-layer model and then generated an empirical equation based on the database. It was worth mentioning that limited work has been reported so far to develop empirical equation models to evaluate mask efficiency.

In this work, a standardized testing system in accordance with the NIOSH equivalent testing standards (e.g., GB2626-2006) was first developed to perform efficiency evaluation of 50 different commercial respirators. All the respirators were measured with their thickness, fiber size, packing density, surface potential, and filtration area. Then charge density was obtained through theoretical efficiency model. and was correlated with surface potential. We then developed an empirical

equation model to predict filtration efficiency of mask minimum efficiency at MPPS. To develop this equation, the three most easily accessible parameters, pressure drop, mask area and surface potential, were utilized. The predicted and experimental efficiencies were then compared with the experimental efficiency data. The model was further validated by using extra new mask samples. The objective of this study is to develop a simple and convenient method for quick evaluation of mask efficiency, which should enable widely available access to quantitatively benchmark mask efficiency, thereby providing guidance for the general public regarding mask selection and practical use.

5.2 Materials and Methods

5.2.1 Materials

The N95, KN95, KF94, and FFP2 respirators that were studied in this work were purchased from various sources, e.g., Amazon.com, Inc., Costco Wholesale Corp., Walmart, Inc., Kroger Co., and CVS Health Corp. 50 samples in this work were evaluated with their specifications and filtration performance. For convenience, only 30 out of 50 different FFRs samples were presented here and were labeled from #1 to #30. In addition, the extra new 5 respirator samples were named #A, #B, #C, #D, and #E for validation of the developed empirical equation model. The obtained specification of the samples will be shown later in Section 5.3.1. All the samples were measured with their thickness, packing density, fiber diameter, mask area, charge density and pressure drop under flow rate of 85 L min^{-1} . The thickness of filter layer was measured by Digital calipers. The packing density was attained through taking ratio of the fiber volume to total volume of the flat sheet media of respirators with a diameter of 47 mm. The effective fiber diameter was calculated through the empirical equation for pressure drop provided by Davies (1973). For determination

of mask area, it is to be noted that the different shape of the mask should be taken into account. This is because, in this study, the tested respirators were entirely mounted in the filter holder, while the respirators have slightly different shapes, which would cause slightly different filtration velocity over the samples, resulting in efficiency differences. Thus, to obtain the real mask area, the pressure drop of the respirator was measured for both its entire full filter at a flow rate of 85 L min⁻¹ and flat sheet media (5 cm in diameter) at a face velocity of 10 cm s⁻¹. Through the mathematical relationship between the pressure drop, face velocity, and filtration area, the real mask area was acquired. Charge density was determined through the theoretical deposition model based on the single fiber theory that was developed in the previous work in Chang et al. (2016). The specific procedures will be included in Section 5.2.2. The charge characteristic of a filter was also evaluated by surface potential via the electrostatic voltmeter (Model: Monroe 244A equipped with a 1017AE probe) and the details will be shown later in Section 5.2.3.

5.2.2 Theoretical deposition model

The theoretical deposition model was originally developed to be used to calculate filtration efficiency of filter media. The detailed theory can be referred to Chang et al. (2016) and Hinds (1999). To be brief, the theoretical particle penetration, P_{theo} , through the filter is usually calculated using the single fiber theory (Wang et al., 2007, 2011; Bahk et al., 2013):

$$P_{theo} = \exp\left(-\frac{4\alpha E_T t}{\pi d_f(1-\alpha)}\right) \quad (5.1)$$

where α is the solidity of the filter, t is the thickness of the filter, d_f is the fiber diameter in the filter media and E_T is the total single fiber efficiency. E_T is the total efficiency due to diffusion (E_D),

interception (E_R), interception of diffusing particles (E_{DR}), impaction (E_I) and electrostatic attraction (E_q) and determined as:

$$E_T = 1 - (1 - E_D)(1 - E_R)(1 - E_{DR})(1 - E_I)(1 - E_q). \quad (5.2)$$

The E_D , E_R , E_{DR} and E_I are calculated as (Wang et al. 2007, 2011):

$$E_D = 0.84\text{Pe}^{-0.43}, \quad (5.3)$$

$$E_R = \frac{1+R}{2\text{Ku}} \left[2\ln(1+R) - 1 + \alpha + \left(\frac{1}{1+R}\right)^2 \left(1 - \frac{\alpha}{2}\right) - \frac{\alpha}{2}(1+R)^2 \right], \quad (5.4)$$

$$E_{DR} = \frac{1.24R^{2/3}}{(\text{Ku}\times\text{Pe})^{1/2}}, \quad (5.5)$$

and

$$E_I = \frac{1}{(2\text{Ku})^2} [(29.6 - 28\alpha^{0.62})R^2 - 27.5R^{2.8}]\text{Stk}, \quad (5.6)$$

where Pe is the Peclet number, Ku is the Kuwabara hydrodynamic parameter, R is the ratio of particle diameter to the fiber diameter and Stk is the Stokes number. The Pe , Ku , and Stk are calculated as:

$$\text{Pe} = \frac{d_f U_0}{D}, \quad (5.7)$$

$$\text{Ku} = \frac{-\ln \alpha}{2} - \frac{3}{4} + \alpha - \frac{\alpha^2}{4}, \quad (5.8)$$

and

$$\text{Stk} = \frac{\rho_p d_p^2 C_c U_0}{18\mu d_f}, \quad (5.9)$$

where U_0 is face velocity, ρ_p is particle density (2.165 g cm^{-3}), d_p is the particle mobility diameter, C_c is the Cunningham slip correction factor and μ is the air viscosity (Ns m^{-2}).

In Eq. (5.1), E_q can be further calculated according to the depositions by the Coulombic force, $E_{qC}(n)$, and the depositions by dielectric polarization force, E_{qD} , as:

$$E_q = 1 - \left(1 - E_{qC}(n)\right) \left(1 - E_{qD}\right) \quad (5.10)$$

where $E_{qC}(n)$ is the function of number of charges, n , the particles carried. The $E_{qC}(n)$ and E_{qD} can be calculated as (Chang et al., 2015):

$$E_{qC}(n) = \left(\frac{1-\alpha}{Ku}\right)^{1/8} \frac{\pi N_{CD}}{1+2\pi N_{CD}^{1/4}} \quad (5.11)$$

N_{CD} is a dimensionless parameter for charged particles through bipolarly charged fibrous filter and defined as:

$$N_{CD} = \frac{c_c \sigma q}{3\pi\mu\varepsilon_0(1+\varepsilon_f)^2 d_p U_0}, \quad (5.12)$$

where σ is the charge density of the fiber ($C\ m^{-2}$), q is the carried charge of particle (C), ε_f is the fabric dielectric constant (1.5 for the polypropylene of electret media used in this study) and ε_0 is the permittivity of the vacuum ($8.85 \times 10^{-12}\ C^2\ N^{-1}\ m^{-2}$).

$$E_{qD} = \left(\frac{1-\alpha}{Ku}\right)^{2/5} \frac{\pi N_{DD}}{1+2\pi N_{DD}^{2/3}} \quad (5.13)$$

and

$$N_{DD} = \frac{2c_c \sigma^2 d_p^2}{3\mu\varepsilon_0(1+\varepsilon_f)^2 \tau^2 d_f U_0} \left(\frac{\varepsilon_p - 1}{\varepsilon_p + 2}\right), \quad (5.14)$$

where N_{DD} is a dimensionless parameter for uncharged particles through bipolarly charged fibrous filter, and ε_p is the relative permittivity of the particle, which is 4.86 in this study.

Therefore, the total theoretical electrostatic penetration should be:

$$P_{theo} = \sum_{n=-10}^{n=10} f(n) \times \exp\left(-\frac{4\alpha E_T(n)t}{\pi d_f(1-\alpha)}\right), n \text{ includes } 0, \quad (5.15)$$

and

$$E_T(n) = 1 - (1 - E_D)(1 - E_R)(1 - E_{DR})(1 - E_I)[1 - E_{qC}(n)](1 - E_{qD}) \quad (5.16)$$

As shown above, to obtain mask efficiency by using the theoretical deposition model involves many mathematical equations and calculations.

Here, it is seen that the charge density was embedded in these equations. To obtain an unknown charge density of filter, if all the other parameters in the equations are known, the charge density can be calculated. This means that all the other parameters need to be measured or determined, including mask efficiency, thickness, packing density, fiber diameter etc. Therefore, given the complexity of obtaining the charge density, it is necessary to find out easily accessible method to characterize the charge state of respirators. According to the mathematical relationship between surface potential and charge density (Antoniou et al., 2011), if the surface electric charge density σ , was assumed as uniformly distributed, the relationship between the two is possible to be correlated. The correlation results were shown in Section 5.3.3. In this work, all the theoretical efficiencies of the samples were obtained and compared with experimental efficiency data, to check the charge density of the samples.

5.2.3 Surface potential measurement

A Trek model 244A electrostatic voltmeter was used to measure the dipolar surface potential of the filter layer. This voltmeter uses a technique which nullifies the field in between the probe

and the filter, therefore does not affect the charge on the filter and thus the measurement (Sachinidou et al. 2018). Specifically, the potential V_p of the voltmeter probe is driven by the electronic circuitry of the instrument at the surface potential V of the monitored surface ($V_p = V$). Thus, the electric field in the airgap between the sample and the probe is nullified. This measurement configuration is equivalent to a capacitor:

$$C = \frac{Q}{V} = \frac{\epsilon_d A}{t}, \quad (5.17)$$

where, C is the capacitance of the capacitor, Q is the charge carried by the surface area A of the sample surface. The surface electric charge density σ , assumed as uniformly distributed, can be expressed as,

$$\sigma = V\epsilon_d/t \quad (5.18)$$

where V is the measured surface potential (i.e., potential difference between the vibrating sensor and the tested surface); ϵ_d is the permittivity of the sample between the electrode and the tested surface; t is the thickness of the sample (Kachi et al., 2011).

The potential at the surface of the sample is,

$$V = \sigma t/\epsilon_d, \quad (5.19)$$

and depends on the surface charge density σ , the thickness of the sample t , and its electric permittivity ϵ_d .

During the surface potential measurement, only the main filter layer of the respirators was measured, and it was positioned onto a grounded metal plate and a noncontact probe of the electrostatic voltmeter was placed 5 mm above the filter layer surface. The samples were in circular shape with a diameter of 5 cm. To obtain more representative and accurate results, 20 spots on the

surface of sample were measured to obtain the average surface potential. It is to be noted that the friction on the surface of filter layer should be avoided as much as possible during measurements. The measurements were repeated for 3 different circle pieces of each different filter medium. To validate the measured surface potential, we further correlate it with the charge density obtained through the theoretical deposition model, given their mathematical relationship, as will be shown in Section 5.3.3.

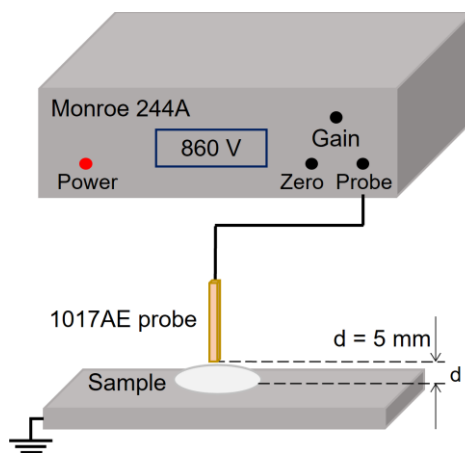


Figure 5. 1 Schematic of surface potential measurement by the electrostatic voltmeter.

5.2.4 Filtration efficiency testing

For assessing particle filtration efficiency, the NIOSH testing standard (TEB-APR-STP-0059) and its equivalent other international testing standards, e.g., GB2626-2006 from China were used based on a photometric method (i.e., mass-based method). The standard procedure for certification of N95 FFRs uses a specialized piece of equipment (TSI 8130 or 8130A) with photometric detection of the aerosol mass concentration upstream and downstream of the filter medium, rather than the size-selective particle counter. The result is a single value for filtration efficiency based on the amount of light scattered by the downstream aerosol over that scattered by the upstream aerosol. The TSI 8130 uses a laser with a wavelength of 780 nm. Light scattered from particles

whose dimensions are less than half the wavelength of the incident laser generally follows Rayleigh scattering, which scales as the sixth power of particle diameter, dp^6 . (Kulkarni et al., 2011) Therefore, the photometric measurement is heavily biased toward detection of the larger particles in a wide particle size distribution. Thus, a significant fraction of the number of particles in the challenging aerosol is essentially invisible to the instrument, which results in overestimation of filtration efficiency among the most efficient filters and underestimation among the least efficient filters within the mass-based method. This suggests that the NIOSH respirator testing protocol may not represent a more challenging aerosol test method for certifying respirators to be used in workplaces containing a wide size range of particles including nanoparticles (< 100 nm size). Therefore, to provide respirator efficiency in the worst scenario, i.e., filtration efficiency at MPPS, which is also the minimum efficiency, both of the mass and number-based efficiencies were evaluated in this work. The experimental setup for mass-based and number-based efficiency measurement was shown in Fig. 5.2.

To measure the mass-based filtration efficiency, GB2626-2006 testing protocol was used. As required by the protocol, the initial efficiency of a respirator was tested using NaCl particles with a number median diameter (NMD) of $0.075 \pm 0.020 \mu\text{m}$ and a geometric standard deviation (δ_g) less than 1.86, generated by a collision-type atomizer (Model 3079, TSI Inc., Shoreview, MN, USA). The NMD and δ_g were monitored by the scanning mobility particle sizer (SMPS, model 3936, TSI Inc., Shoreview, MN). The mass concentration (mg m^{-3}) of the NaCl was determined by the Dusttrak, a light-scattering photometer to measure the mass concentration of particles. The temperature and relative humidity (RH) of the flow in the filtration test were controlled with $25 \pm 5 \text{ }^\circ\text{C}$ and $30 \pm 10 \%$, respectively. The mass concentration of NaCl particles was controlled not to exceed 200 mg/m^3 in the testing process. This concentration of the upstream and downstream were

read from both Dusttrak and SMPS. The testing flow rate was $85 \pm 4 \text{ L min}^{-1}$ which was controlled by the vacuum pump and monitored by the flowmeter shown in Fig. 5.2. Plutonium (Po^{210}) was used to instantly neutralize the NaCl particles generated from the atomizer to be Boltzman charge equivalent.

Before real testing, the procedures as follows were carried out: (1) The scanning mobility particle sizer for monitoring the size distribution of challenging particles and the Dusttrak (model 8530, TSI Inc., Shoreview, MN) for determining the filtration efficiency were first calibrated according to the manuals from TSI. (2) 1~3 wt.% NaCl solution was prepared for the atomizer to generate NaCl particles with a number median diameter (NMD) of $0.075 \pm 0.020 \mu\text{m}$ and a geometric standard deviation (δ_g) less than 1.86. The NMD and δ_g were monitored by the SMPS every time before testing. Fig. 5.3 showed the particle size distribution that was used in this study. (3) The leak tests were performed by using the condensation particle counter (CPC) method. In brief, they are conducted by providing filtered air (with HEPA filters) to the sampling inlet of the CPC. A zero-particle count from the CPC and zero concentration from the Dusttrak is expected to be seen to ensure no leaks in these two instruments. (4) Before determining the filtration efficiency of the respirator, the filtration efficiency without placing the respirator tests were also conducted to ensure that there is no particle transport loss and no leak in the filter holder.

To determine the filtration efficiency of these FFRs, the Dusttrak having detection ranges of $0.001\sim 200 \text{ mg/m}^3$ was used as the particle detector to measure the mass concentration of upstream, C_{up} , and downstream particle concentration, C_{down} , of the respirator sample to determine the filtration efficiency of these FFRs. The filtration efficiency was calculated by using equation below,

$$\eta \% = \left(1 - \frac{C_{down}}{C_{up}} \right) \times 100\% \quad (5.20)$$

The C_{up} and C_{down} were obtained by switching the 3 way-valve to measure the particle concentration upstream and downstream of the respirator, respectively. The concentrations were the average values of 1 minute of sampling. C_{up} and C_{down} were directly recorded and averaged. The tests were run within 10 runs of efficiency measurements to find out the initial efficiency of these FFRs.

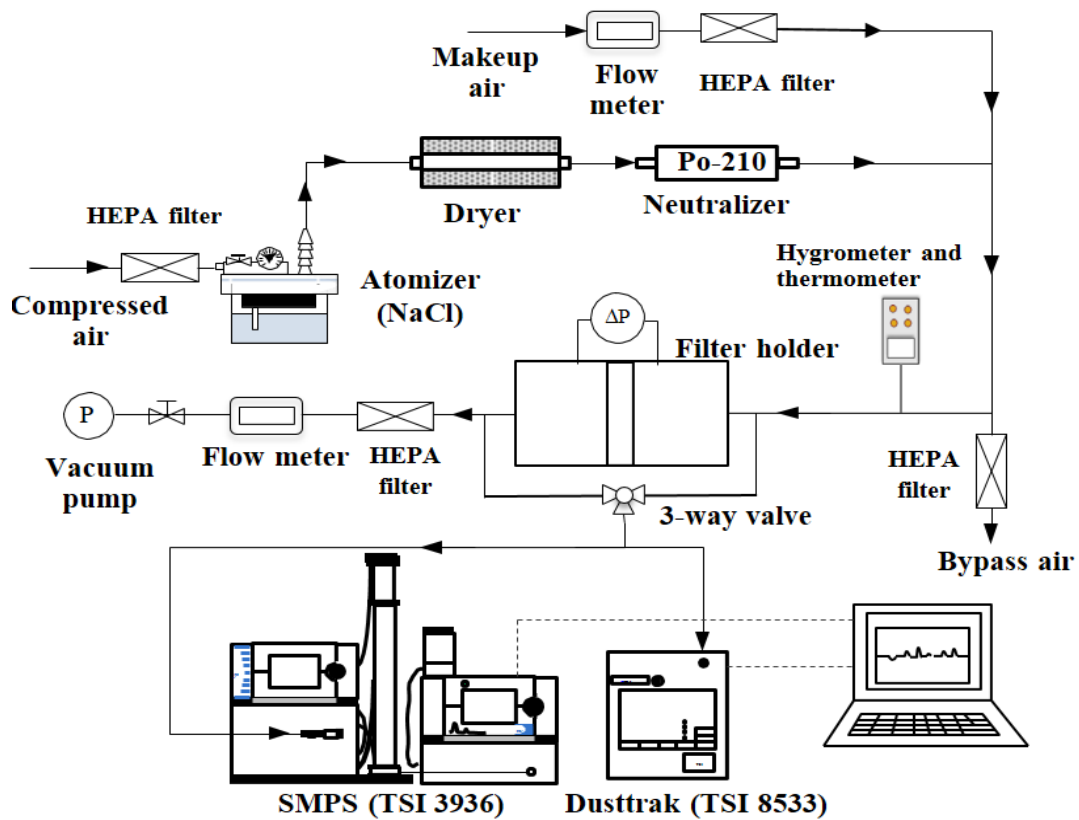


Figure 5. 2 Schematic diagram of experimental setup for measuring filtration efficiency of FFRs.

To measure the number-based filtration efficiency, the procedures are almost same to that of mass-based testing procedure. The only difference is that the size fractional particle concentration from upstream and downstream were recorded by SMPS. In addition, it is worth mentioning that because the efficiency testing was under an aerosol flow rate of 85 L min^{-1} , the upstream concentration of the particle source at smaller particle size and larger particles were low. For more

accurate measurements, different wt% NaCl solution were prepared to generate enough concentration of particles both in smaller particle size range (< 30 nm) and larger particle size range (> 300 nm). To obtain the representative results, measurements for filtration efficiency by every type FFRs were repeated at least four times.

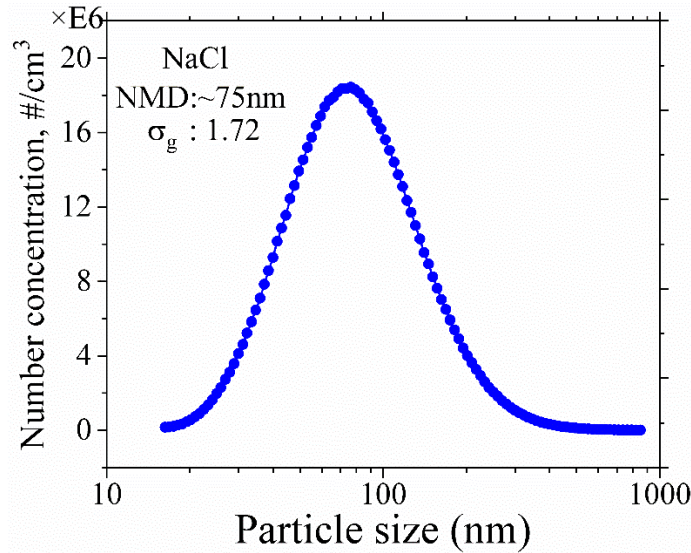


Figure 5. 3 Particle size distribution that was used in the filtration efficiency testing.

5.3 Results and Discussions

5.3.1 Specification of studied masks

Table 5.1 presents the specification of 30 tested respirators. In this table, the mass-based efficiency, number-based efficiency, MPPS, pressure drop, filtration area, thickness, fiber diameter, packing density, charge density and surface potential were included.

From this table, it is seen that respirators (#7, #9 and #23) had mass-based efficiencies larger than 95%, while their number-based efficiencies were smaller than 95%. For respirator #7, it had a very large pressure drop and its MPPS was larger than 100 nm, which demonstrates that it is a mechanical respirator. For respirators #9 and #23, their MPPS were smaller than 50 nm and their

pressure drops were smaller than 85 Pa at a face velocity of around 10 cm s⁻¹. Based on this information, it can be concluded that respirators #9 and #23 are electret respirators. It is clear that whether the mechanical or electret respirators, even though their mass-based efficiency larger than 95%, their number-based efficiency at MPPS can be smaller than 95%, which could pose a risk for people who works in nanoparticle industry, as their respirators could not provide filtration efficiencies of larger than 95%. This table also summarizes the pressure drop for the entire respirator at 85 L min⁻¹ and the flat sheet media at 10 cm s⁻¹. It is shown that the pressure drops range from 25 Pa to 185 Pa for masks entirely mounted in the holder. For the flat sheet media, it is from 37.5 Pa to 237.5 Pa. According to Davies (1973), pressure drop is directly proportional to thickness, face velocity, and inversely proportional to the square of the effective fiber diameter. Meanwhile, pressure drop is also positively related to packing density. Therefore, it is a very important factor to evaluate filtration performance of respirators. In addition, it can easily be seen that mask area varied from sample to sample and was shown to have correlation to mask efficiency. Therefore, it is also reasonable to use mask area as a factor to evaluate mask efficiency. Charge density and surface potential are two variables that describe the charging characteristics of the samples. Their value in this table exhibits their positive correlation, which is consistent with their mathematical relationship. The detailed correlation will be shown in Section 5.3.3. Obviously, charging characteristics of the respirators are significantly essential factors that need to be considered for evaluation of efficiency, especially for the electret respirators. By analyzing the specification of the respirators in Table 5.1, we chose pressure drop, mask area and surface potential as the three most easily accessible parameters of a respirator, together with its corresponding minimum efficiency, for developing an empirical equation model for predicting filtration efficiency.

Table 5. 1 Specification of the studied respirators in this work.

Label (#)	Mass η (%)	Number η at MPPS (%)	MPPS (nm)	Pressure drop ΔP (Pa)	ΔP @10cm/s (Pa)	Filtration area, S (cm ²)	Thickness t (mm)	Fiber diameter d_f (m)	Packing density α	Charge density σ ($\mu\text{C}/\text{m}^2$)	Average surface potential V (V)	Std
1	95.29	95.49	47.9	140	225	227.01	0.32	5.01E-06	0.1784	45	606.6	85.17
2	96.85	95.4	58.3	110	150	192.61	0.55	7.54E-06	0.1812	40	468.13	97.76
3	96.31	95.16	50.5	110	137.5	176.56	0.36	6.07E-06	0.1811	48	572.56	81.16
4	97.21	96.24	62.6	142.5	237.5	235.42	0.35	5.76E-06	0.1953	33	343.60	108.67
5	97.93	95.69	50.5	150	200	188.33	0.34	5.37E-06	0.1894	35	331.3	130.23
6	98.48	95.13	45.3	120	150	176.56	0.35	5.70E-06	0.1797	45	577.53	166.38
7	98.25	90.33	125	185	237.5	181.33	0.32	4.40E-06	0.1799	15	203.56	40.36
8	96.26	95.33	58.3	115	155	190.38	0.40	5.75E-06	0.1676	28	529.22	93.27
9	96.44	86.31	54.2	82.5	120	205.45	0.26	6.08E-06	0.1837	11	136.11	59.45
10	90.52	87.27	93.1	75	102.5	193.04	0.49	7.09E-06	0.1514	15	174.03	11.33
11	86.63	80.78	60.4	72.5	100	194.83	0.46	6.75E-06	0.1454	10	96.54	10.68
12	84.83	80.53	254	92.5	130	198.51	0.47	5.63E-06	0.1350	12	103.23	12.36
13	39.47	20.13	450	25	37.5	211.88	0.39	1.21E-05	0.1661	3	56.47	8.31
14	87.51	83.15	143	67.5	97.5	204.03	0.56	6.57E-06	0.1222	8.5	128.2	20.36
15	46.38	36	294.3	45	62.5	196.18	0.43	9.88E-06	0.1725	2	45.70	5.31
16	97.86	98.93	45.3	170	172.5	143.33	0.44	5.21E-06	0.1748	58	663.26	95.61
17	96.57	97.04	52.3	135	150	156.94	0.48	4.93E-06	0.1417	52	567.67	72.62
18	99.25	97.66	45.3	130	137.5	149.40	0.31	3.74E-06	0.1305	75	594.00	39.64
19	97.92	95.75	52.3	110	155	199.03	0.36	5.32E-06	0.1594	45	477.76	86.11
20	98.92	97.81	34	62.5	77.5	175.15	0.38	4.68E-06	0.0990	95	760.25	137.23
21	98.91	96.55	34	62.5	95	214.70	0.34	4.14E-06	0.0912	55	575.25	101.23
22	97.5	95.7	39.2	70	107.5	216.92	0.31	4.74E-06	0.1203	65	428.40	83.51
23	95.59	90.87	39.2	77.5	100	182.26	0.55	5.59E-06	0.1110	40	376.87	233.44
24	98.09	95.46	60.4	157.5	172.5	154.70	0.36	5.17E-06	0.1835	35	475.45	225.22
25	98.51	96.05	52.3	115	137.5	168.89	0.49	4.91E-06	0.1280	48	586.10	216.45
26	99.86	98.49	29.4	50	75	211.87	0.98	1.02E-05	0.1350	122	1393.06	203.69
27	99.56	98.67	39.2	107.5	127.5	167.53	0.40	5.61E-06	0.1579	85	824.30	125.36
28	90.36	84.58	69.8	67.5	95	198.80	0.41	8.88E-06	0.194	15	145.71	56.31
29	93.63	87.27	45.3	72.5	100	194.82	0.35	7.62E-06	0.1859	25	204.55	86.32
30	91.39	86.63	52.3	68.75	87.5	179.77	0.36	7.65E-06	0.1799	15	169.55	34.75

5.3.2 Comparison of the theoretical and experimental efficiency curve

As discussed previously, in this work, all the theoretical efficiencies of the samples were obtained and compared with experimental efficiency data, to check the charge density of the samples. Here, the theoretical and experimental efficiency curves for 4 representative N95 and N95 equivalent respirators (KN95, KF94, FFP2) were shown here to demonstrate the good agreement between the theoretically calculated efficiencies and experimentally obtained efficiencies in this work, thereby validating the charge density obtained through the theoretical model.

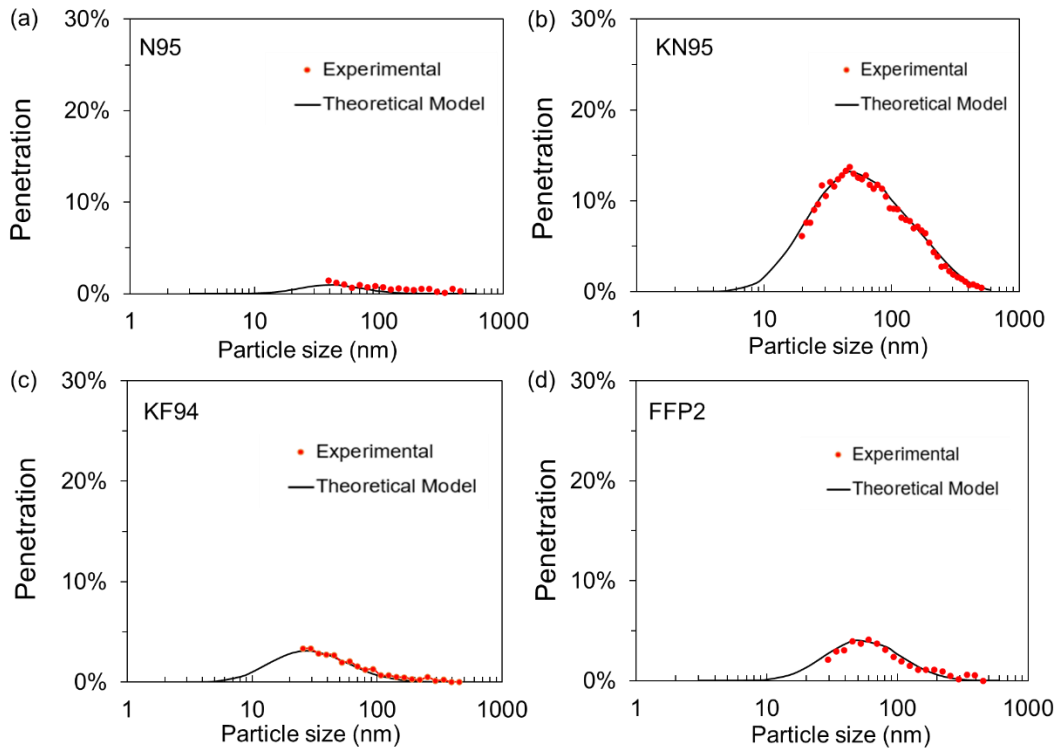


Figure 5. 4 Comparison of the theoretical and experimental efficiency curve of respirator #16 (N95), (a); respirator #9 (KN95), (b); respirator #21 (KF94), (c); respirator #24 (FFP2), (d) respirators.

5.3.3 Correlation of Surface potential and charge density

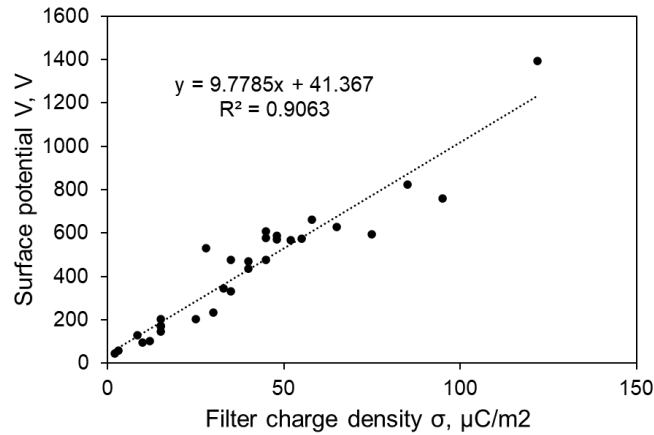


Figure 5. 5 Correlation of Surface potential and charge density of tested respirators.

As aforementioned, to obtain an unknown charge density of filter through the theoretical model, all the other parameters in the equations need to be measured or determined. To identify an easily accessible method for characterizing respirator charge state. It is possible to use surface potential to represent charge density as they have an inherent mathematical relationship (Antoniou et al., 2011), if the surface charge density σ , assumed as uniformly distributed. In addition, as shown in Table 5.1, the charge density and surface potential displayed a positive correlation. Here is the correlation result between the two variables. The correlation results exhibit that filter charge density was well correlated with surface potential, which is consistent with their mathematical relationship.

5.3.4 Empirical correlation of easily accessible parameters

For evaluating mask filtration performance, filtration efficiency and pressure drop are the most important aspects to consider. As pressure drop is easy to measure and it is directly proportional to thickness, face velocity, packing density and inversely proportional to the effective

fiber diameter. In this work, pressure drop was chosen as one of the parameters to be used to develop the empirical equation. As discussed previously, due to the slightly different shapes of respirators, mask area varied from sample to sample, and its value is also related to mask efficiency. Therefore, mask area was also chosen as a factor to evaluate mask efficiency. Further, as demonstrated by positive correlation between charge density and surface potential of the samples shown in Fig. 5.5, the surface potential was selected here to correlate with the efficiency. Therefore, to develop the empirical equation, the three most easily accessible parameters, pressure drop, mask area and surface potential, were utilized in this study. The developed equation was shown below,

$$z = a + b \ln x + c (\ln x)^2 + d (\ln x)^3 + e/y, \quad (5.21)$$

$a = 1.0036$, $b = -0.01725$, $c = 0.09753$, $d = 0.18983$, $e = -0.03338$, $r^2 = 0.96561$,

where z is the filtration efficiency (η), x is the normalized dot product of pressure drop (ΔP) and mask area (S) ($x = \frac{(\Delta P \cdot S)_{Sample}}{(\Delta P \cdot S)_{N95}}$), y is normalized surface potential V ($y = \frac{V_{Sample}}{V_{N95}}$).

Table 5.2 showed the correlation results of 30 samples. It can be seen here that the average deviation of efficiencies predicted by empirical equation is 1.5%. In addition, except for the low efficiency one respirator 15, whose predicted efficiency error is 7.8%, the maximum prediction error for all the other respirator samples, is smaller than 5%. This equation was future validated through new respirator samples.

Table 5. 2 The comparison of the predicted efficiency by empirical equation model with experimental efficiency

Label (#)	x	y	Z experimental	Z predicted	Residual
1	1.304466	0.914574	0.9549	0.973012	0.018112
2	0.869624	0.705802	0.954	0.960143	0.006143
3	0.797159	0.863251	0.9516	0.971684	0.020084
4	1.37695	0.518047	0.9624	0.949883	-0.01252
5	1.1595	0.499503	0.9569	0.937016	-0.01988
6	0.869628	0.870745	0.9513	0.969101	0.017801
7	1.376896	0.306908	0.9033	0.905556	0.002256
8	0.898626	0.797907	0.9533	0.964533	0.011233
9	0.695697	0.205215	0.8631	0.851026	0.010270
10	0.594249	0.262382	0.8727	0.885064	0.012364
11	0.579767	0.145554	0.8078	0.781964	-0.02584
12	0.753675	0.155635	0.8053	0.797568	-0.00773
13	0.217415	0.08514	0.2013	0.190527	-0.01077
14	0.565272	0.193288	0.8315	0.837297	0.005797
15	0.362349	0.068902	0.36	0.438659	0.078659
16	1	1	0.9893	0.970258	-0.01904
17	0.869615	0.855879	0.9704	0.968435	-0.00196
18	0.797175	0.895576	0.9766	0.973079	-0.00352
19	0.89861	0.720321	0.9575	0.960028	0.002528
20	0.449314	1.146232	0.9781	0.953534	-0.02457
21	0.550772	0.867307	0.9655	0.969858	0.004358
22	0.623243	0.645901	0.957	0.961855	0.004855
23	0.579766	0.568215	0.9087	0.952530	0.04383
24	1.000071	0.716838	0.9546	0.957075	0.002475
25	0.79719	0.883666	0.9605	0.972576	0.012076
26	0.43481	2.100323	0.9849	0.960095	-0.02481
27	0.739198	1.242801	0.9867	0.985661	-0.00104
28	0.550782	0.219688	0.8458	0.856416	0.010616
29	0.579737	0.308401	0.8727	0.903043	0.030343
30	0.507282	0.255635	0.8663	0.870359	0.004059

5.3.5 Validation and application of the developed empirical equation

The experimental data from extra new respirator samples was employed to further validate the empirical equation. Table 5.3 summarizes the measured pressure drop, mask area, average surface potential and minimum efficiency of the new respirator samples. The predicted efficiencies by applying the empirical equation model were compared with the experimental efficiencies. Results showed that the maximum error of the efficiency predicted by empirical equation to the experimental database was 2.40%, which is an acceptable error. Therefore, it is reasonable to conclude that the empirical equation model can be used for quick prediction of mask efficiency.

Table 5. 3 The new respirator samples that was used to validate the empirical equation.

New Sample (#)	Pressure drop ΔP (Pa)	Surface area (cm ²)	Measured average surface potential (V)	Measured η at MPPS (%)	Predicted η at MPPS (%)	Residual
A	67.5	204.03	142.08	83.01	85.41	0.0240
B	72.5	199.70	175.47	86.63	88.61	0.0198
C	170	145.40	750.08	98.41	97.10	-0.0131
D	110	199.03	477.25	95.75	96.00	0.0025
E	82.5	192.61	167.36	84.14	88.17	0.0403

The developed empirical equation was further applied to help design the mechanical filters. Respirator #7, #12, #13, #14 and #15 from Table 5.1 as representative mechanical respirators were selected. In Table 5.4, it is suggested that to make the minimum efficiency of the respirators larger than 95%, one can increase the corresponding pressure drop by adjusting the thickness, fiber diameter or packing density of the sample. Here, it is shown that to make the mechanical respirator #7, #12, #13, #14 and #15, have minimum efficiency larger than 95%, their current pressure drop should be increased by 51.2, 205.26, 315.68, 183.86 and 360.60 Pa, respectively.

Table 5. 4 Application of the empirical equation model for mechanical filters.

Label (#)	MPPS (nm)	Number η at MPPS (%)	Pressure drop ΔP (Pa)	Surface area (cm²)	Measured Average surface potential (V)	Predicted η at MPPS (%)	Predicted ΔP	ΔP increase
7	125	90.33	185	181.33	203.56	95.03	236.21	51.21
12	254	80.53	92.50	198.51	89.38	95.02	298.12	205.26
13	450	20.13	25	211.68	56.47	95.03	340.68	315.68
14	143	83.15	67.50	204.03	128.2	95.04	251.36	183.86
15	294	36.13	45	196.18	45.70	95.02	405.60	360.60

5.4 Conclusions

In summary, in this work, we first developed a standardized testing system in accordance with the NIOSH equivalent testing standards (e.g., GB2626-2006) to perform efficiency evaluation of 50 different commercial respirators. Both mass- and number-based efficiencies were evaluated. In addition, all the respirators were measured with their thickness, fiber size, packing density, surface potential, and filtration area. The surface potential was correlated with the charge density that was derived through the theoretical efficiency model. Findings demonstrated a strong correlation between filter charge density and surface potential. An empirical equation model for predicting filtration efficiency of minimum mask efficiency at most penetrating particle size (MPPS) was successfully developed. In this model, the three most readily available parameters were utilized: pressure drop, mask area, and surface potential. The predicted efficiencies obtained by empirical equation showed less than 5% deviation to the experimental efficiencies. The empirical equation was further validated by experimental efficiency data derived from additional new samples. The empirical equation was also successfully applied to help design the mechanical respirators. Overall, this work provided a simple and convenient method for quick evaluation of filtration efficiency, which should enable widely available access to quantitatively benchmark mask efficiency, thereby providing guidance for general public in terms of mask selection and practical use.

Chapter 6. Conclusions and Future Directions

6.1 Conclusions

In this dissertation, in the first section, a newly developed electret HVAC filter media coated with highly porous MOF particles, has been developed and shown to effectively remove fine particulate matter (PM_{2.5}) and volatile organic compounds (VOCs) simultaneously. The second section provides an empirical equation for quickly qualifying commercial respirators. Much effort was put into the sustainable design of MOFs-based materials coated electret filters and the fast evaluation of facepiece filtering respirators. The detailed conclusions from this dissertation are listed below.

6.1.1 Development of MOFs-based materials coated electret filter media for indoor air pollution control

The E-MOFilter, a newly developed electret filter media coated with highly porous MOF particles, has been shown to effectively remove fine particulate matter (PM_{2.5}) and volatile organic compounds (VOCs) simultaneously. The MOF coating on the electret filter has been demonstrated to minimize the increase in pressure drop (ΔP) and degradation of the electret's charge while maintaining PM holding capacities close to the clean electret. The developed E-MOFilter with MIL-125-NH₂ particle coating not only had a decent toluene removal efficiency (>80%) but also maintained its original PM_{2.5} holding capacity. In addition, to mitigate the effects of humidity on VOC removal, the five modification methods to alter MIL-125-NH₂ from inherent hydrophilic into hydrophobic were introduced and studied. The modification method of an external coating of polydimethylsiloxane (PDMS) generated the greatest results, with remarkable initial VOC removal efficiency and the longest VOC breakthrough time at a relative humidity of 50%. Furthermore, a composite photocatalyst (semiconductor@MOF) coated electret filter, designated PE-MOFilter, was developed and found to effectively photodegrade VOC pollutants through the synergistic action of adsorption and photocatalytic oxidation. (PCO). In addition, it was

demonstrated that the proposed photocatalytic PE-MOF filter maintained its high PM filtration efficiency.

In addition to the enhanced performance of novel electret HVAC filters, fundamental interactions between volatile organic compounds and MOF-based materials were also discussed. Specifically, the pore-filling mechanism and hydrogen bonding played significant roles in the adsorption process of VOCs. In addition, plausible factors that promoted photocatalytic efficiency, such as the increased light absorption area, rapid interfacial charge transfer, and enhanced charge carrier separation, were discussed.

6.1.2 Development of an empirical equation for quick respirator efficiency evaluation for individual health protection

N95 and N95 equivalent respirators were measured with their thickness, fiber size, packing density, surface potential, and filtration area. Their efficiencies were evaluated by mass- and number-based methods, respectively. The surface potential was correlated with the charge density derived through the theoretical efficiency model. Findings demonstrated a strong correlation between filter charge density and surface potential. An empirical equation model for predicting the filtration efficiency of minimum mask efficiency at most penetrating particle size was successfully developed. In this model, the three most readily available parameters were utilized: pressure drop, mask area, and surface potential. The predicted efficiencies obtained by empirical equation showed less than 4% deviation to the experimental data. The empirical equation was further validated by experimental efficiency data derived from additional samples. Overall, by providing an empirical equation for fast evaluation of filtration efficiency, this work provides an easily accessible screening method for qualifying respirators so that the general public can make informed decisions about the use of respirators for individual health protection and indoor air pollution control.

6.2 Future Directions

Despite the fact that multiple achievements have been demonstrated in this dissertation and an extensive amount of related work has been reported in previous studies in an effort for indoor air pollution control, further research continues to be necessary in the areas described below:

- (1) Although the examples presented here showed significantly improved efficiency for indoor air pollutants control, the long-term stability and durability of MOF coated electret media under various environmental conditions and usage scenarios is still a concern. Further research can be conducted to explore new MOF materials with improved adsorption capacities, selectivity, and stability, to enhance the performance of MOF coated electret media.
- (2) The production and integration of MOFs with electret media might involve increased costs compared to traditional filters, which could limit their widespread adoption. Therefore, developing more cost-effective methods for MOF synthesis and integration with electret media can help make the technology more accessible and affordable, thereby encouraging its broad adoption.
- (3) Although the empirical equation model developed in this work predicts mask filtration efficiency with less than 4% deviations, the model often needs to be updated and adjusted as new data becomes available. This means that maintaining the model and ensuring its accuracy can be resource intensive. Therefore, continuously updating and refining the model by incorporating new research findings, material innovations, and improved understanding of mask filtration mechanisms can help enhance its predictive capabilities. In addition, to improve the accuracy of the empirical model, advanced statistical methods and machine learning techniques can also be utilized.

Appendix: Vita

YU ZHANG

zhangy74@vcu.edu; 804-664-9560

Education

Ph.D., Mechanical and Nuclear Engineering	Aug 2018 – May 2023
Virginia Commonwealth University – Richmond, VA	
M.S., Safety Engineering	Sep 2016 - Apr 2019
Northeastern University – Shenyang, China	
B.S., Safety Engineering	Sep 2012 - July 2016
Shenyang University of Chemical Technology – Shenyang, China	

Accomplishments

- 4 peer-reviewed journal papers.
- **Zhang, Y.**, He, X., Zhu, Z., Wang, W. N., & Chen, S. C. (2020). Simultaneous removal of VOCs and PM_{2.5} by metal-organic framework coated electret filter media. *Journal of Membrane Science*, 618, 118629; <https://doi.org/10.1016/j.memsci.2020.118629>
- **Zhang, Y.**, Zhu, Z., Wang, W. N., & Chen, S. C. (2022). Mitigating the relative humidity effects on the simultaneous removal of VOCs and PM_{2.5} of a metal-organic framework coated electret filter. *Separation and Purification Technology*, 285, 120309; <https://doi.org/10.1016/j.seppur.2021.120309>
- **Zhang, Y.**, Zhu, Z., Wang, W.N., Chen, S.C. (2023). A Novel Sustainable Semiconductor/Metal-organic Framework Coated Electret Filter for Simultaneous Removal of PM_{2.5} and VOCs. *Aerosol Air Qual. Res.* 23, 220445; <https://doi.org/10.4209/aaqr.220445>
- Zhu, Z., **Zhang, Y.**, Bao, L., Chen, J., Duan, S., Chen, S. C., & Wang, W. N. (2021). Self-decontaminating nanofibrous filters for efficient particulate matter removal and airborne bacteria inactivation. *Environmental Science: Nano*, 8(4), 1081-1095; <https://doi.org/10.1039/D0EN01230K>
- 1 US Patent, Removal of VOCs, and Fine Particulate Matter by Metal Organic Frameworks Coated Electret Media (E-MOFilter), Publication No. 20220274040, Publication Date: Jan 9, 2022.
- 7 presentations at international conferences (Semi-Annual Review Meeting, Center for Filtration Research (CFR), University of Minnesota), 2019-2022
- Graduate School Dissertation Assistantship, Spring, 2023.
- Mentorship for undergraduates on laboratory techniques and research fundamentals, 2020-2021
- National Endeavor Fellowship, China, 2013-2014, (top 1% in the school)
- Liaoning Provincial Government Scholarship, 2014-2015, (top 1% in the school)
- School-level, multiple first/second-prize fellowship, 2012-2018

Skills

- Proficient in nanoparticles synthesis, liquid filtration, PM2.5 filtration, VOCs adsorption and photocatalytic degradation.
- Experienced in multiple material characterization techniques, including XRD, SEM, EDX, XPS, FTIR, Raman, BET analysis, Gas Chromatography (GC), High Performance Liquid Chromatography (HPLC).
- Skilled in aerosol sampling and instrumentation, e.g., Scanning Mobility Particle Sizer (SMPS), Ultrafine Condensation Particle Counter (UCPC), Photometer etc.

Reference:

- Antoniou, A., Dascalescu, L., Vacar, I.-V., Plopeanu, M.-C., Tabti, B., Teodorescu, H.-N.L. (2011). Surface Potential Versus Electric Field Measurements Used to Characterize the Charging State of Nonwoven Fabrics. *IEEE Trans. Ind. Appl.* 47, 1118–1125. <https://doi.org/10.1109/TIA.2011.2127432>
- Alvaro, M., Carbonell, E., Ferrer, B., Llabrés i Xamena, F.X., and Garcia, H. (2007). Semiconductor Behavior of a Metal-Organic Framework (MOF). *Chem. – Eur. J.* 13 (18):5106–5112. doi:10.1002/chem.200601003.
- Ardizzone, S., Bianchi, C.L., Cappelletti, G., Naldoni, A., Pirola, C. (2008). Photocatalytic Degradation of Toluene in the Gas Phase: Relationship between Surface Species and Catalyst Features. *Environ. Sci. Technol.* 42, 6671–6676. <https://doi.org/10.1021/es8009327>
- Augugliaro, V., Coluccia, S., Loddo, V., Marchese, L., Martra, G., Palmisano, L., and Schiavello, M. (1999). Photocatalytic oxidation of gaseous toluene on anatase TiO₂ catalyst: mechanistic aspects and FT-IR investigation. *Appl. Catal. B Environ.* 20 (1):15–27. doi:10.1016/S0926-3373(98)00088-5.
- Bahk, Y., Buha, J., and Wang, J. (2013). Determination of Geometrical Length of Airborne Carbon Nanotubes by Electron Microscopy, Model Calculation and Filtration Method. *Aerosol Sci. Technol.*, 47:776–784.
- Barick, P., Prasad Saha, B., Mitra, R., Joshi, S.V. (2015). Effect of concentration and molecular weight of polyethylenimine on zeta potential, isoelectric point of nanocrystalline silicon carbide in aqueous and ethanol medium. *Ceram. Int.* 41, 4289–4293. <https://doi.org/10.1016/j.ceramint.2014.11.115>
- Bodas, D. and Khan-Malek, C. (2006). Formation of more stable hydrophilic surfaces of PDMS by plasma and chemical treatments. *Microelectron. Eng., Micro- and Nano-Engineering MNE* 2005 83 (4):1277–1279. doi:10.1016/j.mee.2006.01.195.
- Brasche, S. and Bischof, W. (2005). Daily time spent indoors in German homes – Baseline data for the assessment of indoor exposure of German occupants. *Int. J. Hyg. Environ. Health* 208 (4):247–253. doi:10.1016/j.ijheh.2005.03.003.
- Brochot, C., Saidi, M., and Bahloul, A. (2020). Qualitative Knowledge of Filtering Facepiece Respirators for Filtration Performance Tests during the COVID-19 Pandemic -Journal of the International Society for Respiratory Protection-. *Journal of the International Society for Respiratory Protection* 37:94–107.

- Cai, C. and Floyd, E.L. (2020). Effects of Sterilization With Hydrogen Peroxide and Chlorine Dioxide Solution on the Filtration Efficiency of N95, KN95, and Surgical Face Masks. *JAMA Netw. Open* 3 (6): e2012099. doi:10.1001/jamanetworkopen.2020.12099.
- Cao, X., Chen, Z., Lin, R., Cheong, W.-C., Liu, S., Zhang, J., Peng, Q., Chen, C., Han, T., Tong, X., Wang, Y., Shen, R., Zhu, W., Wang, D., and Li, Y. (2018). A photochromic composite with enhanced carrier separation for the photocatalytic activation of benzylic C–H bonds in toluene. *Nat. Catal.* 1 (9):704–710. doi:10.1038/s41929-018-0128-z.
- CDC (2022). Masks and Respirators Cent. Dis. Control Prev. Available at <https://www.cdc.gov/coronavirus/2019-ncov/prevent-getting-sick/types-of-masks.html> (Accessed 29 January 2022).
- CDC (2020). Coronavirus Disease 2019 (COVID-19) Cent. Dis. Control Prev. Available at <https://www.cdc.gov/coronavirus/2019-ncov/science/science-briefs/masking-science-sars-cov2.html> (Accessed 19 December 2021).
- Chang, D.-Q., Chen, S.-C., Fox, A.R., Viner, A.S., and Pui, D.Y.H. (2015). Penetration of Sub-50 nm Nanoparticles Through Electret HVAC Filters Used in Residence. *Aerosol Sci. Technol.* 49 (10):966–976. doi:10.1080/02786826.2015.1086723.
- Chang, D.-Q., Chen, S.-C., and Pui, D.Y.H. (2016). Capture of Sub-500 nm Particles Using Residential Electret HVAC Filter Media-Experiments and Modeling. *Aerosol Air Qual. Res.* 16 (12):3349–3357. doi:10.4209/aaqr.2016.10.0437.
- Chang, D.-Q., Tien, C.-Y., Peng, C.-Y., Tang, M., and Chen, S.-C. (2019). Development of composite filters with high efficiency, low pressure drop, and high holding capacity PM2.5 filtration. *Sep. Purif. Technol.* 212:699–708. doi:10.1016/j.seppur.2018.11.068.
- Chen, Q., Sun, H., Zhang, J., Xu, Y., and Ding, Z. (2019). The hematologic effects of BTEX exposure among elderly residents in Nanjing: a cross-sectional study. *Environ. Sci. Pollut. Res.* 26 (11):10552–10561. doi:10.1007/s11356-019-04492-9.
- Chen, Y., Zhang, S., Cao, S., Li, S., Chen, F., Yuan, S., Xu, C., Zhou, J., Feng, X., Ma, X., Wang, B. (2017). Roll-to-Roll Production of Metal-Organic Framework Coatings for Particulate Matter Removal. *Adv. Mater.* 29, 1606221. <https://doi.org/10.1002/adma.201606221>
- Das, D., Gaur, V., and Verma, N. (2004). Removal of volatile organic compound by activated carbon fiber. *Carbon* 42 (14):2949–2962. doi:10.1016/j.carbon.2004.07.008.
- DeCoste, J.B. and Peterson, G.W. (2014). Metal–Organic Frameworks for Air Purification of Toxic Chemicals. *Chem. Rev.* 114 (11):5695–5727. doi:10.1021/cr4006473.

- Dong, H., Zeng, G., Tang, L., Fan, C., Zhang, C., He, X., He, Y. (2015). An overview on limitations of TiO₂-based particles for photocatalytic degradation of organic pollutants and the corresponding countermeasures. *Water Res.* 79, 128–146. <https://doi.org/10.1016/j.watres.2015.04.038>
- Dou, Y., Zhang, W., and Kaiser, A. (2020). Electrospinning of Metal–Organic Frameworks for Energy and Environmental Applications. *Adv. Sci.* 7 (3):1902590. doi:10.1002/advs.201902590.
- Du, W. and Wang, G. (2020). Indoor Air Pollution was Nonnegligible during COVID-19 Lockdown. *Aerosol Air Qual. Res.* 20 (9):1851–1855. doi:10.4209/aaqr.2020.06.0281.
- Duncan, S., Bodurtha, P., and Naqvi, S. (2021). The protective performance of reusable cloth face masks, disposable procedure masks, KN95 masks and N95 respirators: Filtration and total inward leakage. *PLOS ONE* 16 (10):e0258191. doi:10.1371/journal.pone.0258191.
- Dhand, R. and Li, J. (2020). Coughs and Sneezes: Their Role in Transmission of Respiratory Viral Infections, Including SARS-CoV-2. *Am. J. Respir. Crit. Care Med.* 202 (5):651–659. doi:10.1164/rccm.202004-1263PP.
- Drewnick, F., Pikmann, J., Fachinger, F., Moormann, L., Sprang, F., and Borrmann, S. (2021). Aerosol filtration efficiency of household materials for homemade face masks: Influence of material properties, particle size, particle electrical charge, face velocity, and leaks. *Aerosol Sci. Technol.* 55 (1):63–79. doi:10.1080/02786826.2020.1817846.
- Ereth, M.H., Fine, J., Stamatatos, F., Mathew, B., Hess, D., and Simpser, E. (2021). Healthcare-associated infection impact with bioaerosol treatment and COVID-19 mitigation measures. *J. Hosp. Infect.* 116:69–77. doi:10.1016/j.jhin.2021.07.006.
- Fujishima, A., Honda, K. (1972). Electrochemical Photolysis of Water at a Semiconductor Electrode. *Nature* 238, 37–38. <https://doi.org/10.1038/238037a0>
- Furukawa, H., Cordova, K.E., O’Keeffe, M., and Yaghi, O.M. (2013). The Chemistry and Applications of Metal-Organic Frameworks. *Science*.
- Gao, Z., Wang, J., Muhammad, Y., Zhang, Y., Shah, S.J., Hu, Y., Chu, Z., Zhao, Zhongxing, and Zhao, Zhenxia (2020). Enhanced moisture-resistance and excellent photocatalytic performance of synchronous N/Zn-decorated MIL-125(Ti) for vaporous acetaldehyde degradation. *Chem. Eng. J.* 388:124389. doi:10.1016/j.cej.2020.124389.

- Gustafson, P., Östman, C., and Sällsten, G. (2008). Indoor levels of polycyclic aromatic hydrocarbons in homes with or without wood burning for heating. *Environ. Sci. Technol.* 42 (14):5074–5080.
- Hao, J., Passos de Oliveira Santos, R., and Rutledge, G.C. (2021). Examination of Nanoparticle Filtration by Filtering Facepiece Respirators During the COVID-19 Pandemic. *ACS Appl. Nano Mater.* 4 (4):3675–3685. doi:10.1021/acsanm.1c00139.
- He, X. and Wang, W.-N. (2018). MOF-based ternary nanocomposites for better CO₂ photoreduction: roles of heterojunctions and coordinatively unsaturated metal sites. *J. Mater. Chem. A* 6 (3):932–940. doi:10.1039/C7TA09192C.
- Health, C. for D. and R. (2021). Update: FDA Recommends Transition from Use of Non-NIOSH-Approved and Decontaminated Disposable Respirators - Letter to Health Care Personnel and Facilities. FDA.
- Hinds, W.C. (1999). *Aerosol Technology: Properties, Behavior, and Measurement of Airborne Particles*. John Wiley & Sons.
- Huang, Q., Hu, Y., Pei, Y., Zhang, J., and Fu, M. (2019). In situ synthesis of TiO₂@NH₂-MIL-125 composites for use in combined adsorption and photocatalytic degradation of formaldehyde. *Appl. Catal. B Environ.* 259:118106. doi:10.1016/j.apcatb.2019.118106.
- Huang, K., Song, J., Feng, G., Chang, Q., Jiang, B., Wang, Jun, Sun, W., Li, H., Wang, Jinming, and Fang, X. (2018). Indoor air quality analysis of residential buildings in northeast China based on field measurements and longtime monitoring. *Build. Environ.* 144:171–183. doi:10.1016/j.buildenv.2018.08.022.
- He, X., Fang, H., Gosztola, D.J., Jiang, Z., Jena, P., Wang, W.-N. (2019). Mechanistic Insight into Photocatalytic Pathways of MIL-100(Fe)/TiO₂ Composites. *ACS Appl. Mater. Interfaces* 11, 12516–12524. <https://doi.org/10.1021/acscami.9b00223>
- He, X., Wang, W.-N. (2018). MOF-based ternary nanocomposites for better CO₂ photoreduction: roles of heterojunctions and coordinatively unsaturated metal sites. *J. Mater. Chem. A* 6, 932–940. <https://doi.org/10.1039/C7TA09192C>
- Hu, Q., Di, J., Wang, B., Ji, M., Chen, Y., Xia, J., Li, H., Zhao, Y. (2019). In-situ preparation of NH₂-MIL-125(Ti)/BiOCl composite with accelerating charge carriers for boosting visible light photocatalytic activity. *Appl. Surf. Sci.* 466, 525–534. <https://doi.org/10.1016/j.apsusc.2018.10.020>

- Irokawa, Y., Morikawa, T., Aoki, K., Kosaka, S., Ohwaki, T., and Taga, Y. (2006). Photodegradation of toluene over TiO_2-xN_x under visible light irradiation. *Phys. Chem. Chem. Phys.* 8 (9):1116–1121. doi:10.1039/B517653K.
- Jafari, S., Ghorbani-Shahna, F., Bahrami, A., and Kazemian, H. (2018). Adsorptive removal of toluene and carbon tetrachloride from gas phase using Zeolitic Imidazolate Framework-8: Effects of synthesis method, particle size, and pretreatment of the adsorbent. *Microporous Mesoporous Mater.* 268:58–68. doi:10.1016/j.micromeso.2018.04.013.
- Jayaweera, M., Perera, H., Gunawardana, B., and Manatunge, J. (2020). Transmission of COVID-19 virus by droplets and aerosols: A critical review on the unresolved dichotomy. *Environ. Res.* 188:109819. doi:10.1016/j.envres.2020.109819.
- Jiang, C., Li, S., Zhang, P., and Wang, J. (2013). Pollution level and seasonal variations of carbonyl compounds, aromatic hydrocarbons and TVOC in a furniture mall in Beijing, China. *Build. Environ.* 69:227–232. doi:10.1016/j.buildenv.2013.08.013.
- Jiang, X.-Q., Mei, X.-D., and Feng, D. (2016). Air pollution and chronic airway diseases: what should people know and do? *J. Thorac. Dis.* 8 (1). doi:10.3978/j.issn.2072-1439.2015.11.50.
- Jo, W.-K. and Yang, C.-H. (2009). Granular-activated carbon adsorption followed by annular-type photocatalytic system for control of indoor aromatic compounds. *Sep. Purif. Technol.* 66 (3):438–442. doi:10.1016/j.seppur.2009.02.014.
- Kachi, M., Nemamcha, M., Tabti, B., Dascalescu, L. (2011). Comparison between three measurement methods for characterizing the charge state of granular insulating materials. *J. Electrostat.* 69, 394–400. <https://doi.org/10.1016/j.elstat.2011.05.002>
- Kawase, Y., Isaka, Y., Kuwahara, Y., Mori, K., Yamashita, H. (2019). Ti cluster-alkylated hydrophobic MOFs for photocatalytic production of hydrogen peroxide in two-phase systems. *Chem. Commun.* 55, 6743–6746. <https://doi.org/10.1039/C9CC02380A>
- Kim, B., Lee, Y.-R., Kim, H.-Y., Ahn, W.-S. (2018a). Adsorption of volatile organic compounds over MIL-125-NH₂. *Polyhedron* 154, 343–349. <https://doi.org/10.1016/j.poly.2018.08.010>
- Kim, J.M., Kim, J.H., Lee, C.Y., Jerng, D.W., Ahn, H.S. (2018b). Toluene and acetaldehyde removal from air on to graphene-based adsorbents with micro-sized pores. *J. Hazard. Mater.* 344, 458–465. <https://doi.org/10.1016/j.jhazmat.2017.10.038>
- Kim, K.-D., Park, E.J., Seo, H.O., Jeong, M.-G., Kim, Y.D., Lim, D.C. (2012). Effect of thin hydrophobic films for toluene adsorption and desorption behavior on activated carbon fiber

- under dry and humid conditions. *Chem. Eng. J.* 200–202, 133–139. <https://doi.org/10.1016/j.cej.2012.06.044>
- Kim, S.-N., Kim, J., Kim, H.-Y., Cho, H.-Y., Ahn, W.-S. (2013). Adsorption/catalytic properties of MIL-125 and NH₂-MIL-125. *Catal. Today* 204, 85–93. <https://doi.org/10.1016/j.cattod.2012.08.014>
- Klepeis, N.E., Nelson, W.C., Ott, W.R., Robinson, J.P., Tsang, A.M., Switzer, P., Behar, J.V., Hern, S.C., Engelmann, W.H. (2001). The National Human Activity Pattern Survey (NHAPS): a resource for assessing exposure to environmental pollutants. *J. Expo. Anal. Environ. Epidemiol.* 11, 231–252. <https://doi.org/10.1038/sj.jea.7500165>
- K. Tanabe, K., M. Cohen, S. (2011). Postsynthetic modification of metal–organic frameworks—a progress report. *Chem. Soc. Rev.* 40, 498–519. <https://doi.org/10.1039/C0CS00031K>
- Kulkarni, P., Baron, P.A., Willeke, K. (2011). *Aerosol Measurement: Principles, Techniques, and Applications*. John Wiley & Sons.
- Li, X., Zhu, Z., Zhao, Q., and Wang, L. (2011). Photocatalytic degradation of gaseous toluene over ZnAl₂O₄ prepared by different methods: A comparative study. *J. Hazard. Mater.* 186 (2):2089–2096. doi:10.1016/j.jhazmat.2010.12.111.
- Li, X., Le, Z., Chen, X., Li, Z., Wang, W., Liu, X., Wu, A., Xu, P., and Zhang, D. (2018). Graphene oxide enhanced amine-functionalized titanium metal organic framework for visible-light-driven photocatalytic oxidation of gaseous pollutants. *Appl. Catal. B Environ.* 236:501–508. doi:10.1016/j.apcatb.2018.05.052.
- Li, S., Chen, D.-R., Zhou, F., and Chen, S.-C. (2020). Effects of relative humidity and particle hygroscopicity on the initial efficiency and aging characteristics of electret HVAC filter media. *Build. Environ.* 171:106669. doi:10.1016/j.buildenv.2020.106669.
- Liu, Q., Low, Z.-X., Li, L., Razmjou, A., Wang, K., Yao, J., and Wang, H. (2013). ZIF-8/Zn₂GeO₄ nanorods with an enhanced CO₂ adsorption property in an aqueous medium for photocatalytic synthesis of liquid fuel. *J. Mater. Chem. A1* (38):11563–11569. doi:10.1039/C3TA12433A.
- Lu, W., Wei, Z., Gu, Z.-Y., Liu, T.-F., Park, Jinhee, Park, Jihye, Tian, J., Zhang, M., Zhang, Q., Iii, T.G., Bosch, M., and Zhou, H.-C. (2014). Tuning the structure and function of metal–organic frameworks via linker design. *Chem. Soc. Rev.* 43 (16):5561–5593. doi:10.1039/C4CS00003J.

- Lv, Y., Yao, W., Zong, R., Zhu, Y. (2016). Fabrication of Wide-Range-Visible Photocatalyst Bi₂WO_{6-x} nanoplates via Surface Oxygen Vacancies. *Sci. Rep.* 6, 19347. <https://doi.org/10.1038/srep19347>
- Ma, X., Chai, Y., Li, P., and Wang, B. (2019). Metal-Organic Framework Films and Their Potential Applications in Environmental Pollution Control. *Acc. Chem. Res.* 52 (5):1461-1470. doi:10.1021/acs.accounts.9b00113.
- Maira, A.J., Coronado, J.M., Augugliaro, V., Yeung, K.L., Conesa, J.C., and Soria, J. (2001). Fourier Transform Infrared Study of the Performance of Nanostructured TiO₂ Particles for the Photocatalytic Oxidation of Gaseous Toluene. *J. Catal.* 202 (2):413-420. doi:10.1006/jcat.2001.3301.
- Mamaghani, A.H., Haghghat, F., and Lee, C.-S. (2017). Photocatalytic oxidation technology for indoor environment air purification: The state-of-the-art. *Appl. Catal. B Environ.* 203:247-269. doi:10.1016/j.apcatb.2016.10.037.
- Manisalidis, I., Stavropoulou, E., Stavropoulos, A., and Bezirtzoglou, E. (2020). Environmental and Health Impacts of Air Pollution: A Review. *Front. Public Health* 8:14. doi:10.3389/fpubh.2020.00014.
- Mo, J., Zhang, Y., Xu, Q., Lamson, J.J., Zhao, R. (2009). Photocatalytic purification of volatile organic compounds in indoor air: A literature review. *Atmos. Environ.* 43, 2229-2246. <https://doi.org/10.1016/j.atmosenv.2009.01.034>
- Molavi, H., Shojaei, A., Mousavi, S.A. (2018). Improving mixed-matrix membrane performance via PMMA grafting from functionalized NH₂-UiO-66. *J. Mater. Chem. A* 6, 2775-2791. <https://doi.org/10.1039/C7TA10480D>
- Nguyen, J.G. and Cohen, S.M. (2010). Moisture-Resistant and Superhydrophobic Metal-Organic Frameworks Obtained via Postsynthetic Modification. *J. Am. Chem. Soc.* 132 (13):4560-4561. doi:10.1021/ja100900c.
- Patra, S.S., Nath, J., Panda, S., Das, T., and Ramasamy, B. (2022). Evaluating the filtration efficiency of commercial facemasks' materials against respiratory aerosol droplets. *J. Air Waste Manag. Assoc.* 72 (1):3-9. doi:10.1080/10962247.2021.1948459.
- Plana, D., Tian, E., Cramer, A.K., Yang, H., Carmack, M.M., Sinha, M.S., Bourgeois, F.T., Yu, S.H., Masse, P., Boyer, J., Kim, M., Mo, J., LeBoeuf, N.R., Li, J., and Sorger, P.K. (2021a). Assessing the filtration efficiency and regulatory status of N95s and nontraditional filtering

- face-piece respirators available during the COVID-19 pandemic. *BMC Infect. Dis.* 21 (1):712. doi:10.1186/s12879-021-06008-8.
- Prather, K.A., Wang, C.C., and Schooley, R.T. (2020). Reducing transmission of SARS-CoV-2. *Science* 368 (6498):1422–1424. doi:10.1126/science.abc6197.
- Pui, D.Y.H., Chen, S.-C., and Zuo, Z. (2014). PM_{2.5} in China: Measurements, sources, visibility and health effects, and mitigation. *Particuology* 13:1–26. doi:10.1016/j.partic.2013.11.001.
- Pushpawela, B., Amanatidis, S., Huang, Y., and Flagan, R.C. (2022). Variability of the penetration of particles through facemasks. *Aerosol Sci. Technol.* 56 (2):186–203. doi:10.1080/02786826.2021.2003291.
- Qian, Y., Willeke, K., Grinshpun, S.A., Donnelly, J., and Coffey, C.C. (1998). Performance of N95 Respirators: Filtration Efficiency for Airborne Microbial and Inert Particles. *Am. Ind. Hyg. Assoc. J.* 59 (2):128–132. doi:10.1080/15428119891010389.
- Rezaei, F., Moussavi, G., Bakhtiari, A.R., and Yamini, Y. (2016). Toluene removal from waste air stream by the catalytic ozonation process with MgO/GAC composite as catalyst. *J. Hazard. Mater.* 306:348–358. doi:10.1016/j.jhazmat.2015.11.026.
- Sarigiannis, D.A., Karakitsios, S.P., Gotti, A., Liakos, I.L., and Katsoyiannis, A. (2011). Exposure to major volatile organic compounds and carbonyls in European indoor environments and associated health risk. *Environ. Int.* 37 (4):743–765. doi:10.1016/j.envint.2011.01.005.
- Schilling, K., Gentner, D.R., Wilen, L., Medina, A., Buehler, C., Perez-Lorenzo, L.J., Pollitt, K.J.G., Bergemann, R., Bernardo, N., Peccia, J., Wilczynski, V., and Lattanza, L. (2021). An accessible method for screening aerosol filtration identifies poor-performing commercial masks and respirators. *J. Expo. Sci. Environ. Epidemiol.* 31 (6):943–952. doi:10.1038/s41370-020-0258-7.
- Schneemann, A., Bon, V., Schwedler, I., Senkovska, I., Kaskel, S., and A. Fischer, R. (2014). Flexible metal–organic frameworks. *Chem. Soc. Rev.* 43 (16):6062–6096. doi:10.1039/C4CS00101J.
- Scott Bobbitt, N., L. Mendonca, M., J. Howarth, A., Islamoglu, T., T. Hupp, J., K. Farha, O., and Q. Snurr, R. (2017). Metal–organic frameworks for the removal of toxic industrial chemicals and chemical warfare agents. *Chem. Soc. Rev.* 46 (11):3357–3385. doi:10.1039/C7CS00108H.
- Shah, S.J., Wang, R., Gao, Z., Muhammad, Y., Zhang, H., Zhang, Z., Chu, Z., Zhao, Zhongxing, and Zhao, Zhenxia (2021). IL-assisted synthesis of defect-rich polyaniline/NH₂-MIL-125

- nanohybrids with strengthened interfacial contact for ultra-fast photocatalytic degradation of acetaldehyde under high humidity. *Chem. Eng. J.* 411:128590. doi:10.1016/j.cej.2021.128590.
- Stahl, C., Frederick, K., Chaudhary, S., Morton, C.J., Loy, D., Muralidharan, K., Sorooshian, A., and Parthasarathy, S. (2021). Comparison of the Filtration Efficiency of Different Face Masks Against Aerosols. *Front. Med.* 8:654317. doi:10.3389/fmed.2021.654317.
- Sun, S., Ding, J., Bao, J., Gao, C., Qi, Z., Yang, X., He, B., and Li, C. (2012). Photocatalytic degradation of gaseous toluene on Fe-TiO₂ under visible light irradiation: A study on the structure, activity and deactivation mechanism. *Appl. Surf. Sci.* 258 (12):5031–5037. doi:10.1016/j.apsusc.2012.01.075.
- Tang, M., Chen, S.-C., Chang, D.-Q., Xie, X., Sun, J., and Pui, D.Y.H. (2018a). Filtration efficiency and loading characteristics of PM_{2.5} through composite filter media consisting of commercial HVAC electret media and nanofiber layer. *Sep. Purif. Technol., Filtering a Better Future* 198:137–145. doi:10.1016/j.seppur.2017.03.040.
- Tang, M., Thompson, D., Chang, D.-Q., Chen, S.-C., and Pui, D.Y.H. (2018b). Filtration efficiency and loading characteristics of PM_{2.5} through commercial electret filter media. *Sep. Purif. Technol.* 195:101–109. doi:10.1016/j.seppur.2017.11.067.
- Tran, V.V., Park, D., and Lee, Y.-C. (2020). Indoor Air Pollution, Related Human Diseases, and Recent Trends in the Control and Improvement of Indoor Air Quality. *Int. J. Environ. Res. Public Health* 17 (8):2927. doi:10.3390/ijerph17082927.
- US EPA, O. (2017). Indoor Air Quality. Available at <https://www.epa.gov/report-environment/indoor-air-quality> (Accessed 2 September 2021).
- Usman, M., Mendiratta, S., and Lu, K.-L. (2017). Semiconductor Metal–Organic Frameworks: Future Low-Bandgap Materials. *Adv. Mater.* 29 (6):1605071. doi:10.1002/adma.201605071.
- Walgraeve, C., Demeestere, K., Dewulf, J., Van Huffel, K., Van Langenhove, H. (2011). Diffusive sampling of 25 volatile organic compounds in indoor air: Uptake rate determination and application in Flemish homes for the elderly. *Atmos. Environ.* 45, 5828–5836. <https://doi.org/10.1016/j.atmosenv.2011.07.007>
- Wang, J., Chen, D. R., and Pui, D. Y. H. (2007). Modeling of Filtration Efficiency of Nanoparticles in Standard Filter Media, *J. Nanoparticle Res.*, 9:109–115.

- Wang, J., Kim, S. C., and Pui, D. Y. H. (2011). Measurement of Multi-Wall Carbon Nanotubes Penetration through a Screen Filter and Single-Fiber Analysis. *J. Nanopart. Res.*, 13:4565–4573.
- Wang, X., Liu, J., Leong, S., Lin, X., Wei, J., Kong, B., Xu, Y., Low, Z.-X., Yao, J., Wang, H. (2016). Rapid Construction of ZnO@ZIF-8 Heterostructures with Size-Selective Photocatalysis Properties. *ACS Appl. Mater. Interfaces* 8, 9080–9087. <https://doi.org/10.1021/acsami.6b00028>
- Wang, H., Yu, T., Tan, X., Zhang, H., Li, P., Liu, H., Shi, L., Li, X., and Ye, J. (2016). Enhanced Photocatalytic Oxidation of Isopropanol by HKUST-1@TiO₂ Core–Shell Structure with Ultrathin Anatase Porous Shell: Toxic Intermediate Control. *Ind. Eng. Chem. Res.* 55 (29):8096–8103. doi:10.1021/acs.iecr.6b01400.
- Wang, Y., Guo, L., Zeng, Y., Guo, H., Wan, S., Ou, M., Zhang, S., Zhong, Q. (2019). Amino-Assisted NH₂-UiO-66 Anchored on Porous g-C₃N₄ for Enhanced Visible-Light-Driven CO₂ Reduction. *ACS Appl. Mater. Interfaces* 11, 30673–30681. <https://doi.org/10.1021/acsami.9b04302>
- Wang, T., Wang, Y., Sun, M., Hanif, A., Wu, H., Gu, Q., Sik Ok, Y., W. Tsang, D.C., Li, J., Yu, J., and Shang, J. (2020). Thermally treated zeolitic imidazolate framework-8 (ZIF-8) for visible light photocatalytic degradation of gaseous formaldehyde. *Chem. Sci.* 11 (26):6670–6681. doi:10.1039/D0SC01397H.
- Wang, H., Yu, T., Tan, X., Zhang, H., Li, P., Liu, H., Shi, L., Li, X., Ye, J. (2016). Enhanced Photocatalytic Oxidation of Isopropanol by HKUST-1@TiO₂ Core–Shell Structure with Ultrathin Anatase Porous Shell: Toxic Intermediate Control. *Ind. Eng. Chem. Res.* 55, 8096–8103. <https://doi.org/10.1021/acs.iecr.6b01400>
- Webster, C.E., Drago, R.S., Zerner, M.C. (1998). Molecular Dimensions for Adsorptives. *J. Am. Chem. Soc.* 120, 5509–5516. <https://doi.org/10.1021/ja973906m>
- Xie, R., Lei, D., Zhan, Y., Liu, B., Tsang, C.H.A., Zeng, Y., Li, K., Leung, D.Y.C., Huang, H. (2020). Efficient photocatalytic oxidation of gaseous toluene over F-doped TiO₂ in a wet scrubbing process. *Chem. Eng. J.* 386, 121025. <https://doi.org/10.1016/j.cej.2019.02.112>
- Xu, Y., Zhou, Y., Deng, Y., Xiang, Y., Tan, Y., Tang, H., Zou, H. (2020). Synthesis of Bi₂WO₆@NH₂-MIL-125(Ti): A S-Scheme Photocatalyst with Enhanced Visible Light Catalytic Activity. *Catal. Lett.* 150, 3470–3480. <https://doi.org/10.1007/s10562-020-03258-0>

- Yang, S., Zhu, Z., Wei, F., Yang, X. (2017). Carbon nanotubes / activated carbon fiber-based air filter media for simultaneous removal of particulate matter and ozone. *Build. Environ.* 125, 60–66. <https://doi.org/10.1016/j.buildenv.2017.08.040>
- Yin, S., Chen, Y., Gao, C., Hu, Q., Li, M., Ding, Y., Di, J., Xia, J., Li, H. (2020a). In-situ preparation of MIL-125(Ti)/Bi₂WO₆ photocatalyst with accelerating charge carriers for the photodegradation of tetracycline hydrochloride. *J. Photochem. Photobiol. Chem.* 387, 112149. <https://doi.org/10.1016/j.jphotochem.2019.112149>
- Yin, S., Chen, Y., Li, M., Hu, Q., Ding, Y., Shao, Y., Di, J., Xia, J., Li, H. (2020b). Construction of NH₂-MIL-125(Ti)/Bi₂WO₆ composites with accelerated charge separation for degradation of organic contaminants under visible light irradiation. *Green Energy Environ.* 5, 203–213. <https://doi.org/10.1016/j.gee.2020.03.008>
- Yim, W., Cheng, D., Patel, S.H., Kou, R., Meng, Y.S., and Jokerst, J.V. (2020). KN95 and N95 Respirators Retain Filtration Efficiency despite a Loss of Dipole Charge during Decontamination. *ACS Appl. Mater. Interfaces* 12 (49):54473–54480. doi:10.1021/acsami.0c17333.
- You, R., Zhao, B., and Chen, C. (2012). Developing an Empirical Equation for Modeling Particle Deposition Velocity onto Inclined Surfaces in Indoor Environments. *Aerosol Sci. Technol.* 46 (10):1090–1099. doi:10.1080/02786826.2012.695096.
- Yu, B.F., Hu, Z.B., Liu, M., Yang, H.L., Kong, Q.X., Liu, Y.H. (2009). Review of research on air-conditioning systems and indoor air quality control for human health. *Int. J. Refrig.* 32, 3–20. <https://doi.org/10.1016/j.ijrefrig.2008.05.004>
- Yuan, J., Liu, X., Akbulut, O., Hu, J., Suib, S.L., Kong, J., Stellacci, F. (2008). Superwetting nanowire membranes for selective absorption. *Nat. Nanotechnol.* 3, 332–336. <https://doi.org/10.1038/nnano.2008.136>
- Zeng, X., Huang, L., Wang, C., Wang, J., Li, J., Luo, X. (2016). Sonocrystallization of ZIF-8 on Electrostatic Spinning TiO₂ Nanofibers Surface with Enhanced Photocatalysis Property through Synergistic Effect. *ACS Appl. Mater. Interfaces* 8, 20274–20282. <https://doi.org/10.1021/acsami.6b05746>
- Zhang, W., Hu, Y., Ge, J., Jiang, H.-L., Yu, S.-H. (2014). A Facile and General Coating Approach to Moisture/Water-Resistant Metal–Organic Frameworks with Intact Porosity. *J. Am. Chem. Soc.* 136, 16978–16981. <https://doi.org/10.1021/ja509960n>

- Zhang, Y., Yuan, S., Feng, X., Li, H., Zhou, J., and Wang, B. (2016). Preparation of Nanofibrous Metal–Organic Framework Filters for Efficient Air Pollution Control. *J. Am. Chem. Soc.* 138 (18):5785–5788. doi:10.1021/jacs.6b02553.
- Zhang, B., Zhang, Jianling, Tan, X., Shao, D., Shi, J., Zheng, L., Zhang, Jing, Yang, G., Han, B. (2018). MIL-125-NH₂@TiO₂ Core–Shell Particles Produced by a Post-Solvothermal Route for High-Performance Photocatalytic H₂ Production. *ACS Appl. Mater. Interfaces* 10, 16418–16423. <https://doi.org/10.1021/acsami.8b01462>
- Zhang, X., Lv, X., Shi, X., Yang, Yang, Yang, Yiqiong (2019). Enhanced hydrophobic UiO-66 (University of Oslo 66) metal-organic framework with high capacity and selectivity for toluene capture from high humid air. *J. Colloid Interface Sci.* 539, 152–160. <https://doi.org/10.1016/j.jcis.2018.12.056>
- Zhang, J., Hu, Y., Qin, J., Yang, Z., Fu, M. (2020). TiO₂-UiO-66-NH₂ nanocomposites as efficient photocatalysts for the oxidation of VOCs. *Chem. Eng. J.* 385, 123814. <https://doi.org/10.1016/j.cej.2019.123814>
- Zhang, Y., Chi, H., Zhang, W., Sun, Y., Liang, Q., Gu, Y., Jing, R. (2014). Highly Efficient Adsorption of Copper Ions by a PVP-Reduced Graphene Oxide Based On a New Adsorptions Mechanism. *Nano-Micro Lett.* 6, 80–87. <https://doi.org/10.1007/BF03353772>
- Zhang, Y., He, X., Zhu, Z., Wang, W.-N., Chen, S.-C. (2021). Simultaneous removal of VOCs and PM_{2.5} by metal-organic framework coated electret filter media. *J. Membr. Sci.* 618, 118629. <https://doi.org/10.1016/j.memsci.2020.118629>
- Zhang, Y., Zhu, Z., Wang, W.-N., Chen, S.-C. (2022). Mitigating the relative humidity effects on the simultaneous removal of VOCs and PM_{2.5} of a metal–organic framework coated electret filter. *Sep. Purif. Technol.* 285, 120309. <https://doi.org/10.1016/j.seppur.2021.120309>
- Zhang, Y., Zhu, Z., Wang, W.-N., Chen, S.-C. (2023). A Novel Sustainable Semiconductor/Metal-organic Framework Coated Electret Filter for Simultaneous Removal of PM_{2.5} and VOCs. *Aerosol Air Qual. Res.* 23 (5):220445. doi:10.4209/aaqr.220445.
- Zhao, J., Yang, X. (2003). Photocatalytic oxidation for indoor air purification: a literature review. *Build. Environ.* 38, 645–654. [https://doi.org/10.1016/S0360-1323\(02\)00212-3](https://doi.org/10.1016/S0360-1323(02)00212-3)
- Zhao, X.S., Ma, Q., Lu, G.Q. (Max) (1998). VOC Removal: Comparison of MCM-41 with Hydrophobic Zeolites and Activated Carbon. *Energy Fuels* 12, 1051–1054. <https://doi.org/10.1021/ef980113s>

- Zheng, X., Liu, S., Rehman, S., Li, Z., Zhang, P. (2020). Highly improved adsorption performance of metal-organic frameworks CAU-1 for trace toluene in humid air via sequential internal and external surface modification. *Chem. Eng. J.* 389, 123424. <https://doi.org/10.1016/j.cej.2019.123424>
- Zheng, X., Wu, Z., Yang, J., Rehman, S., Cao, R., Zhang, P. (2021). Metal–Organic Gel Derived N-Doped Granular Carbon: Remarkable Toluene Uptake and Rapid Regeneration. *ACS Appl. Mater. Interfaces* 13, 17543–17553. <https://doi.org/10.1021/acsami.1c01524>
- Zhong, L., Haghghat, F. (2015). Photocatalytic air cleaners and materials technologies – Abilities and limitations. *Build. Environ.* 91, 191–203. <https://doi.org/10.1016/j.buildenv.2015.01.033>
- Zhu, L., Shen, D., Luo, K.H. (2020). A critical review on VOCs adsorption by different porous materials: Species, mechanisms and modification methods. *J. Hazard. Mater.* 389, 122102. <https://doi.org/10.1016/j.jhazmat.2020.122102>
- Zhu, M., Hu, P., Tong, Z., Zhao, Zhongxing, Zhao, Zhenxia (2017). Enhanced hydrophobic MIL(Cr) metal-organic framework with high capacity and selectivity for benzene VOCs capture from high humid air. *Chem. Eng. J.* 313, 1122–1131. <https://doi.org/10.1016/j.cej.2016.11.008>
- Zhu, Z., Bao, L., Pestov, D., Xu, P., Wang, W.-N. (2023). Cellular-level insight into biointerface: From surface charge modulation to boosted photocatalytic oxidative disinfection. *Chem. Eng. J.* 453, 139956. <https://doi.org/10.1016/j.cej.2022.139956>
- Zhu, Z., Zhang, Y., Bao, L., Chen, J., Duan, S., Chen, S.-C., Xu, P., Wang, W.-N. (2021). Self-decontaminating nanofibrous filters for efficient particulate matter removal and airborne bacteria inactivation. *Environ. Sci. Nano* 8, 1081–1095. <https://doi.org/10.1039/D0EN01230K>